View metadata, citation and similar papers at core.ac.uk

brought to you by CORE

provided by University of Wisconsin-Milwaukee

University of Wisconsin Milwaukee
UWM Digital Commons

Theses and Dissertations

May 2019

Mathematical Modeling and Analysis of a Phytoplankton Competition Model Incorporating Preferential Nutrient Uptake

Thomas George Stojsavljevic Jr
University of Wisconsin-Milwaukee

Follow this and additional works at: https://dc.uwm.edu/etd

Part of the Mathematics Commons

Recommended Citation
Stojsavljevic Jr, Thomas George, "Mathematical Modeling and Analysis of a Phytoplankton Competition Model Incorporating Preferential Nutrient Uptake" (2019). *Theses and Dissertations*. 2130.
https://dc.uwm.edu/etd/2130

This Dissertation is brought to you for free and open access by UWM Digital Commons. It has been accepted for inclusion in Theses and Dissertations by an authorized administrator of UWM Digital Commons. For more information, please contact open-access@uwm.edu.

MATHEMATICAL MODELING AND ANALYSIS OF A PHYTOPLANKTON COMPETITION MODEL INCORPORATING PREFERENTIAL NUTRIENT UPTAKE

by

Thomas G. Stojsavljevic Jr.

A Dissertation Submitted in

Partial Fulfillment of the

Requirements for the Degree of

Doctor of Philosophy

in Mathematics

at

The University of Wisconsin-Milwaukee

May 2019

ABSTRACT

MATHEMATICAL MODELING AND ANALYSIS OF A PHYTOPLANKTON COMPETITION MODEL INCORPORATING PREFERENTIAL NUTRIENT UPTAKE

by

Thomas G. Stojsavljevic Jr.

The University of Wisconsin-Milwaukee, 2019
Under the Supervision of Professor Gabriella Pinter

Phytoplankton live in a complex environment with two essential resources forming various gradients. Light supplied from above is never homogeneously distributed in a body of water due to refraction and absorption from biomass present in the ecosystem and from other sources. Nutrients in turn are typically supplied from below. In poorly mixed water columns, phytoplankton can be heterogeneously distributed forming various layering patterns. We present a new reaction-diffusion-taxis model describing the vertical distribution of two phytoplankton species competing for two nutrients, one of which is assumed to be preferred. The parameter space of the model is analyzed for parameter identifiability – the ability for a parameter's true value to be recovered through optimization, and for global sensitivity – the influence a parameter has on model response. Using simulations, we exhibit evidence of thin layer formation for motile phytoplankton in poorly mixed environments. A game theoretic approximation is considered, where the depth of the phytoplankton layer is treated as the strategy the phytoplankton adopt. The evolutionary stable strategy (ESS) is the depth at which the phytoplankton are equally limited by both resources. We analytically derive the ESS of the proposed preferential uptake model along with a related two-species reaction-diffusion-taxis model which only considers one limiting nutrient.

TABLE OF CONTENTS

1 Introduction 1

2 Existing Models 7

2.1 Non-spatial Models 7

2.1.1 Resource Limited Growth 8

2.1.2 Chemostat Model 10

2.2 Spatial Models 12

2.2.1 Klausmeier and Litchman Model 13

2.2.2 Multi-species Klausmeier and Litchman Model 21

3 Proposed Preferential Nutrient Uptake Model 26

3.1 Model Development 27

3.2 Simulation Technique 32

3.2.1 Biomass Advection 35

3.2.2 Biomass Diffusion 38

3.2.3 Nutrient Diffusion 39

3.3 Numerical Illustration and Biological Significance 40

4 Parameter Identification and Global Sensitivity Analysis 47

4.1 Parameter Estimation 47

4.1.1 Deterministic Estimation Problem 48

4.1.2 Parameter Estimation Based on Simulated Data 48

4.2 Global Sensitivity Analysis 56

4.2.1 The Morris Screening Procedure 56

4.2.2 The Sobol Decomposition 66

5 The Evolutionary Stable Strategy 76

5.1 Multi-species Klausmeier and Litchman Model ESS 80

5.2 Preferential Nutrient Uptake Model ESS 96

6 Conclusion and Suggestions for Future Work 117

REFERENCES 120

CURRICULUM VITAE 127

LIST OF FIGURES

2.1 Phase portrait for isolated consumer resource system 9

2.2 Phase portrait for non-conservative consumer resource system 10

2.3 Phase portrait for chemostat model 11

2.4 Klausmeier & Litchman Model Simulations 17

2.5 Multi-Species Klausmeier & Litchman Model Simulations 24

3.1 Preferential Uptake Model Simulation 41

3.2 Preferential Uptake Model Layers 42

3.3 Preferential Uptake Model Species Competition Simulations 43

3.4 Preferential Nutrient Uptake Surface Plots 44

4.1 Klausmeier & Litchman Morris Screening Biomass 58

4.2 Klausmeier & Litchman Morris Screening Nutrient 59

4.3 Multi-species Klausmeier & Litchman Morris Screening Biomass by Species . 61

4.4 Multi-species Klausmeier & Litchman Morris Screening Nutrient 62

4.5 Preferential Uptake Model Morris Screening Biomass by Species 64

4.6 Preferential Uptake Model Morris Screening Nutrients by Nutrient 65

4.7 Klausmeier & Litchman Sobol Decomposition Biomass 69

4.8 Klausmeier & Litchman Sobol Decomposition Nutrient 70

4.9 Multi-species Klausmeier & Litchman Sobol Decomposition Biomass by Species 71

4.10 Multi-species Klausmeier & Litchman Sobol Decomposition Nutrient 72

4.11 Preferential Uptake Model Sobol Decomposition Biomass by Species 73

4.12 Preferential Uptake Model Sobol Decomposition Nutrients by Nutrient . . . 74

5.1 Klausmeier and Litchman Model Simulations with Increasing ν_{max}. 77

5.2 Multi-species Klausmeier and Litchman Model Simulations with Increasing $\nu_{1_{max}}$ and $\nu_{2_{max}}$. 82
5.3 Preferential Nutrient Uptake Model Simulations with Increasing $\nu_{1_{max}}$ and $\nu_{2_{max}}$. 98

LIST OF TABLES

2.1 Model parameters for Klausmeier & Litchman model 16

2.2 Model parameters for Multi-species Klausmeier & Litchman Model 23

3.1 Preferential Uptake Model Parameter Values 46

4.1 Klausmeier & Litchman Parameter Optimization Results for $\alpha = 0.05$ 50

4.2 Klausmeier & Litchman Parameter Optimization Results for $\alpha = 0.1$ 50

4.3 Multi-species Klausmeier & Litchman Parameter Optimization Results for $\alpha = 0.05$ 52

4.4 Multi-species Klausmeier & Litchman Parameter Optimization Results for $\alpha = 0.1$ 53

4.5 Preferential Uptake Model Parameter Estimation Results for $\alpha = 0.05$ 54

4.6 Preferential Uptake Model Parameter Estimation Results for $\alpha = 0.1$ 55

4.7 Klausmeier & Litchman Model Morris Screening Top 5 Parameter Ranking . 60

4.8 Multi-species Klausmeier Model Morris Screening Top 5 Parameter Ranking 63

4.9 Preferential Uptake Model Morris Screening Top 5 Parameter Ranking . . . 65

ACKNOWLEDGMENTS

First I wish to thank Dr. Pinter for all of her insights and support in this project. You have influenced me in many ways, both personally and professionally. The clarity of your work, your commitment to student success, your integrity, willingness to help, and positive outlook will continue to serve as an example in my future career. I am very grateful to you and this work would not have been possible without you.

I would also like to thank Drs. Lauko, Wade, Sun, and Boyd for being on my committee and taking interest in my work. In particular I would like to extend extra gratitude to Drs. Lauko and Wade for their time, expertise, and support.

I wish to thank all of my family and friends who have supported me during my time in graduate school. I am grateful to have the constant help and support from my parents, my sister, and my brother-in-law. To my nephew Colin - one day you will be old enough to read this and know how much joy you bring to my life. To Anastasia, Diego, Murphy, and Nic - you are my chosen family and I am a better person for knowing all of you. To Alie, Amanda, Durham, Joey, Katie, and Rachel - you all have played a major role in my life during my time in the math department. I greatly appreciate your friendship, support, and willingness to bounce around ideas no matter the time.

Finally, I would like to thank the UWM Graduate School and Department of Mathematical Sciences for funding me during my time here. It has been a privilege to have been a member of this department and to have the opportunity to work alongside supportive faculty and staff during my graduate school career.

1 Introduction

In general, phytoplankton are regarded as the community of plants adapted to suspension in the sea or in fresh waters and which are susceptible to passive movement by wind and current. They include algae, diatoms, and cyanobacteria (commonly referred to as blue-green algae). It is estimated that the first phytoplankton (marine cyanobacteria) occurred approximately 3 billion years ago, and since then, have gone on to oxygenate Earth's atmosphere and undergone dramatic diversification (including founding the lineage of terrestrial plants) [39]. Today, phytoplankton account for approximately one half of Earth's primary production, and play a vital role in the biogeochemical cycling of many nutrients including carbon, nitrogen, and phosphorous [3], [9], [39], [61].

As the base of the aquatic food chain, phytoplankton are greatly impacted by human activities [39]. In particular, the effects of climate change on the structure and functioning of ecosystems are far reaching and complex. While elevated carbon dioxide (CO_2) levels are causing acidification of oceans to the detriment of calcifying organisms such as coral, the elevation in CO_2 levels may be beneficial for primary production in both aquatic and terrestrial environments. In addition to altering the timing and distribution of organisms across ecosystems, warming in aquatic ecosystems induces increased thermal stratification [9], [61]. Generally, as thermal stratification increases, nutrient concentrations in the upper mixed layers of oceans and deeper lakes decreases. From this change in the environment there is a corresponding change in the ecological stoichiometry – the field investigating how the elemental composition of organisms affects ecological processes [9], [61].

In 1934, Alfred C. Redfield reported that the ratios between the elements carbon, nitrogen, and phosphorous (C,N, and P respectively) in marine phytoplankton are constant in ratio of 106:16:1 (by atom). This ratio, which went on to be known as the Redfield ratio, was also originally noted to be similar to ratios found in marine environments. The N:P ratio present in phytoplankton was found to be similar to the nitrate:phosphate ratio found in deep

ocean waters. Thus, the elemental composition of phytoplankton were noted to reflect the elemental composition of their environment and vice versa [61]. As global warming and rising CO_2 levels make the ocean more acidic and loaded more with carbon, a similar reflection is observed in the elemental composition of the phytoplankton. This is further exacerbated by the increased thermal stratification and decreased nutrient concentration in the upper mixed layers of bodies of water. The resulting shift of having high carbon nutrients poses a significant risk for the aquatic food chain [9], [61]. Plankton which have a high carbon-to-nutrient ratio are of low nutritional value to zooplankton [61], and thus a poor food source for the primary consumers in the aquatic food chain. These climate induced changes in the elemental makeup of plankton may have a potential cascading effect throughout the entire aquatic food chain [61]. It remains an open area of research as to whether diverse plankton communities can offset the adverse effects of a high carbon-to-nutrient composition and the exact role temperature plays in this relationship [9].

While climate change is a major stress on the environment, it is not a force that acts alone. Many ecosystems are threatened by stressors including increased fragmentation, eutrophication, and pollution [9]. Eutrophication occurs when a body of water becomes overly enriched with minerals and nutrients resulting in excessive plant and algae growths which can result in oxygen depletion in a body of water. The two most common nutrients resulting from human-derived sources are phosphorous and nitrogen [1]. In freshwater environments, phosphorous is the least abundant macronutrient needed by photosynthetic organisms and is the nutrient which limits their growth [1], [30]. Phosphorous can also limit growth in marine environments which sustain high nitrogen inputs, however, nitrogen is often the primary limiting nutrient in marine environments [1]. In estuaries, both nitrogen and phosphorous can co-limit phytoplankton production.

For more than 50 years scientists have recognized that harmful algal blooms (HABs) in freshwater lakes, reservoirs, and slow moving rivers, are stimulated by phosphorous enrichment [1],[22], [23]. In addition to forming thick scums which can be over 1 meter thick,

consisting of billions of cells, and having chlorophyll a concentrations as large as 3,000 μg L^{-1}, many species are able to produce hepatotoxins and neurotoxins which have killed livestock, wildlife, and more rarely humans, in most countries around the world [1]. This relationship is strong enough that the total phosphorous concentration in moderately deep lakes ($\geq$ 10 m) with low abiotic turbidity during the spring season has been used as a predictor for the late summer maximum in cyanobacteria biomass (measured in chlorophyll a) with reasonable success. Similar results have been reported in estuaries in Australia and Scandinavia as well [1].

Over the last several decades, public views and responses to the global HAB problem in estauries and costal waters have shifted. Almost every costal country is affected by multiple harmful or toxic algal species, often in many locations and over broad areas [1], [22], [23]. While poor historical data and new advances in toxin detection methods both play an important role in understanding part of this trend; for resource managers the potential relationship between HABs and accelerated eutrophication of costal waters due to human activity is of utmost importance. Coastal waters are receiving massive and increasing amounts of industrial, agricultural, and sewage runoff through multiple pathways and in urbanized coastal regions, these inputs have already altered the size and content of the nutrient pool which can create a more favorable environment for HABs [1], [22], [23].

Along with the large ecological and environmental hazards that HABs impose on aquatic ecosystems, there is a significant economic cost that is also associated with the increase in HAB events. Currently resource managers estimate that HABs are responsible for millions of dollars lost annually to coastal communities due to the costs of beach cleanup, the closing of fisheries, and decreased tourism. Other estimates, such as those found in section 602(5) of the U.S. Harmful Algal Bloom and Hypoxia Research and Control Act of 1998 concluded that HABs were responsible for $1,000,000,000 over the last decade, and that figure has only increased [22]. Part of the difficulty in estimating the true economic impact is that as bloom events become more widespread and frequent, there are increased cases of paralytic,

diarrhetic, amnesic, or neurotoxic shellfish poisoning resulting from people eating shellfish which accumulated toxins from those algal blooms. The loss of economic productivity from missing work and for hospitalization and treatment from these sources is also in the millions of dollars annually [22].

There have been numerous efforts to find ways to preserve water resevoirs and limit the impact of algal blooms. One of the most recent newsworthy endeavors came from Los Angeles, California in 2015. Due to the extreme drought that was occurring, and wanting to preserve water quality from degradation resulting from algal blooms, over 96 million shade balls with a diameter of 4 inches were released into the Los Angeles reservoir [20]. While it remains an open question as to how successful the black shade balls were in preserving water quality since the shade balls are able to create a thermal blanket which may improve conditions that promote bacterial growth, there was success in reducing water loss due to evaporation. LA officials estimate that up to 300 million gallons of water per year have been conserved by the use of shade balls [20]. However, shade balls are made with high–density polyethylene plastic, which requires crude oil, natural gas, and electricity to produce, and thus can have significant water quantity and quality impacts [20]. Analysis done by Haghighi, Madani, and Hoesktra found that the amount of water needed to produce the shade balls in the typical thickness of 5 mm used during the LA drought was larger than the reduced reservoir evaporation achieved by the balls during the 1.5–year period between the release of the balls (August 2015) and the end of California's drought (March 2017)[20]. Their analysis also showed that while reducing the thickness of the shade balls would be able to result in net positive water conservation, it would also come with operational difficulties of the thermal blanket being less stable and more prone to move. Thus it remains critically important to understand the mechanisms that are responsible for HAB development and to find other sustainable methods for controlling HAB events.

In this dissertation we introduce a new mathematical model which is of interest to the biological community. This model describes the competition between two phytoplankton

species which incorporates preferential nutrient uptake. The role of co-limitation by multiple nutrients is an important dynamic in phytoplankton ecology and until now has not been addressed in the models existing in the literature.

In Chapter 2, we discuss standard approaches to modeling phytoplankton population dynamics and present several existing models. The strengths and limitations these models have are discussed through the use of phase portraits, model simulations, and the results of previous theoretical analysis. The first three models discussed highlight the importance that nutrient in-flows and out-flows have on phytoplankton population dynamics which are naturally present in spatially dependent models. We then present a model first discussed in [35] and a multi-species variant of that model. These models are simulated using biologically significant parameters and the results of the simulations are discussed for their phenomenological ability to capture complex behavior seen in real world data.

The original work in this thesis is presented in Chapters 3, 4, and 5. This work can be categorized into three major tasks:

1. The development of a biologically meaningful model of phytoplankton dynamics which incorporates the role of co-limitation by multiple nutrients via preferential uptake.

2. Numerical experiments and applications that illustrate the behavior of the system and discuss the biological relevance of the proposed model. This includes comparing the phenomological results of the proposed preferential uptake model to existing models in the literature and to field data. Additional work in parameter sensitivity analysis and the results of several inverse problems are also considered in this discussion.

3. The derivation of special equilibrium solutions used to approximate the amount of biomass present and the location of where phytoplankton layers occur.

In Chapter 3 we present the proposed model of phytoplankton competition which incorporates the role of co-limitation by multiple nutrients via preferential nutrient uptake. We describe the necessary biological assumptions along with mathematical formulations for the

preferential nutrient uptake. We then introduce the numerical method needed to conduct model simulations. The results of these numerical simulations are compared to real world data from Lake Michigan as well as existing models in the literature. In particular, parameters responsible for reproducing various layering phenomena seen in nature are discussed.

In Chapter 4, we report on the results of three inverse problems resulting from the preferential uptake model, along with the models presented at the end of Chapter 2 which serve as an inspiration for the proposed model. In particular, we are interested in the ability of each model to recover its original parameter set through solving the inverse problem. Those parameters are deemed to be identifiable and are important to experimental design. Next we analyze the parameter spaces of all three models for global sensitivity. Global sensitivity refers to the influence a parameter has on model response [55]. In this dissertation two different methods of global sensitivity are presented: the Morris screening and the Sobol decomposition. The similarities and differences between the parameters identified by all three models is discussed for both biological relevance and mathematical significance.

In Chapter 5, we derive special equilibrium solutions which can be used to approximate the amount of biomass present and the location of where phytoplankton layers can occur in a body of water. This is done by considering a game theoretic approach where the depth of the layer is treated as a strategy the phytoplankton adopt. Under these assumptions, we solve for the equilibrium distribution of the system. The results of this analysis for the model presented in [35] are summarized. We then rigorously derive the equilibrium distributions of a related two species phytoplankton competition model based off of the model presented in [35] and the proposed preferential uptake model.

We finish the dissertation with suggestions for future work in this area. In particular, further biological considerations which can be incorporated into the proposed model, other types of models, and further statistical analysis are briefly discussed.

2 Existing Models

The dynamics of phytoplankton populations have been the subject of numerous studies. These models can be broadly divided into two categories: non-spatial and spatial models. In this chapter, we summarize several models found in the literature and state results of their analysis if available. In the first section we will focus on simple population models in a non-spatial context. In the second section we consider 1D models of the vertical phytoplankton distributions incorporating limiting factors.

2.1 Non-spatial Models

Adopting the notation used in [51], let $P(t)$ denote the density of a population at time t. The simplest model to consider studying the dynamics of P is given by the first order ordinary differential equation

$$\frac{dP}{dt} = \mu(P)P, \tag{2.1}$$

where the growth rate $\mu(P)$ depends on the population density P. The growth function μ takes into account density dependent factors which can regulate populations such as resource depletion or over-crowding. Typically it is assumed that $\mu(P)$ is monotonically decreasing and eventually becomes negative for large densities. A classic example of a model that fits this form is logistic growth:

$$\frac{dP}{dt} = \mu_0 P\left(1 - \frac{P}{K}\right), \tag{2.2}$$

where μ_0 is the growth rate, K is the carrying capacity of the system and describes the maximum population density that the system can sustain. While models of this form can be used for population density, models of this form lack information about resource limitation.

2.1.1 Resource Limited Growth

We now consider an extension to the basic differential equation model by considering an isolated consumer-resource system. Let $N(t)$ denote the limiting resource concentration. For phytoplankton models this typically is a limiting nutrient such as phosphate or nitrate. The new model becomes a system of differential equations given in the following form

$$\frac{dP}{dt} = \mu(N)P - mP$$

$$\frac{dN}{dt} = -\mu(N)P + mP. \tag{2.3}$$

Here the parameter m is a mortality rate and the growth function $\mu(N)$ is assumed to be defined in such a way that $\mu(0) = 0$ and $\lim_{N\to\infty} \mu(N) = c$, where $0 < c < \infty$, i.e. the growth rate is saturated for large values of N. A standard example is the Michaelis-Menten relation

$$\mu(N) = c\frac{N}{H_N + N}, \tag{2.4}$$

where H_N is the half-saturation constant.

As shown in Figure 2.1, the phase trajectories of the conservative model in the (P, N) plane are straight lines from the initial conditions to an equilibrium state. In this model, nutrient recycling is assumed to be 100% efficient. Thus the above system can be reduced to a one-dimensional model by noting that $S = N + P$ is a constant. This reduction only holds in a closed system.

In general, recycling efficiency will never be 100%. Assuming that only a fraction ε of

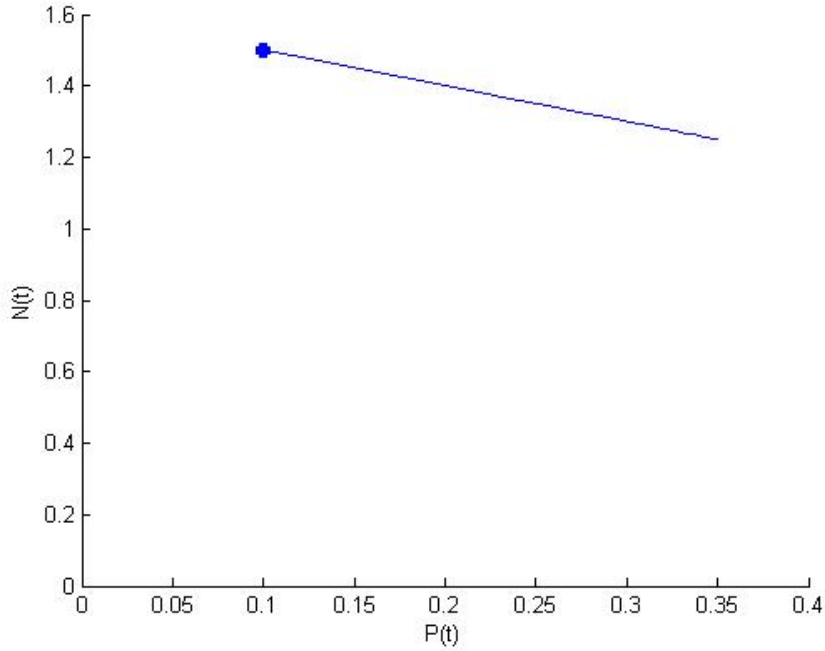

Figure 2.1: Phase trajectory of the model given in (2.3) with Michaelis-Menten growth rate (2.4). The initial value $P(0) = 0.1$ and $N(0) = 1.5$. The other parameters used are $c = 5$, $H_N = 5$, and $m = 1$.

the dead biomass is remineralized, we can modify system (2.3) as

$$\frac{dP}{dt} = \mu(N)P - mP$$

$$\frac{dN}{dt} = -\mu(N)P + \varepsilon mP, \tag{2.5}$$

where $0 < \varepsilon < 1$. The system given in (2.5) is a non-conservative model since we no longer have $S = N + P$ is a constant. As shown in Figure 2.2, the phase trajectory of the non-conservative model leads to the extinction of the population. In general, (2.5) does not admit isolated stationary states in the (P, N) phase plane. Further, for any initial condition, $P(t) \to 0$ as $t \to \infty$ for certain growth functions $\mu(N)$.

The principal issues that the models given in (2.3) and (2.5) have is that neither system

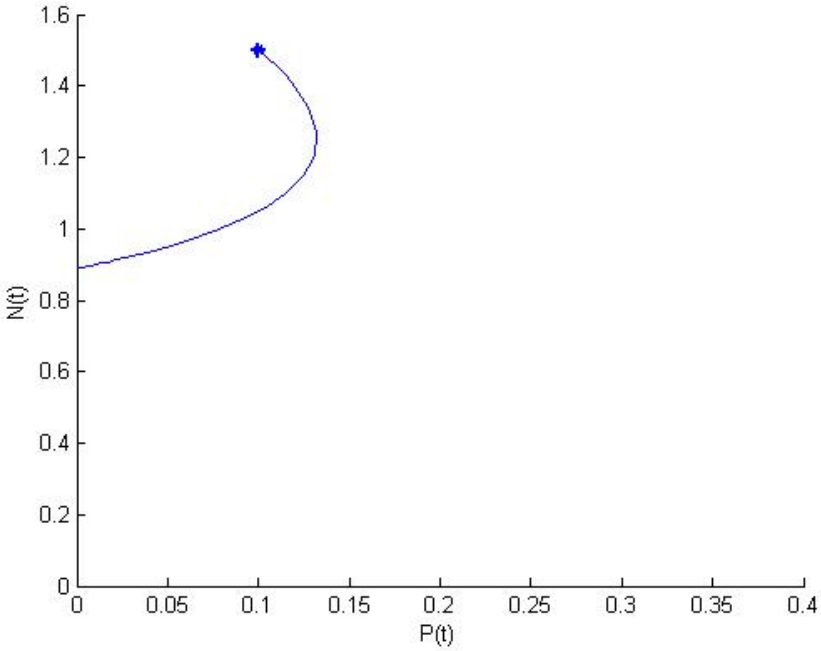

Figure 2.2: Phase trajectory of the model given in (2.5) with Michaelis-Menten growth rate (2.4). The initial value $P(0) = 0.1$ and $N(0) = 1.5$. The other parameters used are $c = 5$, $H_N = 5$, $m = 1$, and $\varepsilon = 0.5$.

contains terms for in-flows and out-flows. While this issue is not present in the spatially dependent models which necessarily have exchanges with the surroundings specified by the boundary conditions, in non-spatial models these exchanges need to be introduced to the models as additional terms. For this we turn our attention to a chemostat model.

2.1.2 Chemostat Model

The following model is adapted from [51]. Consider a well-stirred reactor that contains phytoplankton cells with concentration $P(t)$ and a limiting nutrient with concentration $N(t)$. The chemostat is supplied with the nutrient at an input concentration N_i from an external source. The out-flow contains both phytoplankton cells and the nutrient medium. Assume that the in-flow and out-flow are characterized by the dilution rate δ. The chemostat under

these assumptions is modeled by the following system of ordinary differential equations

$$\frac{dP}{dt} = \mu(N)P - (m+\delta)P$$

$$\frac{dN}{dt} = \delta(N_i - N) - \mu(N)P + \varepsilon m P, \tag{2.6}$$

with $0 < \varepsilon < 1$. The chemostat model is non-conservative since the quantity $S = N + P$ is not constant. However, unlike the previous non-conservative model given in (2.5), the chemostat model attains a stable non-trivial equilibrium. Indeed, when examining the phase portrait given in Figure 2.3, the phase trajectories spiral in the (P, N) plane to an isolated fixed point.

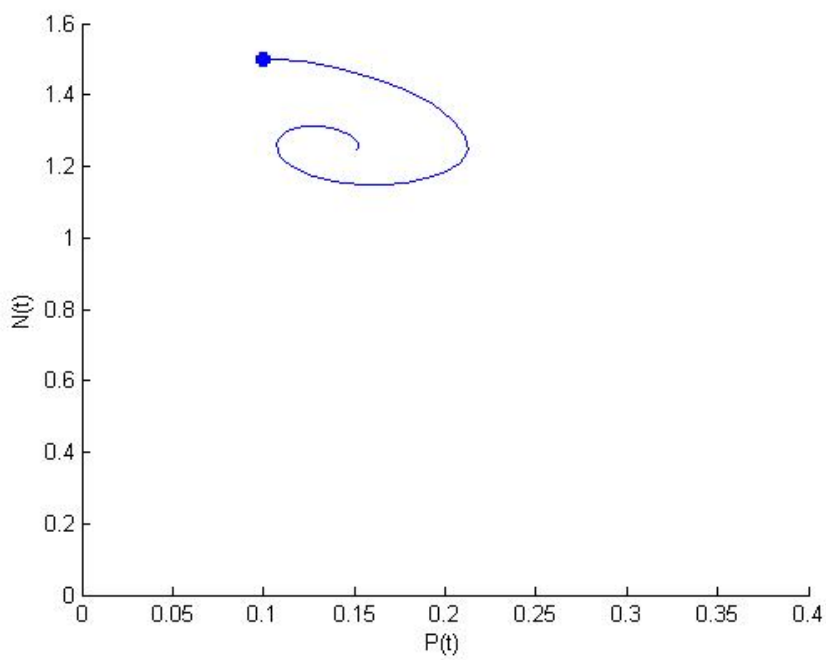

Figure 2.3: Phase trajectory of the model given (2.6) with Michaelis-Menten growth rate (2.4). The initial value $P(0) = 0.1$ and $N(0) = 1.5$ is marked by the closed circle. The other parameters used are $c = 5$, $H_N = 5$, $m = 1$, $\varepsilon = 0.5$, $N_i = 15$, and $\delta = 0.005$.

2.2 Spatial Models

The vertical distribution of phytoplankton in a water column has been the subject of numerous investigations [5],[7],[19],[24],[29],[35],[43]. Prominent vertical patterns observed include deep chlorophyll maxima (DCMs), benthic layers, and surface scums [35],[43]. Deep chlorophyll maxima is the layering phenomenon where biomass accumulation happens beneath the surface of the water column. Surface scums is the layering pattern where up to 90% of the biomass concentration is near the surface resulting in heavy shading of the water. Benthic layers are large biomass acccumulations that are near the sediment layer and often occur in stratified bodies of water. Stratification occurs due to temperature fluxes at the surface and advections within the body of water. The thickness of these layers is controlled by the degree of mixing and can vary from several centimetres to tens of meters [35]. These distributions affect primary production [38] and energy transfers in aquatic ecosystems and are affected by changing environment conditions and global warming [21].

Various mathematical models have been developed to describe the spatial and temporal dynamics of phytoplankton populations [7], [24], [35], [43], [47]. While certain models attribute the layering phenomenon to physical forces such as wind shear, or advections within the body of water and mixing processes, other models suggest that layer formation is due to phytoplankton competing in a stratified environment with non-homogeneous light and nutrient distributions in the vertical dimension. Light is never homogeneously distributed in aquatic environments since it forms a gradient over biomass and other light-absorbing substances [28], [29]. Further, continuous residence in the illuminated layers is neither necessary nor optimal for growth [54]. We restrict our attention to the model presented in [35] and a multi-species variant of that model.

2.2.1 Klausmeier and Litchman Model

The following is a model used to study vertical phytoplankton distributions by Klausmeier and Litchman in [35]. This model incorporates intra-specific competition for light and nutrients in a poorly mixed body of water. For simplifying purposes Klausmeier and Lichtman consider a one dimensional water column where the depth is indexed by z, where $0 \leq z \leq z_b$. The surface of the water column occurs at $z = 0$ and the bottom of the water column is given by z_b. The full model consists of equations for the depth distributions of biomass density, $b(z,t)$, nutrient concentration, $R(z,t)$, and light, $I(z,t)$.

Since light and nutrients form gradients throughout bodies of water, in order to model the change in biomass density it is necessary to know which factor is limiting phytoplankton growth. The functions $f_I(I(z,t))$ and $f_R(R(z,t))$ will be used to represent the phytoplankton growth rate when light and nutrients are limiting respectively. In general, the functions f_I and f_R need to be bounded, strictly increasing functions in I and R respectively. Following Liebig's law of the minimum, the gross phytoplankton growth rate is given by $\min(f_I(I), f_R(R))$. Biomass loss due to grazing, respiration, and death is given by a density and depth independent constant m. Combining these, we define the net per capita growth rate at depth z by $g(z,t) = \min(f_I(I(z,t)), f_R(R(z,t))) - m$.

To complete describing the dynamics of phytoplankton populations, phytoplankton movement needs to be incorporated. Phytoplankton movement is divided into two components: the first being passive movement due to turbulence in the water column and the second being the active movement. For simplicity, Klausmeier and Lichtman only consider phytoplankton species which rely on flagella to swim. Passive movement is modelled by eddy diffusion with diffusion coefficient D_b, which is uniform throughout the water column. This assumption is not necessary and, in general, depth dependent diffusion is permissible. To model the active movement, we introduce a velocity function ν which is dependent on the gradient of the growth rate, $\dfrac{\partial g}{\partial z}$, i.e., $\nu = \nu\left(\dfrac{\partial g}{\partial z}\right)$. Given how phytoplankton might regulate their position

depending on whether light or nutrients are limiting, the biological assumption is introduced that phytoplankton will move up if the conditions are better above than they are below, and phytoplankton will move down if the conditions are better below than they are above, and phytoplankton will not move if the conditions are worse above and below. Positive velocity is oriented upward and associated to the negative z direction. Specifically we assume $\nu(\cdot)$ is an odd, decreasing function which approaches a value ν_{max} as $\frac{\partial g}{\partial z}$ approaches negative infinity and approaches $-\nu_{max}$ as $\frac{\partial g}{\partial z}$ approaches positive infinity.

Combining physical and biological dynamics we can describe the change in phytoplankton biomass by the partial differential equation

$$\begin{aligned}\frac{\partial b}{\partial t} &= (\min(f_I(I), f_R(R)))b - mb + D_b\frac{\partial^2 b}{\partial z^2} + \frac{\partial}{\partial z}\left[\nu\left(\frac{\partial g}{\partial z}\right)b\right] \\ &= [\text{Growth}] - [\text{Loss}] + [\text{Passive Movement}] + [\text{Active Movement}]. \end{aligned} \tag{2.7}$$

Under the assumption that phytoplankton do not enter or leave the water column equation (2.7) has no flux boundary conditions

$$\left[-D_b\frac{\partial b}{\partial z} - \nu\left(\frac{\partial g}{\partial z}\right)b\right]\Bigg|_{z=0} = \left[-D_b\frac{\partial b}{\partial z} - \nu\left(\frac{\partial g}{\partial z}\right)b\right]\Bigg|_{z=z_b} = 0. \tag{2.8}$$

Nutrients in the water column are impacted by diffusion processes and by phytoplankton through consumption and recycling from dead phytoplankton. In [35], the nutrient under consideration is phosphorus due to its role as a limiting nutrient in aquatic ecosystems. Let D_R represent the diffusion coefficient and let ε represent the proportion of the nutrients from dead phytoplankton that is immediately recycled. Then we can describe the change in the nutrients by the partial differential equation

$$\begin{aligned}\frac{\partial R}{\partial t} &= -\frac{b}{Y}\min(f_I(I), f_R(R)) + D_R\frac{\partial^2 R}{\partial z^2} + \varepsilon m\frac{b}{Y} \\ &= -[\text{Uptake}] + [\text{Mixing}] + [\text{Recycling}] \end{aligned} \tag{2.9}$$

where Y is the yield of phytoplankton biomass per unit of nutrient consumed.

It is assumed that nutrients do not leave the system from the surface but are supplied at the bottom of the water column. Nutrients in the sediment are assumed to have constant concentration denoted by R_{in} and diffuse across the sediment-water interface at a rate proportional to the concentration difference at the interface. Under these assumptions we get the boundary conditions

$$\left.\frac{\partial R}{\partial z}\right|_{z=0} = 0, \ \left.\frac{\partial R}{\partial z}\right|_{z=z_b} = h(R_{in} - R(z_b)) \tag{2.10}$$

where the parameter h describes the permeability of the sediment-water interface.

Finally, light at depth z is determined using the Lambert-Beer law with phytoplankton attenuation coefficient a, background attenuation coefficient a_{bg}, and incident light I_{in}. Incident light is assumed to be constant throughout the model simulations, however this assumption can be relaxed to a time dependent function $I_{in}(t)$. Using this we have $I(z,t)$ is given by

$$I(z,t) = I_{in} \exp\left[-\int_0^z (ab(w,t) + a_{bg})dw \right]. \tag{2.11}$$

System (2.7) – (2.11) is a non-local, nonlinear system of integro-partial differential equations for which theoretical analysis has been conducted [11], [12], [13], [14], [25]. A summary of these analysis is presented at the end of this section.

To be able to implement the model, functional representations for f_I, f_R, and ν are needed. In [35] the functions f_I and f_R follow the Michaelis-Menten relation while the function ν is a step function given by $\nu = \nu_{max}$ for $\frac{\partial g}{\partial z} < 0$, $\nu = -\nu_{max}$ for $\frac{\partial g}{\partial z} > 0$, and $\nu = 0$ for $\frac{\partial g}{\partial z} = 0$. In [43] the following velocity function is considered

$$\nu\left(\frac{\partial g}{\partial z}\right) = -\nu_{max} \frac{\frac{\partial g}{\partial z}}{|\frac{\partial g}{\partial z}| + K_{swim}}. \tag{2.12}$$

For the simulations presented here we will be using the above formulation. Using the pa-

rameter values given in Table 2.1, sample model simulations are given in Figure 2.4. The numerical solution to this system uses a finite volume approach with a third-order upwinding scheme used on the advection term and a symmetric difference method for the diffusion terms [27]. For a more thorough description of the method see Chapter 3 Section 2. By altering key parameters distinct layering phenomenon can be exhibited.

Parameter	Explanation	Value	Source
N	Spatial discretization level	100	
z_b	Water column depth (m)	20	[35]
R_{in}	Sediment P concentration (μg P L^{-1})	100	[35]
h	Sediment-water column permeability (m^{-1})	10^{-2}	[35]
I_{in}	Incoming light (μmol photons m^{-2} s^{-1})	1,400	[35]
a_{bg}	Background attenuation coefficient (m^{-1})	0.35	[35], [36]
a	Algal attenuation coefficient (m^{-1} [cells ml^{-1}]$^{-1}$)	10^{-5}	[35], [36]
D_b	Eddy biomass diffusion coefficient (m^2 d^{-1})	10	[35]
D_R	Eddy nutrient diffusion coefficient (m^2 d^{-1})	10	[35]
ν_{max}	Species 1 swimming speed (m d^{-1})	10	[35]
r	Maximum growth rate (d^{-1})	0.4	[35]
m	Loss rate (d^{-1})	0.2	[35]
K_R	P half-saturation constant (μg P L^{-1})	1.0	[35]
K_I	Light half-saturation constant (μmol photons m^{-2} s^{-1})	50	[35]
Y	Yield coefficient (cells ml^{-1} [μg P L^{-1}]$^{-1}$)	10^3	[35]
ε	Recycling coefficient (dimensionless)	0	[43]
K_{swim}	Swimming constant (m^{-1} d^{-1})	0.001	[43]

Table 2.1: Parameters used in simulations unless otherwise noted.

With the parameter values given in Table 2.1 the resulting layer is a DCM. By altering parameters such as ε up to 0.9 and the parameters K_I and K_R to 100 and 0.1 respectively, the resulting equilibrium vertical distribution is a surface scum - the phenomenon where large biomass concentrations happen near the surface and as a result of shading, very little biomass is present in the lower layers. By altering the half-saturation constants K_I and K_R to 0.1 and 50 respectively and keeping $\varepsilon = 0.9$, the resulting equilibrium vertical distribution is a benthic layer - the phenomenon where large biomass concentrations happen near the sediment layer. These situations are illustrated in Figure 2.4 given below.

These layering phenomena that are exhibited are consistent with biological intuition. By

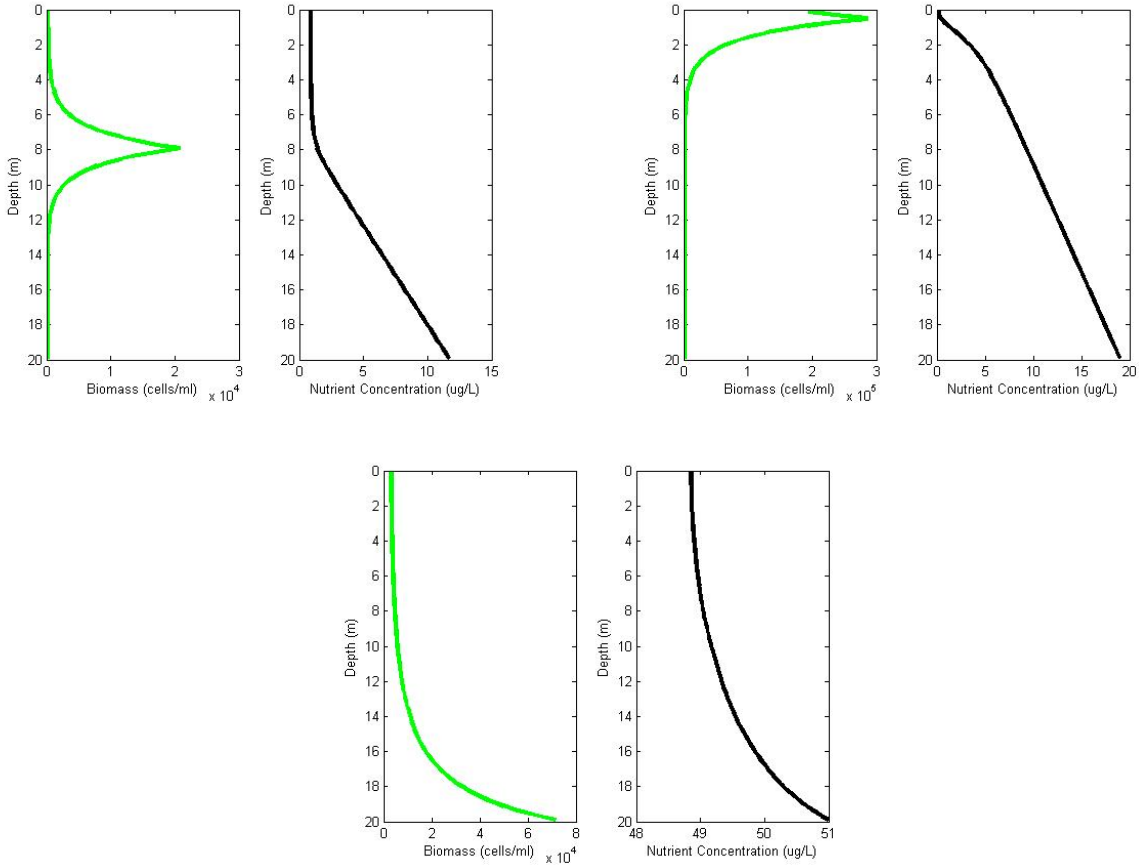

Figure 2.4: Equilibrium vertical distributions of phytoplankton biomass and nutrients determined from System (2.7) – (2.11). The top left represents the DCM distribution, the top right represents the surface scum distribution, and the bottom represents the benthic layer distribution.

altering the half-saturation constants, the resource dependence on light and free nutrient is altered, and by altering the recycling coefficient ε, we are changing the amount of free nutrient released upon cell death that can be utilized by phytoplankton. Thus, when simulating the surface scum, the parameters were altered in such a way that the phytoplankton species had a large light preference, and upon cell death, a large proportion of the nutrient in the cell was assumed to be available for re-uptake by living cells. In comparison, when simulating the surface scum, the preference was switched so that the phytoplankton species had a proportinally larger nutrient presence which is why the layering happened near the sediment layer - the natural source of nutrient in the environment. The ability of this model to replicate

multiple layering phenomenon seen in nature as well being able to define parameters values that are unique to both freshwater and marine environments gives this model a wide range of latitude in practical applications.

The model simulations shown here result from running the model to numerical equilibrium. The existence of positive steady state solutions and asymptotic behavior is established in [11] and [12] respectively. Analysis of similar reaction-diffusion equations and reaction-diffusion advection equations is given in [13], [14], and [25]. A brief summary of their work follows.

The Steady State Solutions

In [11], the problem

$$\begin{cases} -[d_1 u_x + \sigma c(x) u]_x = [g(x) - m]u, & 0 < x < 1, \\ -d_2 v_{xx} = -g(x)u, & 0 < x < 1, \\ d_1 u_x + \sigma c(x) u = 0, & x = 0, 1, \\ v_x(0) = 0, v_x(1) = \beta[v_0 - v(1)], \end{cases} \tag{2.13}$$

is considered where d_1, d_2, m, v_0 and β are positive constants, $g(x) = f(\min\{\alpha v(x), w(x)\})$, $f(s) = \dfrac{rs}{K_I + s}$, and

$$w(x) = w_0 \exp\left[- A_0 x - A \int_0^x u(s) ds \right],$$

with α, r, K_I, A, and A_0 are positive constants. The positive function $c(x)$ is determined by v and w and is defined by

$$c(x) = c_{v,w}(x) = \frac{x - x_0}{\delta + |x - x_0|},$$

where $\delta > 0$ is a small constant and $x_0 \in [0, 1]$ is determined by $\min\{\alpha v(x), w(x)\} = \alpha v(x)$ $\forall x \in [0, x_0)$ and $\min\{\alpha v(x), w(x)\} = w(x)$ $\forall x \in (x_0, 1]$. Note that the function c

is meant to serve as a continuous approximation to the step function used in [35]. The dependence of c on v and w makes this a special quasi-linear problem.

This problem relates to the Klausmeier and Litchman model by using the following normalization and parameter definitions. We normalize the functions given in (2.7), (2.9) and (2.11) by defining $u(x) = b(z_b x)$, $v(x) = R(z_b x)$, and $w(x) = I(z_b x)$ for $0 \leq x \leq 1$. Then define $d_1 = z_b^{-2} D_b$, $d_2 = z_b^{-2} D_R$, $\sigma = \nu_{max} z_b^{-1}$, $A = a z_b Y$, $A_0 = a_{bg} z_b$, $\alpha = K_I K_R^{-1}$, $\beta = h z_b$, $v_0 = R_{in}$, $w_0 = I_{in}$, and $x_0 = z_0 z_b^{-1}$. Finally, by letting $b_t = 0$ and $R_t = 0$, the problem posed in (2.13) is derived. The main results of the analysis done in [11] are as follows.

Proposition 2.2.1. *Fix $\gamma \in (0,1)$ and set $K = \{\phi \in C^{1,\gamma}([0,1]) : \phi$ is nondecreasing in $[0,1]\}$ and $P = \{\phi \in C^{1,\gamma}([0,1]) : \phi$ is nonnegative in $[0,1]\}$. For given $(u,v) \in P \times K$ and $m \geq 0$, define*

$$w = w_0 \exp\left[-A_0 x - A \int_0^x u(s) d(s) \right],$$

$$c(x) = c_{v,w}(x), v_+ = \max\{v, 0\}.$$

Define an abstract operator T(m,u,v) such that T(m,u,v) = (u,v) for $(u,v) \in P \times K$ if and only if (u,v) is a nonnegative solution of (2.13). The operator $T : [0,\infty) \times P \times K \to P \times K$ is completely continuous, and it is Fréchet differentiable at $(m, 0, v_0)$ with respect to (u,v) in the convex set $P \times K$, with derivative operator L_m, where $L_m = (\xi, \eta)$ is the unique solution to the following linear problems:

$$\begin{cases} -(d_1 \xi' + \sigma c^0 \xi)' + (m+1)\xi = f(\min\{\alpha v_0, w_*\})u + u & 0 < x < 1, \\ d_1 \xi' + \sigma c^0 \xi = 0 & x = 0, 1, \end{cases}$$

and

$$\begin{cases} -d_2 \eta'' = -f(\min\{\alpha v_0, w_*\})u & 0 < x < 1, \\ \eta'(0) = 0, \ \eta'(1) + \beta \eta(1) = 0, \end{cases}$$

where $c^0(x) = c_{v_0,w_*}(x)$ *and* $w_* = w_0 \exp(-A_0 x)$. *Moreover,* $(u,v) = T(m,u,v)$ *implies that* $v \in P$ *and (u,v) is a nonnegative solution of* (2.13) *if and only if* $(u,v) = T(m,u,v)$.

Theorem 2.2.2. *For every* $m \in (0, m_*)$ *problem* (2.13) *has at least one positive solution. Moreover, if* m_n *decreases to* 0 *and* (u_n, v_n) *is a positive solution of* (2.13) *with* $m = m_n$, *then* $u_n \to \infty$ *uniformly in* $[0,1]$ *and there exists a unique* $\tau \in \left(0, \dfrac{v_0}{1+\beta^{-1}}\right)$ *determined by*

$$d_2\tau = f(w_0 \exp(-A\sigma_i\tau))\sigma_\tau + \int_{\sigma_\tau}^{\infty} f(w_0 \exp(-Ay))dy$$

such that

$$\frac{u_n(x)}{||u_n||_\infty} \to \left(1 + \frac{x}{\delta}\right)^{\frac{\sigma}{d_1}\delta} \exp\left(-\frac{\sigma}{d_1}x\right), \ v_n(x) \to \tau x + v_0 - \tau(1+\beta^{-1})$$

uniformly in $[0,1]$. *Furthermore, for each* $m \in (0, m_*)$, *there is a positive solution (m,u,v) lying on the global bifurcation branch,* $\Gamma = \{(m,u,v)\} \subset (0,\infty) \times C^{1,\gamma}([0,1]) \times C^{1,\gamma}([0,1])$, *bifurcating from the trivial solution branch* $\Gamma_0 = \{(m,0,v_0) : m \in (-\infty,\infty)\}$ *at* $m = m_*$.

Theorem 2.2.3. *Let* m_* *be defined as above and define* $m^* = -\inf_{x_0 \in [0,1]} \lambda_1(c(x), v_0, w_*)$. *Then*

$$\lim_{\sigma\to\infty} m_*(\sigma) = \lim_{\sigma\to\infty} m^*(\sigma) = f(\min\{\alpha v_0, w_0\}).$$

The analysis done in [12] continues the above work and shows the existence of four critical values $v_{**} < v_* < v^* < v^{**}$ for v_0 - the nutrient concentration in the sediment layer, such that

(i) $x_* = 0$ when $v_0 \geq v^*$, $x_* \in (0,1)$ when $v_0 \in (v_*, v^*)$, and $x_* = 1$ when $v_0 \leq v_*$.

(ii) The total biomass increases with v_0 in the range $v_{**} < v_0 < v^{**}$, but it is constant for $v_0 \geq v^{**}$ or $v_0 \leq v**$. This is under the assumption that v_0 is above a certain threshold level so that biomass can survive.

In [13] the analytic properties of the reaction-diffusion problem with light limitation for a single phytoplankton species is studied. That work is extended in [14] to show that with the inclusion of variable sinking rates, the global dynamics of the model is completely determined by its unique steady-state solution. In [25] the analysis of a nonlocal reaction-diffusion-advection equation modeling the growth of a single phytoplankton species in a water column where the species solely depends on light is analyzed for the existence and uniqueness of positive steady states.

2.2.2 Multi-species Klausmeier and Litchman Model

The previous model can be adapted for the presence of multiple algal species. In general, if N species are present then the following changes to the Klausmeier and Litchman model need to be considered. The same assumptions of biomass growth and movement are kept but are now extended for the presence of N species by allowing for species specific growth, death, diffusion, and active movement. The resulting partial differential equations are given by

$$\begin{aligned}\frac{\partial b_k}{\partial t} &= \min(f_{I,k}(I), f_{R,k}(R))b_1 - m_k b_k + D_{b_k}\frac{\partial^2 b_k}{\partial z^2} + \frac{\partial}{\partial z}\Big[\nu_k\Big(\frac{\partial g_k}{\partial z}\Big)b_k\Big] \\ &= [\text{Growth}] - [\text{Loss}] + [\text{Passive movement}] + [\text{Active movement}] \end{aligned} \tag{2.14}$$

for $k = 1, \ldots, N$. These partial differential equations are given no flux boundary conditions

$$\left[-D_{b_k}\frac{\partial b_k}{\partial z} - \nu_k\left(\frac{\partial g_k}{\partial z}\right)b_k\right]\Bigg|_{z=0} = \left[-D_{b_k}\frac{\partial b_k}{\partial z} - \nu_k\left(\frac{\partial g_k}{\partial z}\right)b_k\right]\Bigg|_{z=z_b} = 0. \tag{2.15}$$

For computational purposes, the functions $f_{I,k}$ and $f_{R,k}$ for $k = 1, \ldots, N$ will take the

Michaelis-Menten form given by

$$f_{I,k}(I(z,t)) = r_k \, \frac{I(z,t)}{I(z,t) + K_{I,k}}, \tag{2.16}$$

and

$$f_{R,k}(R(z,t)) = r_k \, \frac{R(z,t)}{R(z,t) + K_{R,k}}, \tag{2.17}$$

where r_k represents the maximal growth rates of species k and the parameters $K_{I,k}$ and $K_{R,k}$ represent half-saturation constants for light and nutrients for species k. Following [43], the function ν_k will take the form

$$\nu_k\Big(\frac{\partial g_k}{\partial z}\Big) = -\nu_{k_{max}} \, \frac{\frac{\partial g_k}{\partial z}}{|\frac{\partial g_k}{\partial z}| + K_{swim}}. \tag{2.18}$$

Following the conventions of the single species model, let D_R represent the diffusion coefficient of the limiting nutrient and let ε_k represent the proportion of nutrients that are available in the water column from dead phytoplankton by species. The rate of change in the limiting nutrient R is given by the partial differential equation

$$\begin{aligned} \frac{\partial R}{\partial t} &= \sum_{k=1}^{N} \left(-\frac{b_k}{Y_k} \min(f_{I,k}(I), f_{R,k}(R)) + \varepsilon_k \, \frac{b_k}{Y_k} \right) + D_R \, \frac{\partial^2 R}{\partial z^2} \\ &= -[\text{Species } k \text{ Uptake}] + [\text{Species } k \text{ Recycling}] + [\text{Mixing}] \end{aligned} \tag{2.19}$$

where Y_k are the yield of phytoplankton biomass per unit of nutrient consumed for each species respectively. As before, this partial differential equation will have boundary conditions given by

$$\left.\frac{\partial R}{\partial z}\right|_{z=0} = 0, \; \left.\frac{\partial R}{\partial z}\right|_{z=z_b} = h(R_{in} - R(z_b)), \tag{2.20}$$

where the parameter h describes the permeability of the sediment-water interface.

Finally, with phytoplankton attenuation coefficients a_k, background attenuation coefficient a_{bg}, and incident light I_{in}, to describe the change in light at depth z, we modify the

Lambert-Beer law to accommodate the presence of multiple phytoplankton species. We have

$$I(z,t) = I_{in} \exp\left[-\int_0^z \left(\sum_{k=1}^{N} a_k b_k(w,t) + a_{bg} \right) dw \right]. \tag{2.21}$$

The incident light here is assumed to be constant, although this assumption can be relaxed to make the incident light a function of time. Throughout the dissertation, we will be considering the case when $N = 2$.

Parameter	Explanation	Value	Source
N	Spatial discretization level	100	
z_b	Water column depth (m)	20	[35]
R_{in}	Sediment P concentration (μg P L^{-1})	100	[35]
h	Sediment-water column permeability (m^{-1})	10^{-2}	[35]
I_{in}	Incoming light (μmol photons m^{-2} s^{-1})	1,400	[35]
a_{bg}	Background attenuation coefficient (m^{-1})	0.35	[35], [36]
a_1	Species 1 algal attenuation coefficient (m^{-1} [cells ml^{-1}]$^{-1}$)	10^{-5}	[35], [36]
a_2	Species 2 algal attenuation coefficient (m^{-1} [cells ml^{-1}]$^{-1}$)	10^{-5}	[35], [36]
D_{b_1}	Species 1 biomass diffusion coefficients (m^2 d^{-1})	10	[35]
D_{b_2}	Species 2 biomass diffusion coefficients (m^2 d^{-1})	10	[35]
D_R	Nutrient diffusion coefficient (m^2 d^{-1})	10	[35]
$\nu_{1_{max}}$	Species 1 swimming speed (m d^{-1})	10	[35]
$\nu_{2_{max}}$	Species 2 swimming speed (m d^{-1})	10	[35]
r_1	Species 1 maximum growth rates (d^{-1})	0.4	[35]
r_2	Species 2 maximum growth rates (d^{-1})	0.4	[35]
m_1	Species 1 loss rate (d^{-1})	0.2	[35]
m_2	Species 2 loss rate (d^{-1})	0.1	
$K_{R,1}$	P half-saturation constant (μg P L^{-1})	1	[35]
$K_{R,2}$	P half-saturation constant (μg P L^{-1})	10	
$K_{I,1}$	Light half-saturation constant (μmol photons m^{-2} s^{-1})	50	[35]
$K_{I,2}$	Light half-saturation constant (μmol photons m^{-2} s^{-1})	5	
Y_1	Species 1 yield coefficient (cells ml^{-1} [μg P L^{-1}]$^{-1}$)	10^3	[35]
Y_2	Species 2 yield coefficient (cells ml^{-1} [μg P L^{-1}]$^{-1}$)	10^3	[35]
ε_1	Species 1 recycling coefficient (dimensionless)	0	[43]
ε_2	Species 2 recycling coefficient (dimensionless)	0	[43]
K_{swim}	Swimming constant (m^{-1} d^{-1})	0.001	[43]

Table 2.2: Parameters used in simulations unless otherwise noted.

The case of $N = 2$ is of particular concern since it allows for the development and analysis of a mathematical framework for the theory of competition and modes of coexistence between multiple phytoplankton species. Theoretical analysis of a similar reaction-diffusion model in the case when $N = 2$ has considered in [13] under the hypothesis of light limitation only. Based on the work done in [14] the bistable behavior exhibited in [52] can only occur with the assumption of nutrient limitation as well.

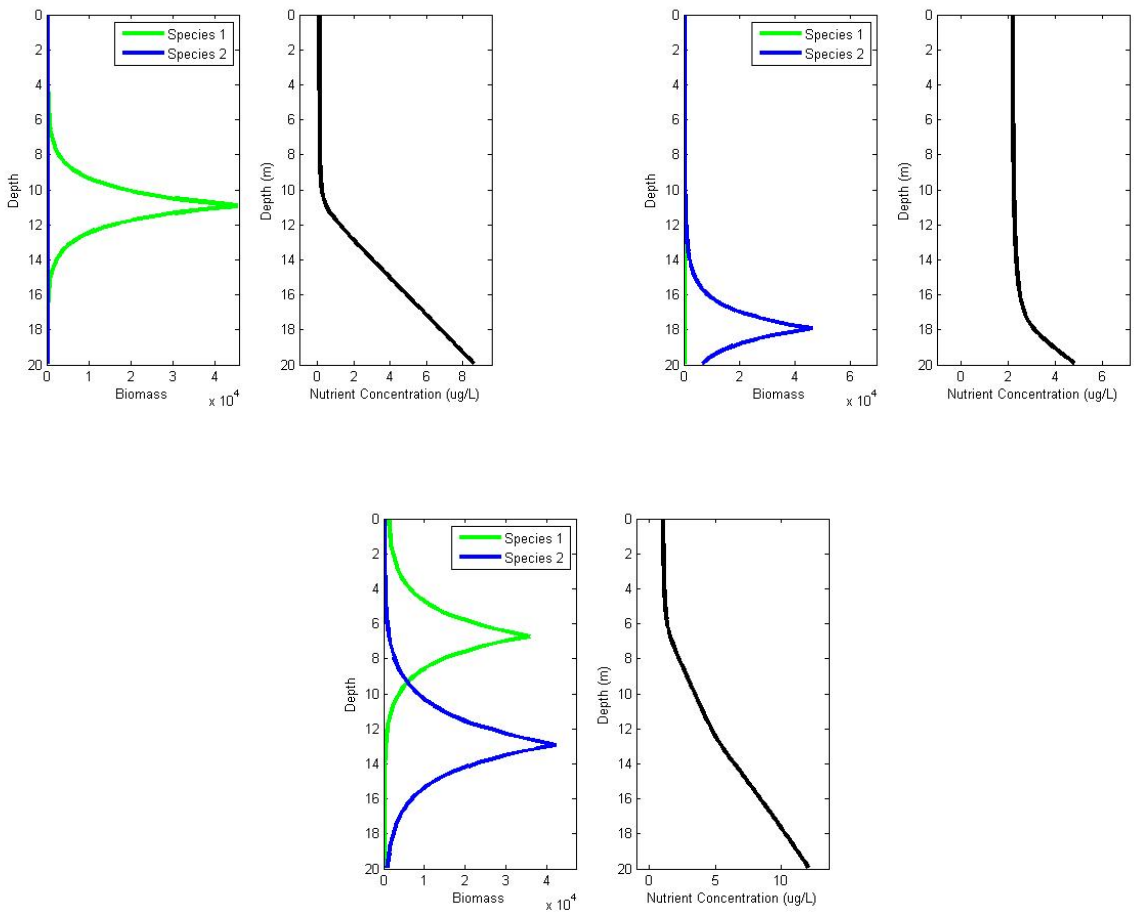

Figure 2.5: Equilibrium vertical distributions of phytoplankton biomass and nutrients determined from Equations (2.14) – (2.21). The top left represents the case when Species 1 out competes Species 2, the top right represents the case when Species 2 out competes Species 1, and the bottom represents the case of bistability between the two species resulting in coexistence.

Sample model simulations using the parameter values given in Table 2.2 are given above. This model has the same ability to replicate multiple layering phenomena as the single species

model was able to capture. The advantage to considering multi-species models over the single species version is the ability to investigate biological questions of how multiple phytoplankton species are able to coexist. By altering certain parameters, there are two distinct outcomes that occur. The first scenario is competitive exclusion. This occurs when one species is able to out compete with the other resulting in one of the competitors becoming extinct. Examining Figure 2.5 these scenarios are illustrated in the top left and top right. This was accomplished by setting the mortality coefficients m_1 and m_2 to be equal and making the winner have a growth rate of 0.5 while the loser had a lower growth rate of 0.1. The second scenario that can occur is coexistence. This is illustrated in the bottom panel of Figure 2.5. This was accomplished by using the parameter values assigned in Table 2.2 and changing the parameters $\nu_{1_{max}} = 7$, $\nu_{2_{max}} = 6$, and $\varepsilon_1 = \varepsilon_2 = 0.75$.

While the multi-species model is able to explore more complex questions of ecosystem structure than the single species version, the model does not account for other complexities that arise. In particular, the models described assume that there is only one nutrient present in the system which is limiting growth and that the phytoplankton only utilize this resource for growth. This is an idealized situation and the biogeochemical interactions that phytoplankton have with their environment are complex [49]. As an example, the species *Mycrocistis* which forms toxic blooms, prefers to acquire nitrogen from ammonia rather than nitrate [7], both of which are available in the environment. Models incorporating preferential nutrient uptake have yet to be considered and analyzed. We propose a new phytoplankton competition model which incorporates this nutrient dynamic and present numerical illustrations of how this model compares to previous models in the literature.

3 Proposed Preferential Nutrient Uptake Model

It is generally understood that the rate of nitrate (NO_3^-) uptake by phytoplankton is severely reduced by the presence of ammonium (NH_4^+). This effect is referred to either as 'inhibition' of nitrate uptake by ammonium or by 'preference' for ammonium [10]. Work done to support this theory can be found in [10], [40], [44], [60], and others. Evidence includes both laboratory studies of nitrate assimilation by green algae [44], field studies in marine ecosystems, and theoretical considerations [40], [60]. The existing theoretical considerations made to support the preference for ammonium over nitrate are a result of the energy requirements needed to utilize both resources. While nitrate and ammonium are both available in the environment and are susceptible to diffusion processes, there is an eight electron difference in the utilization of ammonium over nitrate [19]. In order for nitrate to be utilized by phytoplankton it must undergo two chemical reactions summarized below:

$$NO_3^- \xrightarrow[\text{NR}]{2e^-} NO_2^- \xrightarrow[\text{NiR}]{6e^-} NH_4^+$$

The first reaction involves the enzyme nitrate reductase (NR) which costs two electrons and reduces nitrate to nitrite (NO_{2^-}). The second reaction involves the enzyme nitrite reductase (NiR) which costs six electrons and reduces nitrite to ammonium. However, further work has shown that the nitrate-ammonium relationship is in fact difficult to explain by one simple mechanism and that both inhibition (an indirect interaction) and preference (a direct interaction) can be observed [8], [10]. These interactions can vary across environmental conditions and phytoplankton species but can be tested for separately in laboratory settings. Until the process of nitrate uptake is fully understood, it is not possible to accurately model the response of nitrate uptake to environmental conditions or to model its relationship to biomass productivity [10]. This is especially important for the development of models of harmful algal blooms, a matter of significant public health importance, and one of great interest to biologists, government officials, and aquatic based industries.

In this chapter we first introduce a new model of phytoplankton competition which incorporates preferential nutrient uptake. We then give a detailed explanation of the numerical methods used to simulate the model. Finally, we conduct several simulations of this new model to examine the layer formation patterns that are exhibited along with competitive outcomes by altering certain model parameters. These simulations will be analyzed for their biological significance and compared to existing models in the literature. In particular, simulated phytoplankton distributions will be compared to data from Lake Michigan presented in [5], [6], and [45].

3.1 Model Development

The proposed model studies the coexistence of two phytoplankton species, b_1 and b_2, in a water column where there are two nutrients, R_1 and R_2, present with the assumption that one nutrient is preferentially taken up. Without loss of generality, it is assumed that R_1 is the preferred nutrient. The full model consists of a non-local, nonlinear system of integro-partial differential equations for the depth distributions of biomass densities $b_1(z,t)$ and $b_2(z,t)$, the limiting nutrient concentrations $R_1(z,t)$ and $R_2(z,t)$, and light $I(z,t)$. For simplifying purposes we consider a one dimensional water column index by z, where $0 \leq z \leq z_b$ where $z = 0$ represents the surface and $z = z_b$ represents the depth of the water column. We further assume that the water column is not stratified.

Biomass densities are assumed to be limited by the availability of light and nutrients. The functions $f_{I,1}(I(z,t))$ and $f_{I,2}(I(z,t))$ will represent the phytoplankton growth rate when light is limiting for species 1 and species 2, respectively, while the functions $f_{R,1}(R_1(z,t), R_2(z,t))$ and $f_{R,2}(R_1(z,t), R_2(z,t))$ represent the phytoplankton growth rate when nutrients are limiting for species 1 and 2, respectively. The gross phytoplankton growth rate of each species follows the Liebig law of the minimum so that the per-capita growth rate will be given by the equations $g_k(z,t) = \min[f_{I,k}(I(z,t)), f_{R,k}(R_1(z,t), R_2(z,t))] - m_k$, where m_k is the loss rate, and the index $k = 1, 2$ represents the respective species.

Each phytoplankton species is assumed to move within the water column. Their movement is affected by the processes of diffusion and active movement. Passive movement is modeled by eddy diffusion with diffusion coefficients D_{b_1} and D_{b_2} which are assumed to be uniform throughout the water column. This assumption is not necessary and, in general, depth dependent diffusion is permissible [27], [43]. To model the active movement, we introduce a velocity function ν which is dependent on the gradient of the growth rate, $\frac{\partial g_k}{\partial z}$, i.e. $\nu = \nu_k\left(\frac{\partial g_k}{\partial z}\right)$ for $k = 1, 2$ [46]. Given how phytoplankton can regulate their position, to an extent, depending on whether light or nutrients are limiting, the biological assumption is introduced that phytoplankton will move up if the conditions are better above than they are below, and phytoplankton will move down if the conditions are better below than they are above, and phytoplankton will not move if the conditions are worse above and below [35]. Positive velocity is oriented upward and associated to the negative z direction. Specifically we assume $\nu(\cdot)$ is an odd, decreasing function which approaches a value $\nu_{k_{max}}$ as $\frac{\partial g_k}{\partial z}$ approaches negative infinity and approaches $-\nu_{k_{max}}$ as $\frac{\partial g_k}{\partial z}$ approaches positive infinity for $k = 1, 2$ [33] [35],[43],[46].

The resulting partial differential equations for biomass densities are given by

$$\begin{aligned}\frac{\partial b_1}{\partial t} &= \min(f_{I,1}(I), f_{R,1}(R_1, R_2))b_1 - m_1 b_1 + D_{b_1}\frac{\partial^2 b_1}{\partial z^2} + \frac{\partial}{\partial z}\Big[\nu_1\Big(\frac{\partial g_1}{\partial z}\Big)b_1\Big] \\ &= [\text{Growth}] - [\text{Loss}] + [\text{Passive movement}] + [\text{Active movement}] \qquad (3.1)\end{aligned}$$

and

$$\begin{aligned}\frac{\partial b_2}{\partial t} &= \min(f_{I,2}(I), f_{R,2}(R_1, R_2))b_2 - m_2 b_2 + D_{b_2}\frac{\partial^2 b_2}{\partial z^2} + \frac{\partial}{\partial z}\Big[\nu_2\Big(\frac{\partial g_2}{\partial z}\Big)b_2\Big] \\ &= [\text{Growth}] - [\text{Loss}] + [\text{Passive movement}] + [\text{Active movement}]. \qquad (3.2)\end{aligned}$$

These partial differential equations are given no flux boundary conditions

$$\left[D_{b_1}\frac{\partial b_1}{\partial z}+\nu_1\left(\frac{\partial g_1}{\partial z}\right)b_1\right]\Bigg|_{z=0}=\left[D_{b_1}\frac{\partial b_1}{\partial z}+\nu_1\left(\frac{\partial g_1}{\partial z}\right)b_1\right]\Bigg|_{z=z_b}=0, \tag{3.3}$$

and

$$\left[D_{b_2}\frac{\partial g_2}{\partial z}+\nu_2\left(\frac{\partial g_2}{\partial z}\right)b_2\right]\Bigg|_{z=0}=\left[D_{b_2}\frac{\partial g_2}{\partial z}+\nu_2\left(\frac{\partial g_2}{\partial z}\right)b_2\right]\Bigg|_{z=z_b}=0. \tag{3.4}$$

The functions $f_{R,1}(R_1,R_2)$ and $f_{R,2}(R_1,R_2)$ used to model the inhibition of the uptake of the second nutrient R_2 by the presence of the first nutrient R_1 take the form of a modified Michaelis-Menten relation given by

$$f_{R,1}(R_1(z,t),R_2(z,t))=r_1\left(\frac{R_1(z,t)}{K_{R_1,1}+R_1(z,t)}+\frac{R_2(z,t)}{K_{R_2,1}+R_2(z,t)}\,\frac{\lambda^n}{\lambda^n+R_1(z,t)}\right) \tag{3.5}$$

and

$$f_{R,2}(R_1(z,t),R_2(z,t))=r_2\left(\frac{R_1(z,t)}{K_{R_1,2}+R_1(z,t)}+\frac{R_2(z,t)}{K_{R_2,2}+R_2(z,t)}\,\frac{\lambda^n}{\lambda^n+R_1(z,t)}\right), \tag{3.6}$$

where r_1 and r_2 are the maximal growth rate of species 1 and species 2, respectively, and the parameters $K_{R_1,1}$ and $K_{R_2,1}$ represent the saturation constants for species 1 with the corresponding nutrient, the parameters $K_{R_1,2}$ and $K_{R_2,2}$ represent the saturation constants for species 2 with the corresponding nutrient, $K_{I,1}$ and $K_{I,2}$ represent the light saturation constants for species 1 and 2 respectively, and λ is an inhibition coefficient. Following [32] the functions $f_{I,k}$ for $k=1,2$ are hyperbolic tangent functions of the form

$$f_{I,1}(I(z,t))=r_1\tanh\left(\frac{I(z,t)}{K_{I,1}}\right), \tag{3.7}$$

and

$$f_{I,2}(I(z,t))=r_2\tanh\left(\frac{I(z,t)}{K_{I,2}}\right). \tag{3.8}$$

The use of hyperbolic tangent functions over the classic Michaelis-Menten relation is due to better results from regression analysis on experimental data [32].

As in [43], the active movement functions ν_1 and ν_2 take the form

$$\nu_1\Big(\frac{\partial g_1}{\partial z}\Big) = -\nu_{1_{max}} \frac{\frac{\partial g_1}{\partial z}}{|\frac{\partial g_1}{\partial z}| + K_{swim}} \tag{3.9}$$

and

$$\nu_2\Big(\frac{\partial g_2}{\partial z}\Big) = -\nu_{2_{max}} \frac{\frac{\partial g_2}{\partial z}}{|\frac{\partial g_2}{\partial z}| + K_{swim}}. \tag{3.10}$$

Nutrients in the water column are impacted by diffusion processes and by phytoplankton through consumption and recycling. Let D_{R_1} and D_{R_2} represent the diffusion coefficients of the two nutrients, respectively, and let $\varepsilon_{1,1}$, $\varepsilon_{2,1}$, $\varepsilon_{1,2}$, and $\varepsilon_{2,2}$ represent the proportion of nutrients that are available in the water column from dead phytoplankton where the indexing on the recycling coefficients is done in the order of species, nutrient. Since both species use both nutrients to grow, it is necessary to determine the proportion of each nutrient lost to uptake processes. Define the functions γ and ρ by

$$\gamma_k(R_1) = r_k \frac{R_1}{K_{R_1,k} + R_1} \tag{3.11}$$

and

$$\rho_k(R_1, R_2) = r_k \frac{R_2}{K_{R_2,k} + R_2} \frac{\lambda^n}{\lambda^n + R_1} \tag{3.12}$$

for $k = 1, 2$. These functions will be used to give the appropriate proportion of each nutrient uptaken by each species. Using these modifications and the physical and biological assumptions consistent with the multi-species Klausmeier and Litchman model, the partial

differential equations for the nutrients are given by

$$\begin{aligned}\frac{\partial R_1}{\partial t} =& -\frac{b_1}{Y_1}\min(f_{I,1}(I), f_{R,1}(R_1,R_2))\,\frac{\gamma_1(R_1)}{f_{R,1}(R_1,R_2)} + \varepsilon_{1,1}m_1\,\frac{b_1}{Y_1}\\ &-\frac{b_2}{Y_2}\min(f_{I,2}(I), f_{R,2}(R_1,R_2))\,\frac{\gamma_2(R_1)}{f_{R,2}(R_1,R_2)} + \varepsilon_{2,1}m_2\,\frac{b_2}{Y_2}\\ &+ D_{R_1}\frac{\partial^2 R_1}{\partial z^2}\\ &= -[\text{Species 1 Uptake}] + [\text{Species 1 Recycling}] - [\text{Species 2 Uptake}]\\ &+ [\text{Species 2 Recycling}] + [\text{Mixing}]\end{aligned} \tag{3.13}$$

and

$$\begin{aligned}\frac{\partial R_2}{\partial t} =& -\frac{b_1}{Y_1}\min(f_{I,1}(I), f_{R,1}(R_1,R_2))\,\frac{\rho_1(R_1,R_2)}{f_{R,1}(R_1,R_2)} + \varepsilon_{1,2}m_1\,\frac{b_1}{Y_1}\\ &-\frac{b_2}{Y_2}\min(f_{I,2}(I), f_{R,2}(R_1,R_2))\,\frac{\rho_2(R_1,R_2)}{f_{R,2}(R_1,R_2)} + \varepsilon_{2,2}m_2\,\frac{b_2}{Y_2}\\ &+ D_{R_2}\frac{\partial^2 R_2}{\partial z^2}\\ &= -[\text{Species 1 Uptake}] + [\text{Species 1 Recycling}] - [\text{Species 2 Uptake}]\\ &+ [\text{Species 2 Recycling}] + [\text{Mixing}].\end{aligned} \tag{3.14}$$

For boundary conditions on the nutrient equations, assume that nutrients cannot enter or leave the water column from the surface, and that both nutrients are supplied from the bottom. Assume nutrients in the sediment have a constant concentration. Let the concentration of nutrient 1 in the sediment be denoted by R_{in_1} and let the concentration of nutrient 2 in the sediment be denoted by R_{in_2}. Then the boundary conditions for equations (3.13) and

(3.14) are given respectively by

$$\left.\frac{\partial R_1}{\partial z}\right|_{z=0} = 0, \ \left.\frac{\partial R_1}{\partial z}\right|_{z=z_b} = h(R_{in_1} - R_1(z_b)) \tag{3.15}$$

and

$$\left.\frac{\partial R_2}{\partial z}\right|_{z=0} = 0, \ \left.\frac{\partial R_2}{\partial z}\right|_{z=z_b} = h(R_{in_2} - R_2(z_b)), \tag{3.16}$$

where h represents the permeability of the sediment-water interface.

Finally, to describe the change in light at depth z, we modify the Lambert-Beer law to accommodate the presence of multiple phytoplankton species. The Lambert-Beer law becomes

$$I(z,t) = I_{in} \exp\left[-\int_0^z (a_1 b_1(w,t) + a_2 b_2(w,t) + a_{bg}) dw \right], \tag{3.17}$$

where the parameters I_{in}, a_1, a_2 and a_{bg} represent the incident light, species specific light attenuation coefficients, and background attenuation coefficient, respectively [34]. The incident light is considered to be constant in our simulations, although this assumption can be relaxed to admit a time dependent function $I_{in}(t)$. This model is based on [35] with the addition of another phytoplankton species, the competition for two nutrient resources, one of which is assumed to be preferred, and light dependence on growth functions consistent with experimental results.

3.2 Simulation Technique

In order to simulate the model, we use a finite volume method [27]. Under this approach the spatial differential operators given in equations (3.1), (3.2), (3.13), and (3.14) as well as the integral term given in equation (3.17) will be replaced by discrete approximations. This will result in a large system of ordinary differential equations of the form

$$\frac{d\mathbf{b}(t)}{dt} = \mathbf{F}(\mathbf{b}(t)), \ t \geq 0 \tag{3.18}$$

where the vector $\mathbf{b} \in \mathbb{R}^{4N}$ contains the components $b_i(t)$ and $R_i(t)$ resulting from the discretization. Since (3.18) is still continuous in time the resulting system of ODEs are solved by numerical integration. The ODE model given in (3.18) is generally stiff, thus to solve the system numerically, an implicit integration method is needed. In this treatment, we implemented the model in MATLAB, and integrated using MATLAB's ODE solver ode15s [2].

To begin we define a spatial grid on the one dimensional water column $0 \leq z \leq z_b$. Let $s_0 = 0$, $s_i = \left(i - \frac{1}{2}\right)\Delta z$, and $s_{N+1} = z_b$ be the spatial grid where $\Delta z = \dfrac{z_b}{N}$. Here N will represent the partition of the water column and will represent the number of ODEs each of the b_i and R_i in equations (3.1), (3.2), (3.13), and (3.14) are partitioned into. For convenience, the method will be explained using only one species and one nutrient. To simplify notation, for $i = 1, \ldots, N$ let $b_i(t)$ denote an approximation to $b(s_i, t)$. A visual representation of the discretization adapted from [27] is given below.

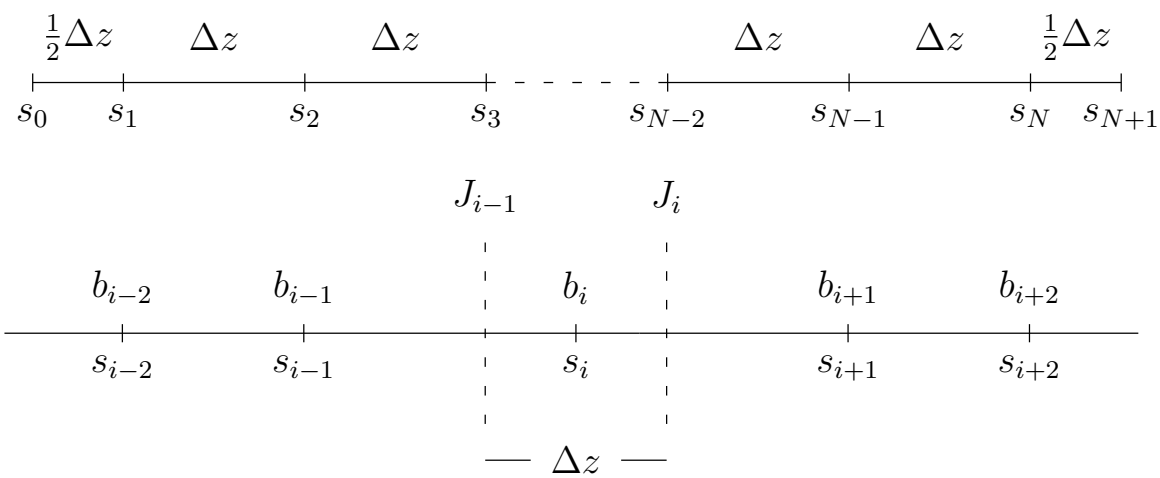

To discretize the spatial derivatives at the points s_i present in the diffusion and active movement terms in equations (3.1) and (3.2), a finite volume approach is used. First define the flux of the phytoplankton by

$$J(z,t) = -\Big(\nu_k b(z,t) + D_b \frac{\partial b}{\partial z}(z,t)\Big). \tag{3.19}$$

The minus sign on the diffusion term is present to indicate that turbulent diffusion is in the direction opposite to the biomass concentration while the minus sign on the active movement term is a result of the orientation of the velocity.

As demonstrated in the figure above, assume there is an imaginary box of size Δz around the point s_i and we denote the fluxes at the side of these 'boxes' by $J_i \approx J(s_i + \frac{1}{2}\Delta z, t)$ which depends on the numerical values b_i. Doing this, conservation of J is obtained since the outflow of one part of one box will serve as the input for the adjacent box. Further, observe that equations (3.1) and (3.2) can be rewritten using J in the following form

$$\frac{\partial b}{\partial t}(z,t) = g(z,t)b(z,t) - \frac{\partial J}{\partial z}(z,t). \tag{3.20}$$

Thus our interest is in approximating $\dfrac{\partial J}{\partial z}$ at the point $z = s_i$. To form the approximation we first split the flux into two components

$$\frac{\partial J}{\partial z}(z,t) = -\Big(\frac{\partial A}{\partial z}(z,t) + \frac{\partial P}{\partial z}(z,t)\Big) \tag{3.21}$$

where A represents the active movement portion of the flux while P represents the portion of passive movement in the flux $\left(D_b \dfrac{\partial b}{\partial z}\right)$.

We use the approximation

$$\frac{\partial J}{\partial z}(z,t) \approx \frac{J_i - J_{i-1}}{\Delta z} = -\Big(\frac{A_i - A_{i-1}}{\Delta z} + \frac{P_i - P_{i-1}}{\Delta z}\Big). \tag{3.22}$$

What follows is a description of determining the approximation for J_i. For the advection term in equations (3.1) and (3.2) (the active movement) a third-order upwind scheme is used. The diffusion terms present in equations (3.1), (3.2), (3.13), and (3.14) (the passive movement) are handled using a symmetric discretization.

3.2.1 Biomass Advection

Under the assumptions laid out in the previous section, phytoplankton will move up or down in the water column depending on growth conditions. Thus to determine A_i under the upwinding scheme, first we need to separate the cases when $\nu_i > 0$ (upward movement) and $\nu_i < 0$ (downward movement). Further, movement near the surface of the water column and near the bottom of the water column have to be treated separately. No flux boundary conditions tell us that there cannot be upward movement at the surface or any downward motion on the bottom. However phytoplankton can swim up to the surface and down to the bottom. The approximation at the surface will rely on the terms A_0, A_1, and A_2 and the bottom will rely on A_{N-2}, A_{N-1}, and A_N. The rest of the water column will rely on the terms A_i for $i = 2, \ldots, N-2$.

First consider phytoplankton that are in the water column but are not at the surface or the bottom. To implement the upwinding scheme it is necessary to know which direction the phytoplankton are swimming. When the phytoplankton are swimming down towards the bottom the flow is from left to right in the figure. For that reason more information will be used from the left. Similarly, when phytoplankton are swimming up towards the surface, the flow is from the right to the left. Separating the cases for $\nu_i > 0$ and $\nu_i < 0$ we get that the upwinding scheme in general can be given by the formula

$$\begin{aligned} A_i &= \frac{1}{6}\nu_i(2b_i + 5b_{i+1} - b_{i+2}) * (\nu_i > 0) + \frac{1}{6}\nu_i(-b_{i-1} + 5b_i + 2b_{i+1}) * (\nu_i < 0) \\ &= [\text{Upward movement}] + [\text{Downward movement}]. \end{aligned} \tag{3.23}$$

Thus the approximation to $\dfrac{\partial A}{\partial z}$ is given by

$$\begin{aligned}\frac{A_i - A_{i-1}}{\Delta z} =& \frac{1}{6\Delta z}\Big(\nu_i(2b_i + 5b_{i+1} - b_{i+2}) * (\nu_i > 0) \\ &+ \nu_i(-b_{i-1} + 5b_i + 2b_{i+1}) * (\nu_i < 0) \\ &- \nu_{i-1}(2b_{i-1} + 5b_i - b_{i+1}) * (\nu_{i-1} > 0) \\ &- \nu_{i-1}(-b_{i-2} + 5b_{i-1} + 2b_i) * (\nu_{i-1} < 0)\Big). \end{aligned} \tag{3.24}$$

Combining like terms and reorganizing we get

$$\begin{aligned}\frac{A_i - A_{i-1}}{\Delta z} =& \frac{1}{6\Delta z}\Big(\nu_{i-1} * (\nu_{i-1} < 0)b_{i-2} - (\nu_i * (\nu_i < 0) + 2\nu_{i-1} * (\nu_{i-1} > 0) \\ &- 5\nu_{i-1} * (\nu_{i-1} < 0))b_{i-1} + (2\nu_i * (\nu_i > 0) + 5\nu_i * (\nu_i < 0) \\ &- 5\nu_{i-1} * (\nu_{i-1} > 0) - 2\nu_{i-1} * (\nu_{i-1} < 0))b_i + (5\nu_i * (\nu_i > 0) \\ &+ 2\nu_i * (\nu_i < 0) + \nu_{i-1} * (\nu_{i-1} > 0))b_{i+1} - \nu_i * (\nu_i > 0)b_{i+2}\Big). \end{aligned} \tag{3.25}$$

Now consider phytoplankton near the surface of the water column. The upwinding scheme used on A_i for $i = 2, \ldots, N-2$ has to be modified to get the upwinding scheme for A_0 and A_1. Given that the system is closed we have $A_0 = 0$. To compute A_1, observe that A_1 depends only on b_1, b_2, and b_3. Using this, A_1 can be computed using the formula

$$A_1 = \nu_1 * (\nu_1 < 0)\Big(\frac{b_1 + b_2}{2}\Big) + \frac{1}{6}\nu_1 * (\nu_1 > 0)(2b_1 + 5b_2 - b_3). \tag{3.26}$$

Using the same strategy as before we construct the approximations $\dfrac{\partial A}{\partial z}$ for $z = s_1$ and $z = s_2$. For $z = s_1$ we get

$$\begin{aligned}\frac{\partial A}{\partial z}(s_1, t) \approx \frac{A_1 - A_0}{\Delta z} = \frac{1}{6\Delta z}\Big(&(3\nu_1 * (\nu_1 < 0) + 2\nu_1 * (\nu_1 > 0))b_1 \\ &+ (3\nu_1 * (\nu_1 < 0) + 5\nu_1 * (\nu_1 > 0))b_2 - \nu_1 * (\nu_1 > 0)b_3\Big). \end{aligned} \tag{3.27}$$

For $z = s_2$ we get

$$\frac{\partial A}{\partial z}(s_2, t) \approx \frac{A_2 - A_1}{\Delta z} = \frac{1}{6\Delta z}\Big((-\nu_2 * (\nu_2 < 0) - 3\nu_1 * (\nu_1 < 0) - 2\nu_1 * (\nu_1 > 0))b_1$$
$$+ (2\nu_2 * (\nu_2 > 0) + 5\nu_2 * (\nu_1 < 0) - 5\nu_1 * (\nu_1 > 0) - 3\nu_1 * (\nu_1 < 0))b_2$$
$$+ (5\nu_2 * (\nu_2 > 0) + 2\nu_2 * (\nu_2 < 0) + \nu_1 * (\nu_1 > 0))b_3 - \nu_2 * (\nu_2 > 0)b_4\Big). \tag{3.28}$$

Finally, consider phytoplankton near the bottom of the water column. As with the computations near the surface, the upwinding scheme for A_{N-1} and A_N has to be modified. As with A_0, since the system is closed it follows that $A_N = 0$. To compute A_{N-1} observe that A_{N-1} will depend on b_{N-2}, b_{N-1}, and b_N. Hence we get

$$A_{N-1} = \nu_{N-1} * (\nu_{N-1} > 0)\Big(\frac{b_N + b_{N-1}}{2}\Big) + \frac{1}{6}\nu_{N-1} * (\nu_{N-1} < 0)(-b_{N-2} + 5b_{N-1} + 2b_N). \tag{3.29}$$

Using this we can finish constructing the approximations of $\frac{\partial A}{\partial z}$ by computing the terms at $z = s_{N-1}$ and $z = s_N$. At $z = s_N$ we get

$$\frac{\partial A}{\partial z}(s_N, t) \approx \frac{A_N - A_{N-1}}{\Delta z} = \frac{1}{6\Delta z}\Big(\nu_{N-1} * (\nu_{N-1} < 0)b_{N-2}$$
$$+ (-3\nu_{N-1} * (\nu_{N-1} > 0) - 5\nu_{N-1} * (\nu_{N-1} < 0))b_{N-1}$$
$$+ (-3\nu_{N-1} * (\nu_{N-1} > 0) - 2\nu_{N-1} * (\nu_{N-1} < 0))b_N\Big). \tag{3.30}$$

Finally, at $z = s_{N-1}$ we get

$$\frac{\partial A}{\partial z}(s_{N-1},t) \approx \frac{A_{N-1}-A_{N-2}}{\Delta z} = \frac{1}{6\Delta z}\Big(\nu_{N-2} * (\nu_{N-2} < 0) b_{N-3}$$
$$+ (-\nu_{N-1} * (\nu_{N-1} < 0) - 2\nu_{N-2} * (\nu_{N-2} > 0)$$
$$- 5\nu_{N-2} * (\nu_{N-2} < 0)) b_{N-2} + (5\nu_{N-1} * (\nu_{N-1} < 0)$$
$$+ 3\nu_{N-1} * (\nu_{N-1} > 0) - 5\nu_{N-2} * (\nu_{N-2} > 0)$$
$$- 2\nu_{N-2} * (\nu_{N-2} < 0)) b_{N-1}$$
$$+ (2\nu_{N-1} * (\nu_{N-1} < 0) + \nu_{N-2} * (\nu_{N-2} > 0)) b_N\Big). \tag{3.31}$$

Using these approximations, one can construct the active movement matrix, $A_{\mathcal{M}}$, such that $A_{\mathcal{M}}\mathbf{b}$ gives the approximations to $\frac{\partial A}{\partial z}$. The active movement matrix will be an $N \times N$ sparse matrix whose coefficients are given by the velocities ν_i with their corresponding positive and negative parts. This matrix will be a banded matrix which has non-zero elements in the two diagonal arrays above and the two diagonal arrays below the main diagonal, and non-zero elements in the main diagonal.

3.2.2 Biomass Diffusion

To finish the discretization of the biomass flux, the spatial derivatives present from the diffusion term need to be approximated. Unlike the active movement problem where a symmetric difference can produce unwanted numerical artifacts [27], we use a symmetric method to discretize the diffusion for both the biomass and the nutrients.

Let $P_i = P(s_i + \frac{1}{2}\Delta z)$. Since the system is closed for phytoplankton at the surface and the bottom of the water column, we have $P_0 = P_N = 0$. For $i = 1, \ldots, N-1$ we have

$$P_i = D_i \frac{b_{i+1} - b_i}{\Delta z}. \tag{3.32}$$

Using equation (3.32) we form the approximations to the diffusion term $\frac{\partial P}{\partial z}$ in equation

(3.19) using the appropriate differences. Computing the differences we get

$$\frac{P_1 - P_0}{\Delta z} = \frac{1}{(\Delta z)^2}(D_1 b_1 - D_1 b_2), \tag{3.33}$$

$$\frac{P_i - P_{i-1}}{\Delta z} = \frac{1}{(\Delta z)^2}(-D_i b_{i+1} + (D_i + D_{i-1})b_i - D_i b_{i+1}), \tag{3.34}$$

$$\frac{P_N - P_{N-1}}{\Delta z} = \frac{1}{(\Delta z)^2}(-D_{N-1} b_{N-1} + D_{N-1} b_N). \tag{3.35}$$

Thus the resulting biomass diffusion matrix, $P_{\mathcal{M}}$, will be an $N \times N$ tridiagonal matrix. The main diagonal will consist of $\frac{1}{(\Delta z)^2}D_1$, $\frac{1}{(\Delta z)^2}(D_i + D_{i-1})$, and $\frac{1}{(\Delta z)^2}D_{N-1}$. The upper and lower diagonals will consist of elements of the form $-\frac{1}{(\Delta z)^2}D_i$ where $i = 2, \ldots, N$ for the lower diagonal and $i = 1, \ldots, N-1$ for the upper diagonal.

3.2.3 Nutrient Diffusion

While the nutrient diffusion matrix that results from the discretization is almost identical to the biomass diffusion matrix constructed above there is a key difference. Unlike the biomass, the model developed is not assumed to be a closed system for the nutrients. The boundary terms given in equations (3.15) and (3.16) show that nutrients can be supplied from the sedimentary layer at the bottom of the water column. So while equations (3.33) and (3.34) will still be valid for the nutrients equation, (3.35) will no longer hold in this circumstance.

Using the boundary term for $\frac{\partial R}{\partial z}$ at $z = z_b$ we can define P_N by the equation

$$P_N = \frac{D_N}{\Delta z}\Big(h(R_{in} - R_N)\Big). \tag{3.36}$$

Proceeding as we did before, we now calculate the approximation of $\frac{\partial P}{\partial z}(z,t)$ at $z = s_N$.

Using equation (3.35) (making the change from b_i to R_i) we get

$$\frac{P_N - P_{N-1}}{\Delta z} = \frac{1}{(\Delta z)^2}(-D_N h R_{in} + (D_N h + D_{N-1})R_N + -D_{N-1}R_{N-1}).$$

3.3 Numerical Illustration and Biological Significance

Parameter interpretation and values used for the simulations can be found in Table 3.1 given at the end of this section. The constants for light and nutrients used in the growth rate affect the proportion of light and nutrients needed by a species. For this reason, these parameters are chosen such that $K_{I,2} < K_{I,1}$. This way the competing species will have growth functions defined in such a way that the first species has a growth rate with proportionally larger requirement on light while the second species has a growth rate with proportionally larger nutrient requirements. With these assumptions, the phytoplankton species have potential natural niches located at different depths that they will want to occupy.

For initial conditions suppose $b_1(z,0) = b_2(z,0) = 10^4$ cells ml^{-1}, $R_1(z,0) = 2.25$ μg L^{-1}, and $R_2(z,0) = 2.1$ μg L^{-1} holds for all z, $0 \leq z \leq z_b$. To investigate the phytoplankton layering patterns, model simulations are run for a time period long enough for numerical changes in phytoplankton and nutrient distributions to approximately stabilize. For simplifying purposes we consider situations when $\nu_{max_1} = \nu_{max_2}$ and $\varepsilon_{1,1} = \varepsilon_{1,2} = \varepsilon_{2,2} = \varepsilon_{2,2}$, although these assumptions can be relaxed.

As hypothesized, the model under this parametrization gives a vertically heterogeneous water column. Studying the left panel in Figure 3.1 we can see that the two species form layers whose thickness and location within the water column vary. While this result supports the hypothesis of MacArthur and Levins (1964) to explain why various phytoplankton species coexist, it is not necessarily feasible to consider this approach when studying field data. To get a better understanding of how the model compares to field data, relative fluorescence is simulated along with light transmission. While the model may not match field data quantitatively [5], [6], [35], [43], the model simulations do qualitatively agree with what

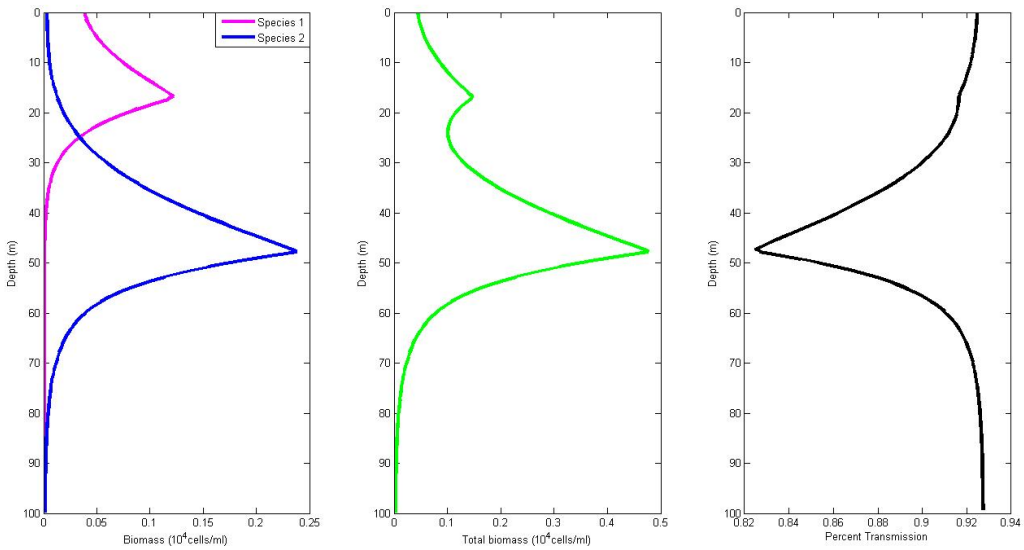

Figure 3.1: Left Panel: Species specific biomass vs. depth. Middle Panel: Simulated relative fluorescence vs. depth. Right Panel: Simulated light transmission vs depth.

is seen in Lake Michigan. In particular, the presence of multiple phytoplankton layers of varying depths is a key phenomological behavior that the proposed model has successfully captured. Similarly, the behavior of the simulated light transmission data as it relates to peaks in phytoplankton biomass is qualitatively similar to that seen in the literature [5], [6], [43].

In addition to capturing the qualitative behavior of what is seen in Lake Michigan the model is also able to capture other layering phenomenon. For the remaining model simulations presented in this chapter, we will be using $z_b = 20$ as is used in the Klausmeier and Litchman model. By changing the model parameters we can see the formation of surface scums, deep chlorophyll maxima, and benthic layers. We will illustrate these examples below along with which parameters from Table 3.1 need to be altered.

The multiple DCMs present in the top left are a result from the following parameter changes from the values given in Table 3.1: $a_{bg} = 0.35$, $\nu_{1_{max}} = 8$, $\nu_{2_{max}} = 6$, $K_{I,1} = 100$, and $K_{I,2} = 1$. To produce the surface scum seen in the top right panel the following parameters changes were made: $a_1 = 10^{-3}$, $a_2 = 10^{-2}$, $a_{bg} = 0.35$, $\nu_{1_{max}} = \nu_{2_{max}} = 10$, $K_{R_1,1} =$

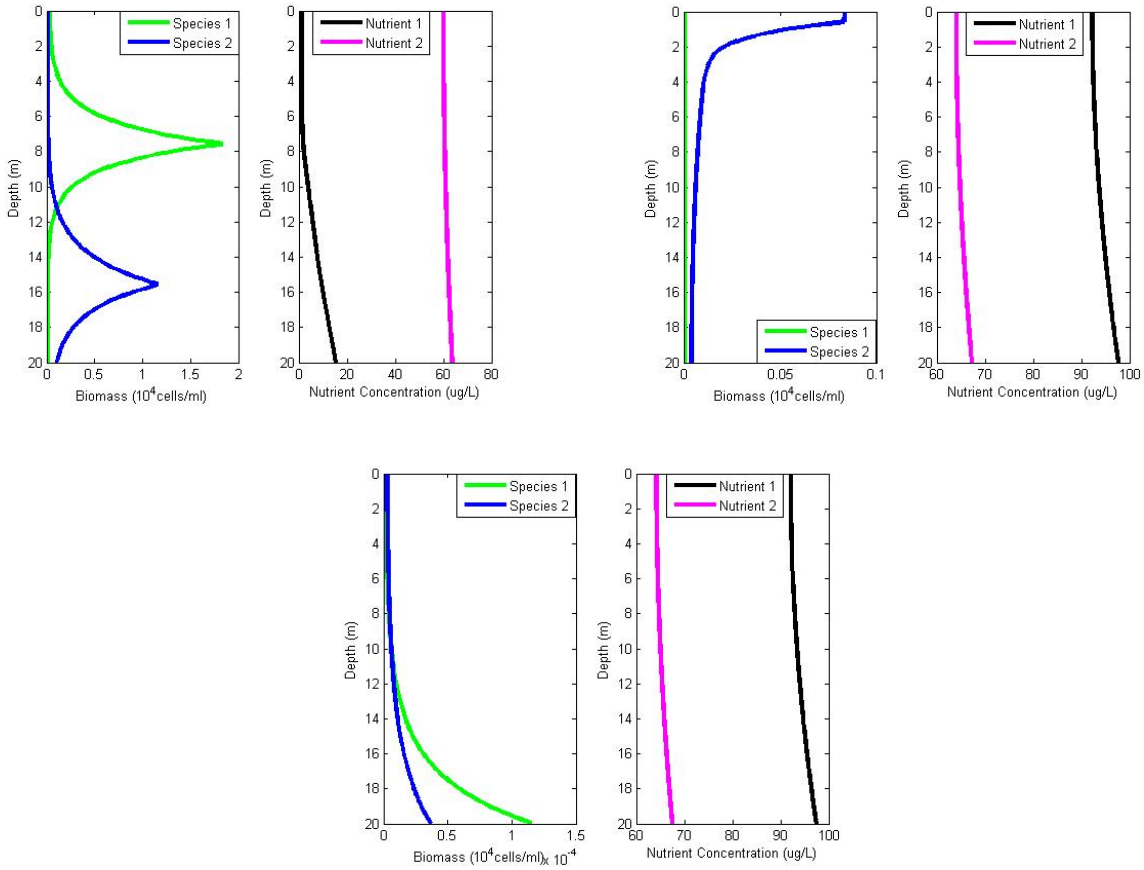

Figure 3.2: Equilibrium vertical distributions of phytoplankton biomass and nutrients determined from Equations (3.1) –(3.17). The top left represents the DCM distribution, the top right represents the surface scum distribution, and the bottom represents the benthic layer distribution.

$K_{R_2,1} = 1,\ K_{R_1,2} = K_{R_2,2} = 10,\ K_{I,1} = 100,\ \ K_{I,2} = 5$ and $\varepsilon_{1,1} = \varepsilon_{1,2} = \varepsilon_{2,1} = \varepsilon_{2,2} = 0.9$. The resulting surface scum is reasonable to expect since the algal attenuation coefficients impact the amount of light that is absorbed by the biomass and influences the level of self shading that occurs. Further, by increasing the amount of nutrients that are released back into the environment upon cell death and increasing the speed in which phytoplankton are able to move, the need to go deeper into the water column in search of nutrients is minimized. To produce the benthic layer demonstrated in the bottom panel, the following parameter changes were made: $a_1 = 10^{-7}, a_2 = 10^{-6},\ a_{bg} = 0.35,\ \nu_{1_{max}} = \nu_{2_{max}} = 10,\ K_{R_1,1} = K_{R_2,1} = 100,\ K_{R_1,2} = K_{R_2,2} = 500,\ K_{I,1} = 0.1, K_{I,2} = 0.5,$ and $\varepsilon_{1,1} = \varepsilon_{1,2} = \varepsilon_{2,1} = \varepsilon_{2,2} = 0.9$. Un-

like with the surface scum where the parameter changes were made to favor light intensive conditions, the benthic layer requires light to be able to permeate further in depth in the water column so that self-shading is minimized and the nutrient saturation requirements are increased so that phytoplankton will reside in the lower depths.

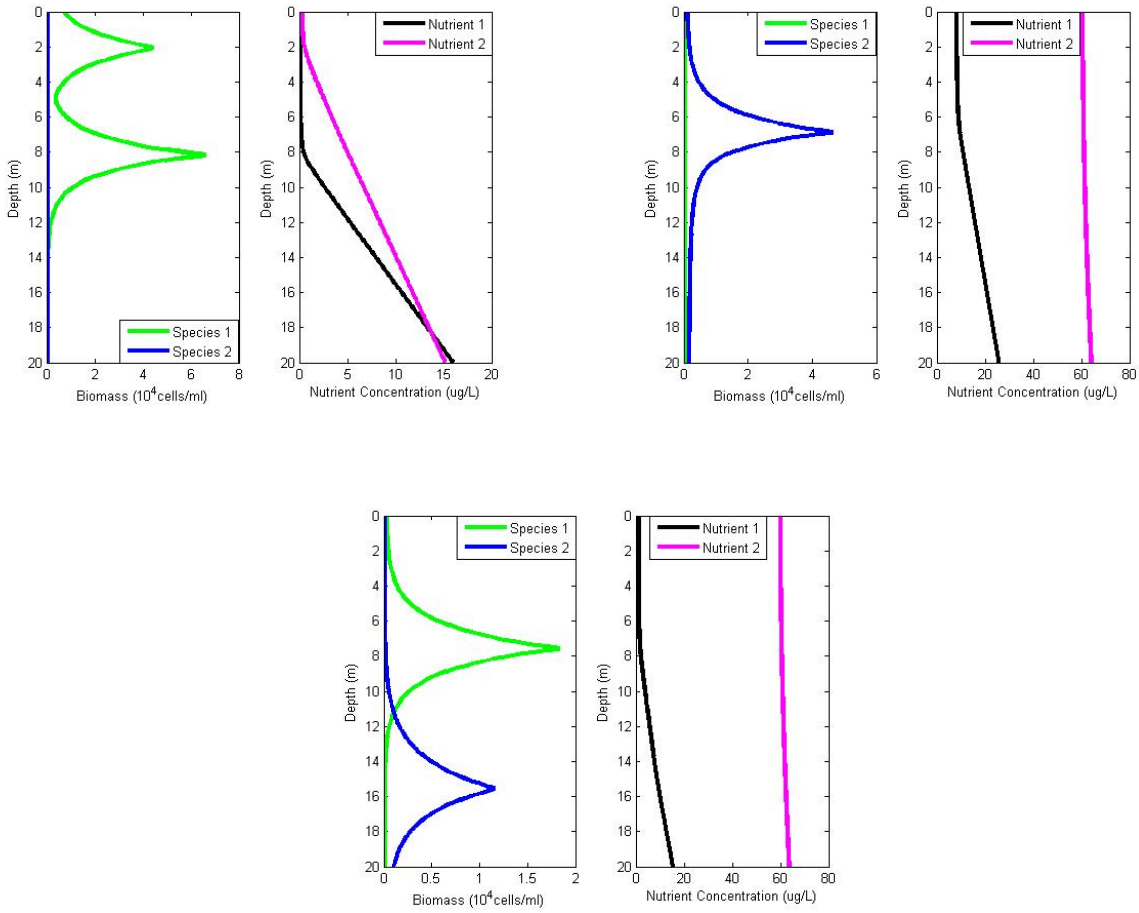

Figure 3.3: Equilibrium vertical distributions of phytoplankton biomass and nutrients determined from Equations (3.1) –(3.17). The top left represents the case when Species 1 out competes Species 2, the top right represents the case when Species 2 out competes Species 1, and the bottom represents the case of bistability between the two species resulting in coexistence.

Besides being able to replicate common layering phenomena seen in field data, these simulations also capture insights into the nutrient dynamics present in an ecosystem when one nutrient is assumed to be preferentially uptaken over the other. As can be seen in Figure 3.2, it is not always the case that the preferred nutrient, R_1, is utilized more than

the secondary source R_2. This outcome is largely determined by the saturation constants $K_{R_1,1}$, $K_{R_1,2}$, $K_{R_2,1}$, $K_{R_2,2}$, $K_{I,1}$, and $K_{I,2}$. These differences are displayed in Figure 3.4. Notably, this figure also demonstrates the importance of differences in nutrient utilization for coexistence. In Figure 3.2, the surface scum contains only b_2 while b_1 is extinct. When looking at the respective nutrient uptake plots in Figure 3.4 for the surface, it is clearly seen that both species have a similar uptake pattern. However, due to the differences in mortality rates ($m_1 > m_2$) species 2 out-competed species 1 and competitive exclusion is the final result.

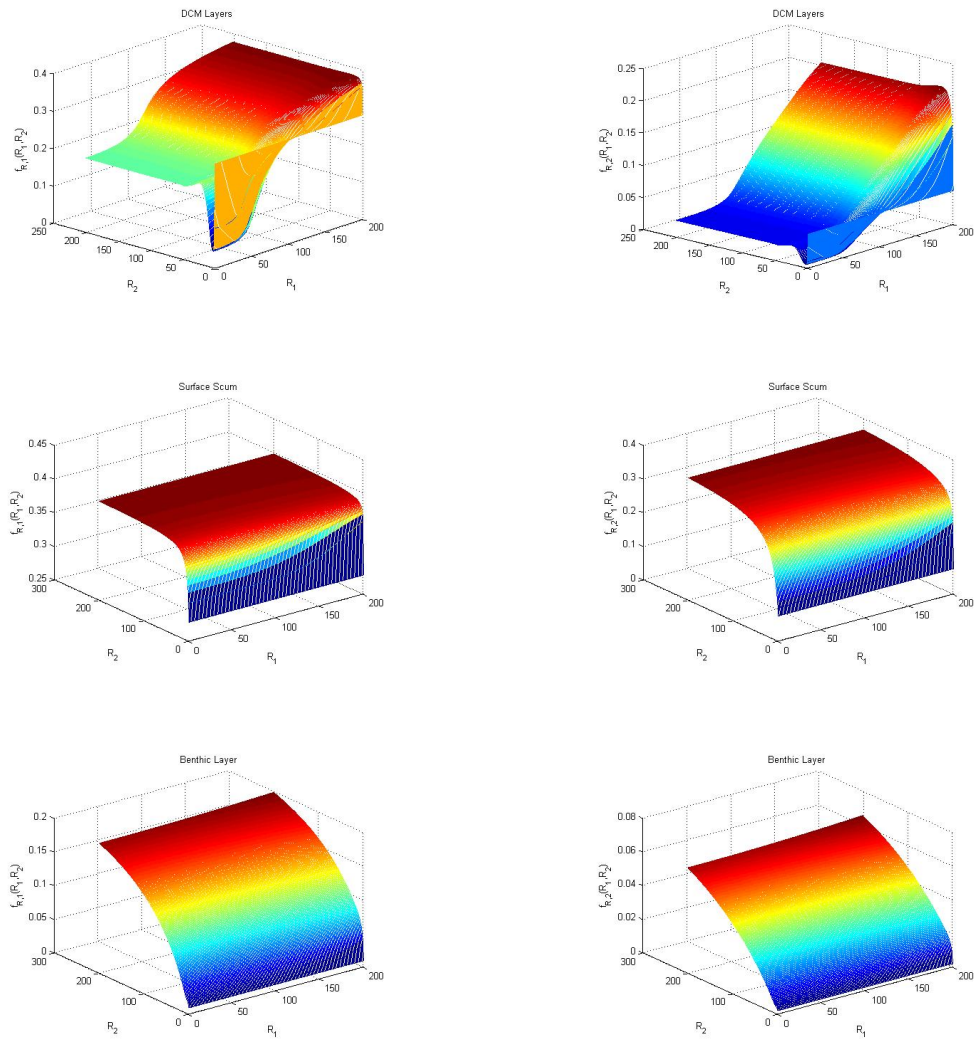

Figure 3.4: Surface plots for Equations (3.5) and (3.6) modeling the preferential nutrient uptake using the same parameters as in Figure 3.2 showing the differences in nutrient utilization by the competing phytoplaknton species.

As with the multi-species version of the Klausmeier and Litchman model, our proposed preferential uptake model is able to exhibit cases where competitive exclusion of each species occurs and cases of bistable coexistence demonstrated in Figure 3.3. To simulate the case where only the first species survives the following parameters from Table 3.1 were altered: $a_{bg} = 0.35$, $\nu_{1_{max}} = \nu_{2_{max}} = 10$, $r_1 = 0.5$, $r_2 = 0.2$, $m_1 = 0.1$, $K_{I,1} = 50$, and $K_{I,2} = 1$. In comparison, to simulate the case where only the second species survives the following parameters were altered: $a_{bg} = 0.35$, $\nu_{1_{max}} = \nu_{2_{max}} = 10$, $r_1 = 0.2$, $r_2 = 0.5$, $K_{I,1} = 50$, and $K_{I,2} = 1$. Finally, the bistable coexistence simulation is identical to the simulation of the DCM distribution shown in Figure 3.2.

Currently the model simulations are performed using parameters reported from the literature, and while biologically feasible, they may not be suitable for all environments. For example, parameters used in a marine environment would not be suitable for a freshwater ecosystem such as Lake Michigan. Further, since the parameters are species dependent, there can be a wide range of accepted values which can be influenced by factors that are unique to the environment. Given the large number of parameters present in the PDE models it is necessary to use various statistical techniques to analyze the parameter space. This analysis in turn can be used to design experiments in laboratory settings and to accurately make predictions for conditions which will result in large blooms for a specific body of water.

Parameter	Explanation	Value	Source
N	Spatial discretization level	200	
z_b	Water column depth (m)	100	[35]
R_{in_1}	Sediment concentration Nutrient 1 (μg L^{-1})	150	
R_{in_2}	Sediment concentration Nutrient 2 (μg L^{-1})	100	[35]
h	Sediment-water column permeability (m^{-1})	10^{-2}	[35]
I_{in}	Incoming light (μmol photons m^{-2} s^{-1})	1,400	[35]
a_{bg}	Background attenuation coefficient (m^{-1})	0.15	[35], [36]
a_1	Species 1 algal attenuation coefficient (m^{-1} [cells ml^{-1}]$^{-1}$)	10^{-5}	[35], [36]
a_2	Species 2 algal attenuation coefficient (m^{-1} [cells ml^{-1}]$^{-1}$)	10^{-4}	[35], [36]
D_{b_1}	Species 1 biomass diffusion coefficients (m^2 d^{-1})	10	[35]
D_{b_2}	Species 2 biomass diffusion coefficients (m^2 d^{-1})	10	[35]
D_{R_1}	Nutrient 1 diffusion coefficient (m^2 d^{-1})	10	[35]
D_{R_2}	Nutrient 2 diffusion coefficient (m^2 d^{-1})	10	[35]
$\nu_{1_{max}}$	Species 1 swimming speed (m d^{-1})	1	[35]
$\nu_{2_{max}}$	Species 2 swimming speed (m d^{-1})	1	[35]
r_1	Species 1 maximum growth rates (d^{-1})	0.4	[35]
r_2	Species 2 maximum growth rates (d^{-1})	0.4	[35]
m_1	Species 1 loss rate (d^{-1})	0.2	[35]
m_2	Species 2 loss rate (d^{-1})	0.1	
$K_{R_1,1}$	Nutrient 1 saturation constant for Species 1 (μg L^{-1})	1	[35]
$K_{R_1,2}$	Nutrient 1 saturation constant for Species 2 (μg L^{-1})	1	[35]
$K_{R_2,1}$	Nutrient 2 saturation constant for Species 1 (μg L^{-1})	15	
$K_{R_2,2}$	Nutrient 2 saturation constant for Species 2 (μg L^{-1})	15	
$K_{I,1}$	Light saturation constant for Species 1 (μmol photons m^{-2} s^{-1})	120	[35]
$K_{I,2}$	Light saturation constant for Species 2 (μmol photons m^{-2} s^{-1})	0.1	
Y_1	Species 1 yield coefficient (cells ml^{-1} [μg L^{-1}]$^{-1}$)	10^3	[35]
Y_2	Species 2 yield coefficient (cells ml^{-1} [μg L^{-1}]$^{-1}$)	10^3	[35]
$\varepsilon_{i,1}$	Species i Nutrient 1 recycling coefficient (dimensionless)	0	[43]
$\varepsilon_{i,2}$	Species i Nutrient 2 recycling coefficient (dimensionless)	0	[43]
K_{swim}	Swimming constant (m^{-1} d^{-1})	0.001	[43]
λ	Nutrient uptake inhibition factor (dimensionless)	0.8	
n	Shaping parameter	24	

Table 3.1: Parameters used in simulations unless otherwise noted.

4 Parameter Identification and Global Sensitivity Analysis

One of the principal challenges to modeling algal bloom dynamics are the non-stationary and non-linear dynamics due to the complex interaction of physical, chemical, and biological parameters affecting growth and accumulation of biomass [64]. Traditional statistical methods such as multiple linear regression and autoregressive moving average models are thus difficult to implement in this situation [48]. In this chapter we analyze the parameter spaces of three models - the Klausmeier and Litchman model, the multispecies variant of their model, and the proposed preferential uptake model. The parameter spaces of all three models are analyzed for parameter identifiability: the ability for a parameter's true value to be recovered through optimization, and for global sensitivity: the influence a parameter has on model response [55].

4.1 Parameter Estimation

In order to implement the model and run simulations, values for the model parameters need to be supplied. Ranges for some of these quantities are reported in [7], [24], [35], [43], [47]. While quantities such as incident light and depth of the water column can be easily measured, other parameters are either difficult to measure or have wide reported ranges. Thus we resort to parameter estimation based on data. However, when experimental or field data is unavailable, the parameter estimation problem can be done on simulated data [4]. Analysis of estimation techniques and results using simulated data provide information about which parameters can be identified computationally. Further, solving estimation problems on simulated data provide insights into the type of data that is needed, as well as how frequently it must be collected in order to successfully identify unknown parameters.

4.1.1 Deterministic Estimation Problem

To solve the inverse problem, we set up a deterministic estimation problem using the simulated data with random noise. Adopting the notation used in [4], let B_i be observations taken for T_n time values. We want to estimate the parameters q in the parameter space $Q = \mathbb{R}^m$ where m is the number of parameters in the vector q. To this end we seek to minimize

$$J(q, B) = \sum_{i=1}^{T_n} \frac{1}{||B_i||_2} ||Y(t_i; q) - B_i||_2 + P(q) \tag{4.1}$$

over $q \in Q$, where Y is a model given estimate of the total biomass in the water column, $P(q)$ is a penalty function to prevent parameters from taking on negative values, and $||\cdot||_2$ is the 2-norm.

Numerous algorithms exist to solve the optimization problem given by (4.1). In this discussion we utilized MATLAB's *fminsearch* function which uses the Nelder-Mead algorithm [37].

4.1.2 Parameter Estimation Based on Simulated Data

We analyze the sensitivity of the model to the inverse problem by solving the minimization problem using synthetic data. To generate the simulated data, we run the model with a chosen set of parameters q. We form observations $B_i = Y(t_{2i}; q)$ according to the model given estimate of the total biomass and then add various levels of random noise to form the synthetic data set. Thus we define $B_i^{\mathcal{N}}$ by

$$B_i^{\mathcal{N}} = (1 + \eta_i^{\mathcal{N}}(\alpha))B_i, \tag{4.2}$$

where $\eta_i^{\mathcal{N}}$ is a normally distributed random variable with mean 0 and standard deviation of $\frac{\alpha}{3}$. This corresponds to 99.74% of $\eta_i^{\mathcal{N}}$ taking values in the interval $[-\alpha, \alpha]$. The parameter

estimation problem was solved using noise levels $\alpha = 5\%$ and 10% to analyze the impact random noise in the data set has on the model's ability to recover the original parameters. The parameter estimation problem on simulated data was solved for the Klausmeier and Litchman model, the multi-species variant of their model, and the proposed model incorporating preferential nutrient uptake.

The Klausmeier and Litchman Model

In this application, $q \in \mathbb{R}^{12}$ is a vector of the form

$$q = [R_{in}, h, I_{in}, a_{bg}, a, r, m, K_R, K_{I,}, Y, \varepsilon, K_{swim}]^T,$$

and

$$\begin{aligned} Y(t;q) =& \frac{z_b}{2}\left(\sum_{k=1}^{N} b(w_{k+1}, t, q) + b(w_k, t, q)\right) \\ \approx& \int_0^{z_b} b(w, t, q)dw. \end{aligned} \tag{4.3}$$

Note that the diffusion parameters D_b and D_R along with the swimming speed ν_{max} were excluded from the parameter vector. These parameters were not included due to the numerical stability of the solution to the inverse problem. When the diffusion coefficients are large, artificial oscillations are introduced into the solution and when the swimming speed is made too large, the numerical solutions become singular.

Solving the parameter estimation problem, model simulations with 5% and 10% noise were generated. Each parameter in q was augmented by 5% from the reported values in literature and was used as an initial guess in the optimization routine. The results of these experiments are given in Tables 4.1 and 4.2.

Overall, the two parameter estimation problems give results which are consistent with the original parameter values with total error of 1.38% and 2.53% for $\alpha = 0.05$ and $\alpha = 0.1$

Parameter	Original Value	Recovered Value	Relative Error
R_{in}	100	95.630	-0.0437
h	0.01	0.0102	0.0237
I_{in}	1400	1517.65	0.0840
a_{bg}	0.35	0.348	-0.0049
a	1.0×10^{-5}	1.01×10^{-5}	0.0112
r	0.4	0.409	0.0234
m	0.2	0.208	0.0377
K_R	1	1.081	0.0809
K_I	50	52.686	0.0537
Y	1000	1059.635	0.0596
ε	0.3	0.323	0.0753
K_{swim}	0.001	0.0011	0.1074

Table 4.1: Comparing the original and recovered values of the parameters in q when $\alpha = 0.05$.

Parameter	Original Value	Recovered Value	Relative Error
R_{in}	100	101.824	0.0182
h	0.01	0.00992	-0.0085
I_{in}	1400	1518.67	0.0848
a_{bg}	0.35	0.341	-0.0247
a	1.0×10^{-5}	1.04×10^{-5}	0.0373
r	0.4	0.402	0.0060
m	0.2	0.204	0.0177
K_R	1	1.119	0.1188
K_I	50	55.092	0.1018
Y	1000	1026.329	0.0263
ε	0.3	0.326	0.0867
K_{swim}	0.001	0.00110	0.0990

Table 4.2: Comparing the original and recovered values of the parameters in q when $\alpha = 0.1$.

respectively. Since the optimized parameter values are close to the original parameter values, we can say that the parameters in q are identifiable. The parameters with the largest relative error in both estimation problems were I_{in}, K_R, ε, and K_{swim}. While I_{in} is an identifiable parameter, in practical applications this term would not be included in the parameter estimation problem since it is possible to accurately measure incident light both in the field and in laboratory settings with minimal difficulty. As for the other parameters, the absolute error is small and within the reported literature values.

Multi-species Klausmeier and Litchman Model (N=2)

In this application, $q \in \mathbb{R}^{19}$ is a vector of the form

$$\begin{aligned} q =& [R_{in}, h, I_{in}, a_{bg}, a_1, a_2, r_1, r_2, m_1, m_2, K_{R,1}, K_{R,2}, K_{I,1}, K_{I,2}, Y_1, Y_2, \varepsilon_1, \\ & \varepsilon_2, K_{swim}]^T, \end{aligned}$$

and

$$\begin{aligned} Y(t;q) =& \frac{z_b}{2}\left[\sum_{k=1}^{N}(b_1(w_{k+1},t,q)+b_1(w_k,t,q))+\sum_{k=1}^{N}(b_2(w_{k+1},t,q)+b_2(w_k,t,q))\right] \\ \approx& \int_0^{z_b}(b_1(w,t,q)+b_2(w,t,q))dw. \end{aligned} \tag{4.4}$$

Note that the diffusion parameters D_{b_1}, D_{b_2}, D_R and the swimming speeds $\nu_{1_{max}}$ and $\nu_{2_{max}}$ were excluded from the parameter vector.

Solving the parameter estimation problem, model simulations with 5% and 10% noise were generated. Each parameter in q was augmented by 5% from the reported values in literature and was used as an initial guess in the optimization routine. The results of solving the inverse problem with $\alpha = 0.05$ and $\alpha = 0.1$ are given in Tables 4.3 and 4.4.

Overall, the two parameter estimation problems give results which are consistent with the original parameter values and with total error of 1.45% and 2.91% for $\alpha = 0.05$ and $\alpha = 0.1$ respectively. Since the optimized values are close to the original values, in this case we say that the parameters in q are identifiable.

The parameters with largest relative error in both estimation problems were I_{in}, $K_{R,1}$, $K_{R,2}$, $K_{I,2}$, and ε_1. As before, the parameter I_{in} can be excluded from the parameter vector q in practical applications while the other parameters would be useful to include. While the relative error for these terms is larger than for the other parameters in q, the absolute error is small. Additionally, the optimized parameter values are within the acceptable ranges of the reported literature values.

Parameter	Original Value	Recovered Value	Relative Error
R_{in}	100	104.973	0.0497
h	0.01	0.0098	-0.0233
I_{in}	1400	1581.18	0.1294
a_{bg}	0.35	0.350	0.0011
a_1	1.0×10^{-5}	9.983×10^{-6}	-0.0017
a_2	1.0×10^{-5}	9.655×10^{-6}	-0.0345
r_1	0.4	0.395	-0.0132
r_2	0.4	0.449	0.1233
m_1	0.2	0.207	0.0347
m_2	0.1	0.102	0.0169
$K_{R,1}$	1	0.896	-0.1036
$K_{R,2}$	10	11.169	0.1169
$K_{I,1}$	50	49.725	-0.0055
$K_{I,2}$	5	6.350	0.2699
Y_1	1000	1064.78	0.0648
Y_2	1000	978.273	-0.0217
ε_1	0.1	0.120	0.2043
ε_2	0.1	0.103	0.0328
K_{swim}	0.001	0.00105	0.0595

Table 4.3: Comparing the original and recovered values of the parameters in q when $\alpha = 0.05$.

Another important feature of these results is the larger relative error in the optimized values for the half-saturation parameters $K_{I,1}$, $K_{I,2}$, $K_{R,1}$, and $K_{R,2}$. In the multi-species model, these parameters were chosen so that one species is a better light competitor while the other species is a better nutrient competitor. These parameters help determine the preferred depth these species reside in within the water column. The deviations presented in the recovered values compared to the original model values further highlights the importance that these parameters have on understanding phytoplankton population dynamics along side the more biologically obvious parameters such as the growth and loss rates.

Parameter	Original Value	Recovered Value	Relative Error
R_{in}	100	104.970	0.0497
h	0.01	0.0102	0.0185
I_{in}	1400	1498.81	0.0706
a_{bg}	0.35	0.344	-0.0169
a_1	1.0×10^{-5}	1.037×10^{-5}	0.0371
a_2	1.0×10^{-5}	1.029×10^{-5}	0.0285
r_1	0.4	0.430	0.0750
r_2	0.4	0.418	0.0456
m_1	0.2	0.218	0.0904
m_2	0.1	0.105	0.0518
$K_{R,1}$	1	1.085	0.0846
$K_{R,2}$	10	10.709	0.0709
$K_{I,1}$	50	52.939	0.0588
$K_{I,2}$	5	5.537	0.1074
Y_1	1000	1074.19	0.0742
Y_2	1000	1033.74	0.0337
ε_1	0.1	0.107	0.0724
ε_2	0.1	0.105	0.0481
K_{swim}	0.001	0.00105	0.0482

Table 4.4: Comparing the original and recovered values of the parameters in q for $\alpha = 0.1$.

Preferential Nutrient Uptake Model

In this application, $q \in \mathbb{R}^{26}$ is a vector of the form

$$\begin{aligned} q =& [R_{in_1}, R_{in_2}, h, I_{in}, a_{bg}, a_1, a_2, r_1, r_2, m_1, m_2, K_{R_1,1}, K_{R_1,2}, K_{R_2,1}, \\ & K_{R_2,2}, K_{I,1}, K_{I,2}, Y_1, Y_2, \varepsilon_{1,1}, \varepsilon_{1,2}, \varepsilon_{2,1}, \varepsilon_{2,2}, K_{swim}, \lambda, n]^T, \end{aligned}$$

and

$$\begin{aligned} Y(t;q) =& \frac{z_b}{2}\left[\sum_{k=1}^{N}(b_1(w_{k+1},t,q)+b_1(w_k,t,q)) + \sum_{k=1}^{N}(b_2(w_{k+1},t,q)+b_2(w_k,t,q))\right] \\ \approx & \int_0^{z_b}(b_1(w,t,q)+b_2(w,t,q))dw, \end{aligned} \tag{4.5}$$

as before with the multi-species Klausmeier and Litchman model. Note that the diffusion parameters D_{b_1}, D_{b_2}, D_{R_1}, D_{R_2} and the swimming speeds $\nu_{1_{max}}$ and $\nu_{2_{max}}$ were excluded

from the parameter vector. As stated before, this exclusion was made due to issues with numerical stability of the solution to the model.

Solving the parameter estimation problem, model simulations with 5% and 10% noise were generated. Each parameter in q was augmented by 5% from the reported values in literature and was used as an initial guess in the optimization routine. The results of solving the inverse problem with $\alpha = 0.05$ and $\alpha = 0.1$ are given in Tables 4.5 and 4.6.

Parameter	Original Value	Recovered Value	Relative Error
R_{in_1}	150	174.386	0.1626
R_{in_2}	100	107.932	0.0793
h	0.01	0.00993	-0.0073
I_{in}	1400	1219.38	-0.1290
a_{bg}	0.15	0.156	0.0421
a_1	1.0×10^{-5}	1.18×10^{-5}	0.1796
a_2	1.0×10^{-4}	9.49×10^{-5}	-0.0505
r_1	0.4	0.375	-0.0619
r_2	0.4	0.408	0.0189
m_1	0.2	0.203	0.0156
m_2	0.1	0.099	-0.0078
$K_{R_1,1}$	1	0.775	-0.2250
$K_{R_1,2}$	1	1.052	0.0518
$K_{R_2,1}$	10	13.128	0.3128
$K_{R_2,2}$	10	7.720	-0.2280
$K_{I,1}$	50	77.521	0.5504
$K_{I,2}$	5	5.183	0.0366
Y_1	1000	975.930	-0.0241
Y_2	1000	1080.346	0.0803
$\varepsilon_{1,1}$	0.1	0.107	0.0656
$\varepsilon_{2,1}$	0.1	0.0870	-0.1310
$\varepsilon_{1,2}$	0.1	0.098	-0.0190
$\varepsilon_{2,2}$	0.1	0.138	0.3782
K_{swim}	0.001	0.00088	-0.1235
λ	0.8	1.046	0.3069
n	4	3.905	-0.0238

Table 4.5: Comparing the original and recovered values of the parameters in q for $\alpha = 0.05$.

Overall, the two parameter estimation problems give estimated parameters that are close to the true values with error of 4.15% and 8.32% error for $\alpha = 0.05$ and $\alpha = 0.1$ respectively. The parameters with the largest relative error in both estimation problems were a_1, $K_{R_1,1}$,

Parameter	Original Value	Recovered Value	Relative Error
R_{in_1}	150	156.262	0.0417
R_{in_2}	100	108.142	0.0814
h	0.01	0.00840	-0.1602
I_{in}	1400	1452.37	0.0374
a_{bg}	0.15	0.168	0.1172
a_1	1.0×10^{-5}	3.71×10^{-6}	-0.6292
a_2	1.0×10^{-4}	9.89×10^{-5}	-0.0112
r_1	0.4	0.403	0.0063
r_2	0.4	0.419	0.0480
m_1	0.2	0.201	0.0074
m_2	0.1	0.100	0.0039
$K_{R_1,1}$	1	1.144	0.1438
$K_{R_1,2}$	1	0.875	-0.1247
$K_{R_2,1}$	10	10.539	0.0539
$K_{R_2,2}$	10	9.968	-0.0032
$K_{I,1}$	50	92.603	0.8521
$K_{I,2}$	5	4.806	-0.0388
Y_1	1000	1108.37	0.1084
Y_2	1000	1124.76	0.1248
$\varepsilon_{1,1}$	0.1	0.113	0.1279
$\varepsilon_{2,1}$	0.1	0.091	-0.0924
$\varepsilon_{1,2}$	0.1	0.108	0.0816
$\varepsilon_{2,2}$	0.1	0.108	0.0842
K_{swim}	0.001	0.0010	0.0012
λ	0.8	1.084	0.3548
n	4	4.776	0.1940

Table 4.6: Comparing the original and recovered values of the parameters in q for $\alpha = 0.1$.

$K_{I,1}$, and λ . While the optimized values differ from the true value, they are within the reported ranges in the literature and are biologically feasible. The parameters a_1, $K_{R_1,1}$, and $K_{I,1}$ are species dependent and can have a wide range of values [49].

Further, while there are ways to empirically determine the algal attenuation coefficients and light and nutrient saturation constants in a laboratory setting, the experiments are time consuming and can be expensive. The parameter λ is dependent on the relationship between the two nutrients and can include factors such as which nutrient is more limiting in the environment (important in estuaries when comparing the availability of phosphorous and nitrogen) and which one is more energetically efficient to uptake (important in ma-

rine environments when comparing different forms of nitrogen uptake such as nitrate and ammonium).

4.2 Global Sensitivity Analysis

Beyond parameter identifiability, another important aspect of a model's parameter space is measuring how parameters interact to influence the dynamics of the model. Various methods such as local sensitivity analysis, global sensitivity analysis and Bayesian methods are available to test how important parameters and groups of parameters are to model dynamics [55].

Global sensitivity analysis has an advantage over Bayesian methods since these methods tend to not require prior information which is needed for a Bayesian approach and are only dependent on the structure of the model itself. Two common measures for global sensitivity analysis are given by Morris screening and Sobol decomposition [55]. The Sobol decomposition is a variance based method which is sensitive to the size of the parameter space and the complexity of the model. Screening methods provide an alternative for identifying critical parameters and are able to generally provide a ranking for parameters in terms of importance. However, unlike the variance based methods, screening methods are not able to quantify how much more important one parameter is compared to another [55].

4.2.1 The Morris Screening Procedure

Consider the model $y = f(q)$ where $q = [q_1, \ldots, q_n]$ is the set of parameters scaled such that $q_i \in [0, 1]$. To construct the Morris screening, partition $[0, 1]$ into ℓ-levels. Then the elementary effect associated with the i-th input is given by the difference quotient

$$d_i(q) = \frac{f(q_1, \ldots, q_{i-1}, q_i + \Delta, \ldots, q_n) - f(q_1, \ldots, q_n)}{\Delta} = \frac{f(q + \Delta e_i) - f(q)}{\Delta} \tag{4.6}$$

where the step size Δ is chosen from the set

$$\Delta \in \left\{ \frac{1}{\ell - 1}, \ldots, 1 - \frac{1}{\ell - 1} \right\} = \Gamma_\ell. \tag{4.7}$$

The elementary effects d_i approximate large scale, local sensitivity at the point q. The step size is taken large to cover the entire parameter space. For r sample points, the sensitivity measures for q_i are the sample mean and the sample variance given by

$$\mu_i^* = \frac{1}{r} \sum_{j=1}^{r} |d_i^j(q)| \tag{4.8}$$

and

$$\sigma_i^2 = \frac{1}{r-1} \sum_{j=1}^{r} \left(d_i^j(q) - \frac{1}{r} \sum_{j=1}^{r} d_i^j(q) \right)^2, \tag{4.9}$$

where

$$d_i^j = \frac{f(q^j + \Delta e_i) - f(q^j)}{\Delta} \tag{4.10}$$

is the elementary effect associated with the i-th parameter in the j-th sample [55]. The mean quantifies the individual impact that a parameter has on the output while the variance estimates the effects of interactions with other inputs. As with the parameter estimation problem, the Morris screening procedure was performed on the Klausmeier and Litchman model, the multi-species variant of their model, and the proposed model incorporating preferential nutrient uptake. Of particular interest are the different parameters that will be identified as significant as more complex biological dynamics are introduced to the models and what parameters, if any, are consistently identified.

The Klausmeier and Litchman Model

In this application, $q \in \mathbb{R}^{15}$ is a vector of the form

$$q = [R_{in}, h, I_{in}, a_{bg}, a, D_R, D_b, \nu_{max}, r, m, K_R, K_I, Y, \varepsilon, K_{swim}]^T.$$

Note that unlike the parameter estimation problem, the diffusion coefficients and the swimming speed are included. When implementing this procedure, ℓ was chosen sufficiently large ($\ell = 10$) and was done 50 times before constructing μ and σ^2.

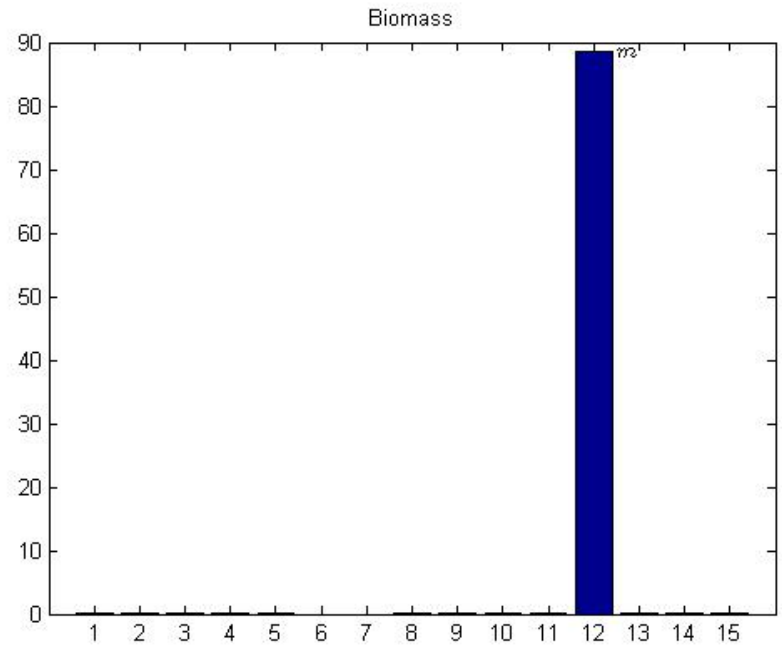

Figure 4.1: Morris screening results for the phytoplankton biomass. Parameters in the q vector are on the horizontal axis in order as listed in the vector. The averages μ_i are displayed on the vertical axis.

Examining Figure 4.1, we immediately see that for $b(z,t)$ the most important parameter in q is q_{12} which corresponds to the mortality coefficient m. Based on theoretical analysis of this model in [11], [12], [13], and [25], this result is consistent since the death rate impacts the existence of unique positive steady state solutions to the system. It can be further shown that when the death rate is above a critical level, then the solution of the biomass equation converges to 0 uniformly as $t \to \infty$ [14].

For the limiting nutrient $R(z,t)$, the Morris screening procedure highlights a different set of parameters for consideration. As can be seen in Figure 4.2, the parameters now highlighted by the procedure are $q_1,\ q_2,\ q_{10},\ q_{13},$ and q_{14} which correspond to the parameters $R_{in},\ h,\ m,\ Y,$ and ε. As with the biomass, the parameter m also makes an appearance as

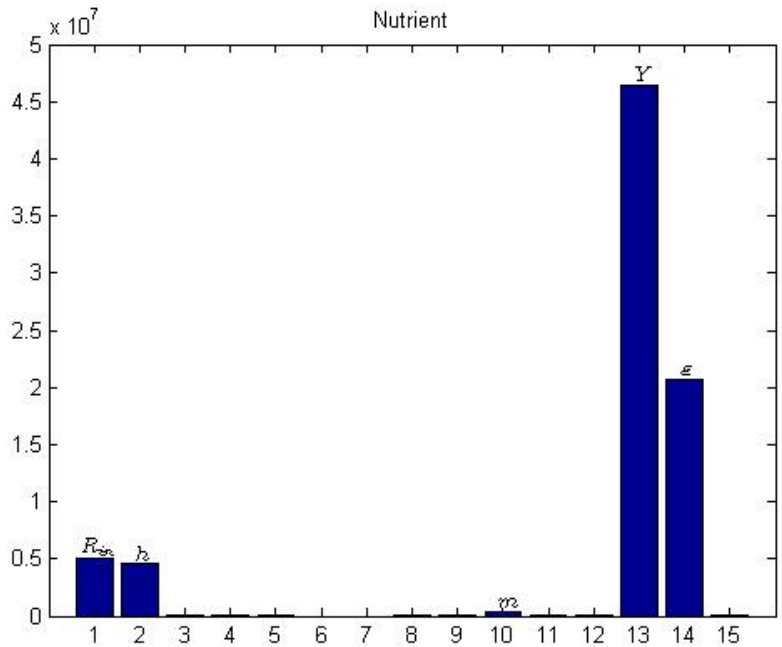

Figure 4.2: Morris screening results for the liming nutrient. Parameters in the q vector are on the horizontal axis in order as listed in the vector. The averages μ_i are displayed on the vertical axis.

an important parameter. However, compared to the other four parameters present, it is the least important. The remaining parameters are all connected with terms used to model the nutrient dynamics. R_{in} and h are parameters in the boundary term at $z = z_b$ which corresponds to nutrients in the sediment layer that are able to released into the water column. The parameter Y, the yield coefficient, relates to how much nutrient a cell is able to uptake while the parameter ε is the recycling coefficient and relates to the proportion of nutrient released back into the environment upon cell death. These parameters are consistent with biological intuition about the system.

Ranking of the top 5 parameters for $b(z,t)$ and $R(z,t)$ are given in Table 4.7. An important note is that D_R, D_b, and K_R had a mean of 0 under the Morris screening. This indicates that these parameters are not influential for the model and can be fixed in subsequent model sensitivity analysis, and uncertainty quantification to reduce model complexity [55].

Ranking	$b(z,t)$	$R(z,t)$
1	m	Y
2	I_{in}	ε
3	r	R_{in}
4	a_{bg}	h
5	K_I	m

Table 4.7: Ranking the top 5 most important parameters in q from the Morris screening.

Multi-species Klausmeier and Litchman Model (N=2)

In this application, $q \in \mathbb{R}^{24}$ is a vector of the form

$$q = [R_{in}, h, I_{in}, a_{bg}, a_1, a_2, D_R, D_{b_1}, D_{b_2}, \nu_{1_{max}}, \nu_{2_{max}}, r_1, r_2, m_1, m_2, K_{R,1}, K_{R,2}, K_{I,1}, K_{I,2}, Y_1, Y_2, \varepsilon_1, \varepsilon_2, K_{swim}]^T.$$

Note the diffusion coefficients and the swimming speeds are included in this procedure. When implementing this procedure, ℓ was chosen sufficiently large (ℓ=10) and was done 50 times before constructing μ and σ^2.

Examining Figure 4.3, we can see immediately that for $b_1(z,t)$ the most important parameters in q are q_4, q_{18}, and q_{15} which correspond to the parameters a_{bg}, $K_{I,1}$, and m_2 respectively. In contrast to the single species model, in the Morris screening results, the parameters highlighted by that procedure for b_1 as being significant were a_{bg} and $K_{I,1}$-parameters relating to light absorption and light utilization by the first phytoplankton species. This is consistent with how the model was parameterized originally: the parameters were chosen such that $K_{I,2} < K_{I,1}$, $K_{R,1} < K_{R,2}$, and $m_1 \neq m_2$ so that the first species has a growth rate with proportionally larger requirement on light availability, the second species has a growth rate with proportionally larger requirement on nutrient availability, and we exclude the possibility of the principle of competitive exclusion resulting in the extinction of one of the phytoplankton species. Also of note, it is the mortality rate of the second species m_2 rather than m_1 which is highlighted as important for species 1. This is consistent with the

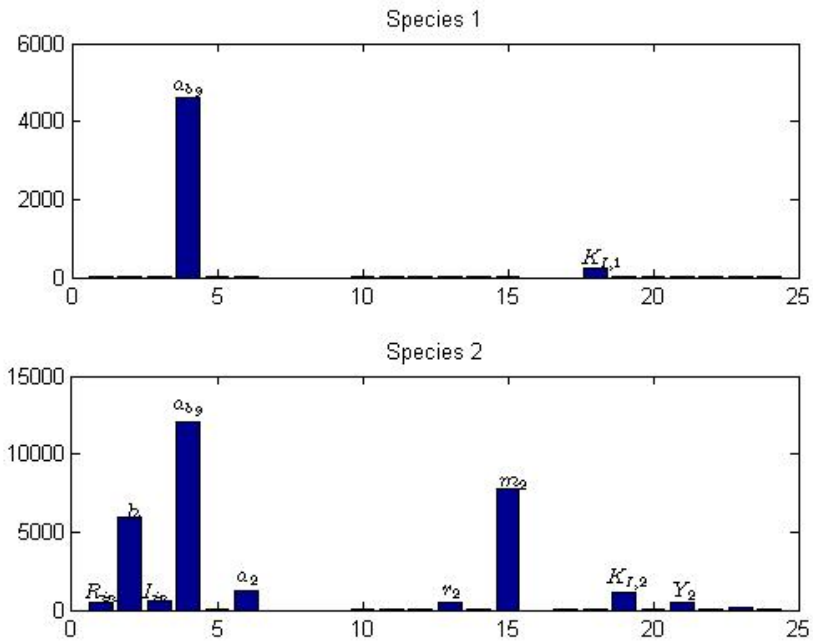

Figure 4.3: Morris screening results for the phytoplankton biomass by species. Parameters in the q vector are on the horizontal axis in order as listed in the vector. The averages μ_i are displayed on the vertical axis.

hypothesis that coexistence in spatially variable habitats can result from a growth based trade-off [26], [53],[56], [63].

Indeed, when examining Figure 4.3 for $b_2(z,t)$ we see immediately that the most important parameters in q are q_4, q_{15}, q_2, q_6, and q_{19} which correspond to a_{bg}, m_2, h, a_2, and $K_{I,2}$, respectively. While m_2 is a natural candidate for parameter importance for $b_2(z,t)$ since it corresponds to the death rate of the second species, the most important parameter highlighted by the Morris screening was the background attenuation coefficient a_{bg}. This term appears in Equation (2.21) and it accounts for light absorbed by inorganic sediments. Since the parameters were chosen in such a way that the second species would require proportionally less light than nutrients, the importance in how much light is absorbed throughout the depth of the water column further highlights the importance of light dynamics in phytoplankton populations. This is further reinforced by the appearance of the attenuation coefficient a_2 and the half-saturation constant $K_{I,2}$. Finally, given the model parametrization, the im-

portance of the parameter h is consistent with phytoplankton which reside deeper in the water column close to the sediment layer where nutrients are able to be introduced into the environment as the second species is constructed.

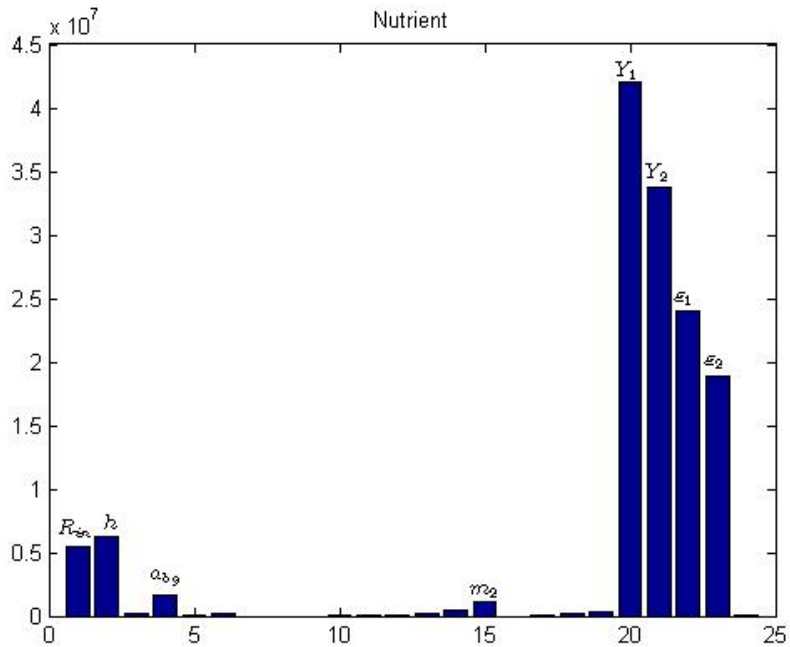

Figure 4.4: Morris screening results for the limiting nutrient. Parameters in the q vector are on the horizontal axis in order as listed in the vector. The averages μ_i are displayed on the vertical axis

For the limiting nutrient $R(z,t)$, the Morris screening procedure highlights a different group of parameters for importance from the biomass but consistent with the results from the one species model. Examining Figure 4.4 we see that the most important parameters in q are q_{20}, q_{21}, q_{22}, q_{23}, q_2, and q_1 which correspond to the parameters Y_1, Y_2, ε_1, ε_2, h, and R_{in} respectively. These parameters are consistent with the construction of $R(z,t)$ since they all appear in Equations (2.19) and (2.20). From physical considerations, h and R_{in} are logical since it describes how nutrients enter the water column from the sediment layer at the bottom: the more porous the sediment layer is and the more nutrient rich the sediment is, the more nutrients will diffuse into the water column. Physiologically, ε_1 and ε_2 have a similar relationship. While ε_1, $\varepsilon_2 \in [0,1]$, the closer to 1 these parameters are, the larger the

portion of nutrients are released into the environment upon phytoplankton death.

Ranking	$b_1(z,t)$	$b_2(z,t)$	$R(z,t)$
1	a_{bg}	a_{bg}	Y_1
2	$K_{I,1}$	m_2	Y_2
3	m_2	h	ε_1
4	$\nu_{1_{max}}$	a_2	ε_2
5	m_1	$K_{I,2}$	h

Table 4.8: Ranking the top 5 most important parameters in q from the Morris screening.

The top 5 parameter rankings for $b_1(z,t)$, $b_2(z,t)$, and $R(z,t)$ are given in Table 4.8 above. One interesting feature to note is that for all three equations the parameters D_{b_1}, D_{b_2}, D_R, $K_{R,1}$, and $K_{R,2}$ had a mean of 0 under the Morris screening. This would indicate that these parameters are not influential for the model and can be fixed in subsequent model calibration, sensitivity analysis, and uncertainty quantification to reduce model complexity [55].

Preferential Nutrient Uptake Model

In this application, $q \in \mathbb{R}^{32}$ is a vector of the form

$$\begin{aligned} q =&[R_{in_1}, R_{in_2}, h, I_{in}, a_{bg}, a_1, a_2, D_{R_1}, D_{R_2}, D_{b_1}, D_{b_2}, \nu_{1_{max}}, \nu_{2_{max}}, \\ &r_1, r_2, m_1, m_2, K_{R_1,1}, K_{R_1,2}, K_{R_2,1}, K_{R_2,2}, K_{I,1}, K_{I,2}, Y_1, Y_2, \\ &\varepsilon_{1,1}, \varepsilon_{1,2}, \varepsilon_{2,1}, \varepsilon_{2,2}, K_{swim}, \lambda, n]^T. \end{aligned}$$

Note the diffusion coefficients and the swimming speeds are included in this procedure. When implementing this procedure, ℓ was chosen sufficiently large (ℓ=10) and was done 50 times before constructing μ^* and σ^2.

Examining Figure 4.5 we see that the most important parameters for $b_1(z,t)$ in q are q_{17}, q_4, and q_{16} which correspond to the parameters m_2, I_{in}, and m_1 respectively. From a biological perspective, I_{in} and m_1 are expected as they represent incident light and the death rate of the first phytoplankton species respectively. For $b_2(z,t)$ we see that the most

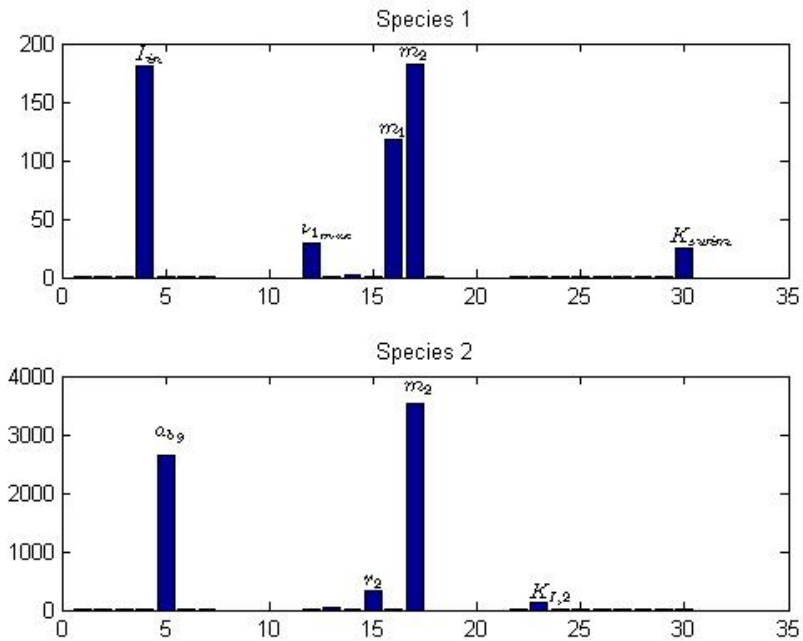

Figure 4.5: Morris screening results for the phytoplankton biomass by species. Parameters in the q vector are on the horizontal axis in order as listed in the vector. The averages μ_i^* are displayed on the vertical axis.

important parameters in q are q_{17}, q_5, and q_{15} which correspond to the parameters m_2, a_{bg} and r_2 respectively.

The parameter m_2, representing the loss rate of species 2, was chosen so that the principle of competitive exclusion would not hold allowing for the coexistence of the two phytoplankton species in the model simulations. For that reason its importance for b_1 and b_2 is expected. Having both I_{in} and a_{bg} being identified by the screening procedure emphasizes the importance of understanding how phytoplankton species compete and utilize light for coexistence.

For the nutrients $R_1(z,t)$ and $R_2(z,t)$ the Morris screening procedure highlights a different group of parameters for importance. Examining Figure 4.6 we see that the most important parameters in q for $R_1(z,t)$ are q_{25}, q_{27}, and q_8 which correspond to Y_2, $\varepsilon_{1,2}$, and r_2 respectively. In comparison, for $R_2(z,t)$ the parameters q_{25}, q_{29}, and q_{24} which correspond to Y_2, $\varepsilon_{2,2}$, and Y_1 are the top three ranked parameters. Given the assumptions of how the biomass groups were constructed – one species favoring light, the other favoring nutrients

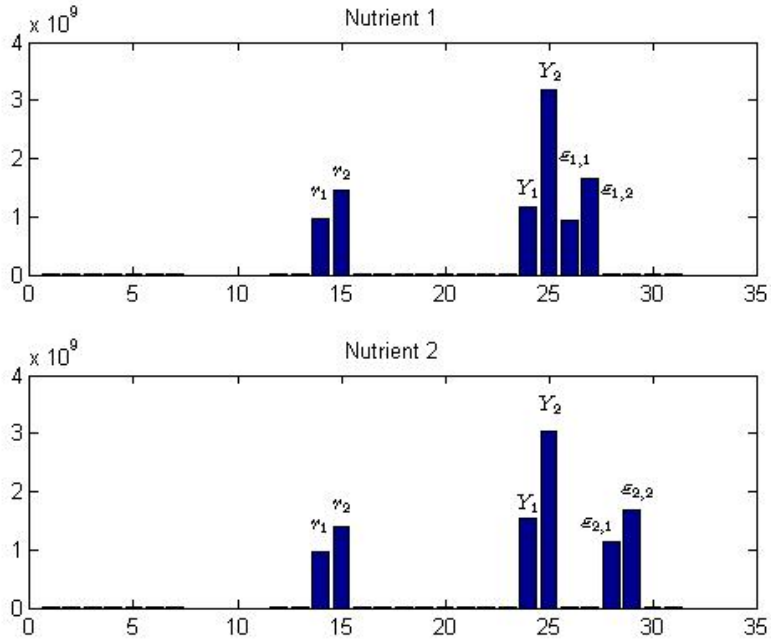

Figure 4.6: Morris screening results for the nutrients. Parameters in the q vector are on the horizontal axis in order as listed in the vector. The averages μ_i^* are displayed on the vertical axis

– the dependence on the amount of nutrient in each cell and how much of the preferred nutrient released upon cell death is biologically feasible to allow coexistence.

Parameter rankings for $b_1(z,t)$, $b_2(z,t)$, $R_1(z,t)$, and $R_2(z,t)$ are given in Table 4.9 below.

Ranking	$b_1(z,t)$	$b_2(z,t)$	$R_1(z,t)$	$R_2(z,t)$
1	m_2	m_2	Y_2	Y_2
2	I_{in}	a_{bg}	$\varepsilon_{1,2}$	$\varepsilon_{2,2}$
3	m_1	r_2	r_2	Y_1
4	$\nu_{1_{max}}$	$K_{I,2}$	Y_1	r_2
5	K_{swim}	$\nu_{2_{max}}$	r_1	$\varepsilon_{2,1}$

Table 4.9: Ranking the top 5 most important parameters in q from the Morris screening.

The diffusion parameters D_{b_1}, D_{b_2}, D_{R_1} and D_{R_2} as well as the shape parameter n all had a mean of 0 under the Morris screening. This indicates that these parameters are not influential for the model and can be fixed in subsequent model calibration, sensitivity analysis, and uncertainty quantification to reduce model complexity [55]. Other parameters that were highlighted such as swimming speeds and light half saturation constants further demonstrate

the importance of phytoplankton's potential abilities to regulate their position in bodies of water to adapt to various resource gradients.

4.2.2 The Sobol Decomposition

The construction of the Sobol decomposition is adapted from [55] and [62]. Consider the scalar valued non-linear model $Y = f(q)$ where $q = [q_1, q_2, \ldots, q_p]$ is defined so that the q_i are independent random variables uniformly distributed on $[0, 1]$. The Sobol indices are based on a second-order High Dimensional Model Representation (HDMR) given by

$$f(q) \approx f_0 + \sum_{i=1}^{p} f_i(q_i) + \sum_{1 \leq i < j \leq p} f_{ij}(q_i, q_j), \tag{4.11}$$

where f_0 is a constant, f_i is a function of q_i, f_{ij} is a function of q_i and q_j, etc.

Since the representation is not unique, constraints are placed to ensure uniqueness of the representation. This is accomplished by minimizing the functional

$$\mathcal{J} = \int_{[0,1]^p} \Big[f(q) - \Big(f_0 + \sum_{i=1}^{p} f_i(q_i) + \cdots + \sum_{i_1 < \cdots < i_s} f_{i_1 i_2 \ldots i_s}(q_{i_1}, q_{i_2}, \ldots, q_{i_s}) \Big) \Big]^2 dq \tag{4.12}$$

subject to

$$\int_0^1 f_{i_1 i_2 \ldots, i_s}(q_{i_1}, \ldots, q_{i_s}) dq_{i_k} = 0 \tag{4.13}$$

for $k = 1, \ldots, s$ and $s = 1, \ldots, p$ so that all the terms in the function decomposition are orthogonal. The component functions f_i and f_{ij} are given by

$$f_i = \int_{[0,1]^{p-1}} f(q) \; dq_{\sim i} \tag{4.14}$$

and

$$f_{ij} = \int_{[0,1]^{p-2}} f(q) \; dq_{\sim i,j}, \tag{4.15}$$

where the notation $dq_{\sim i}$ represents $dq_1, \ldots, dq_{i-1}, dq_{i+1}, \ldots, dq_p$.

The Sobol decomposition method uses the expansion given in equation (4.9) to quantify the contribution of each parameter to the variance of the response. The total variance of the response Y is defined by

$$D = \mathrm{Var}(Y) = \int_0^1 f^2(q)\ dq - f_0^2, \tag{4.16}$$

where f_0 is the mean response given by

$$f_0 = \int_0^1 f(q)\ dq. \tag{4.17}$$

To define the Sobol indices, we rewrite D as the sum of variances due to first-order and second-order parameter interactions by

$$D = \sum_{i=1}^{p} D_i + \sum_{1 \le i < j \le p} D_{ij}, \tag{4.18}$$

where

$$D_i = \int_0^1 f_i^2(q_i)\ dq_i \tag{4.19}$$

and

$$D_{ij} = \int_{[0,1]^2} f_{ij}^2(q_i, q_j)\ dq_i dq_j. \tag{4.20}$$

The Sobol indices are then defined by

$$S_i = \frac{D_i}{D}, \text{ and } S_{ij} = \frac{D_{ij}}{D}, \tag{4.21}$$

for $i, j = 1, \ldots, p$. The indices given by S_i are the first-order sensitivity indices and measure the contribution of the parameter q_i on the response variance, while the indices given by S_{ij} measure the interaction of parameters q_i and q_j on the response variance.

The computation of first and second-order indices requires $p + \frac{p(p-1)}{2}$ model responses. To

reduce the computational cost, total sensitivity indices S_{T_i} which quantify the total impact of a parameter q_i on the response are defined by

$$S_{T_i} = S_i + \sum_{j=1}^{p} S_{ij}. \tag{4.22}$$

As with the parameter estimation problem and the Morris screening procedure, the Sobol Decomposition was performed on the Klausmeier and Litchman model, the two species variant of their model, and the proposed model incorporating preferential nutrient uptake. Similarly to the Morris screening, of particular interest are the different parameters that will be identified as significant as more complex biological dynamics are introduced to the models and what parameters, if any, are consistently identified. In this application the vector q is the same as the vector used in the Morris screening.

The Klausmeier and Litchman Model

As with the Morris screening, for the biomass term $b(z,t)$, the main parameter of importance that is highlighted is the mortality coefficient m as shown in Figure 4.7. The consistency between both methods in accordance with the established theoretical analysis is significant as it indicates that these methods are able to consistently detect influential parameters.

The next most significant parameters identified by the Sobol decomposition method for this model are q_5, q_3, q_{12}, and q_9 which correspond to the parameters a, I_{in}, K_I, and r. However the order of magnitude for a is 10^{-7}, while the other parameters are of order of magnitude 10^{-8}. Unlike the Morris screening method which is able to give just an ordered ranking, the Sobol decomposition can determine that the mortality parameter m is much more significant since it has an order of magnitude of 10^{-1} which is significantly larger than the next highest ranked terms.

Unlike the biomass term where the global sensitivity analysis gave consistent results for ranking parameter importance, when the nutrient term $R(z,t)$ is analyzed additional

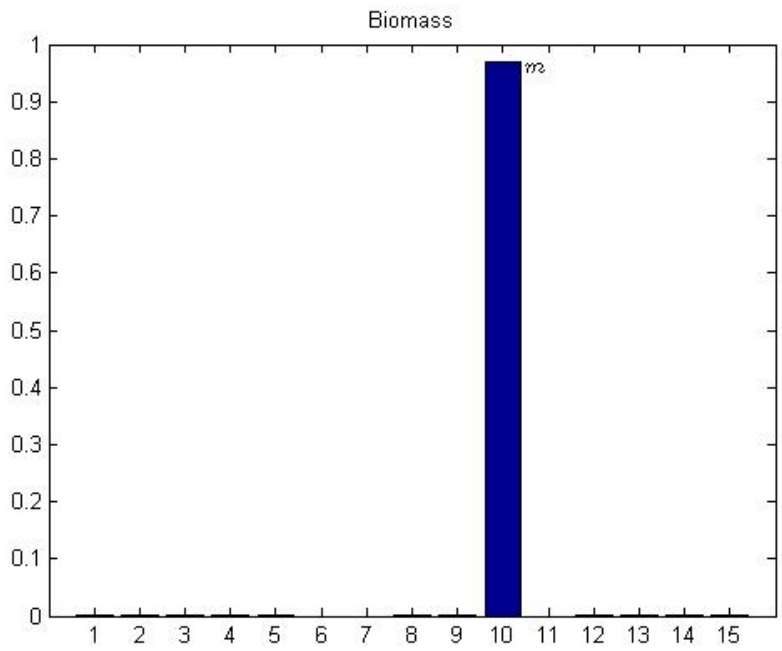

Figure 4.7: Sobol decomposition results for the biomass. Parameters in the q vector are on the horizontal axis in order as listed in the vector. The total sensitivity indices S_T are displayed on the vertical axis.

parameters are filtered out. In the Morris screening, the parameters R_{in}, h, m, Y, and ε were the top 5 parameters in ranking while in the Sobol decomposition the two parameters that are highlighted as significant are Y and ε as demonstrated in Figure 4.8. Under the Sobol decomposition, the parameter m is order of magnitude of 10^{-2} while the parameters R_{in} and h are both of order 10^{-8} which is significantly smaller than the rankings of Y and ε. While these parameters were all consistent with the biological intuition about the system, this result suggests that these parameters do not play as critical of a role in the overall dynamics of $R(z,t)$ in numerical simulations as compared to Y and ε.

As with the Morris screening, the parameters D_R, D_b, and K_R had a total sensitivity index of 0 for both the biomass and the nutrient terms. This carries the same interpretation as it did in the case of the Morris screening stated previously.

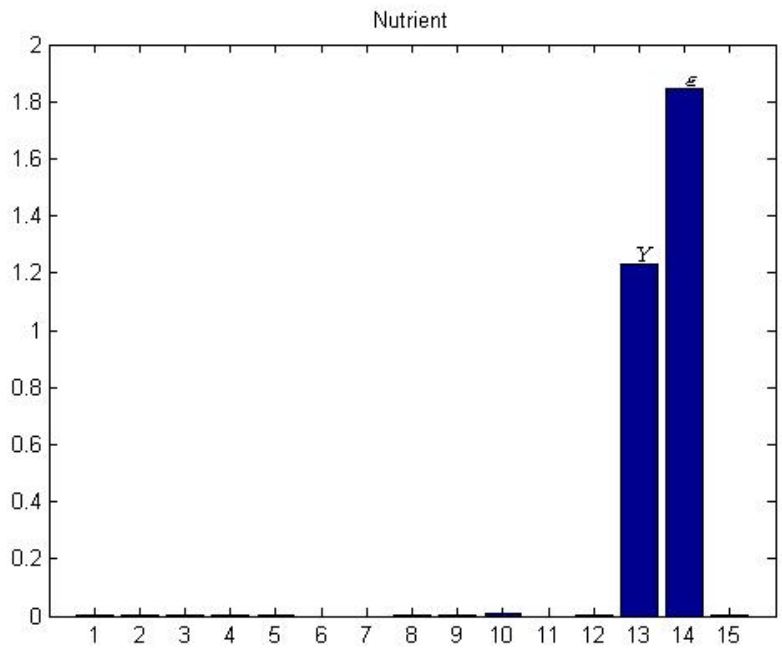

Figure 4.8: Sobol decomposition results for the limiting nutrient. Parameters in the q vector are on the horizontal axis in order as listed in the vector. The total sensitivity indices S_T are displayed on the vertical axis.

Multi-species Klausmeier and Litchman Model (N=2)

Unlike the Morris screening results presented in Figure 4.3, the Sobol decomposition results given in Figure 4.9 show that the mortality rates m_1 and m_2 have the largest impact on $b_1(z,t)$ and $b_2(z,t)$ respectively. The other parameters in the vector q have orders of magnitude 10^{-5} and lower for $b_1(z,t)$ and 10^{-6} and lower for $b_2(z,t)$. While the parameters that showed up in the Morris screening as being significant are among the next highest ranked in the Sobol decomposition, the difference in the order of magnitude is significant. This result is consistent with theoretical analysis of a related two species phytoplankton competition model considered in [13].

Similarly to the one species variant, when the multi-species Klausmeier and Litchman models parameter space is analyzed with the Sobol decomposition, the number of parameters identified as significant is filtered down to the yield coefficient Y_1 and Y_2 along with the

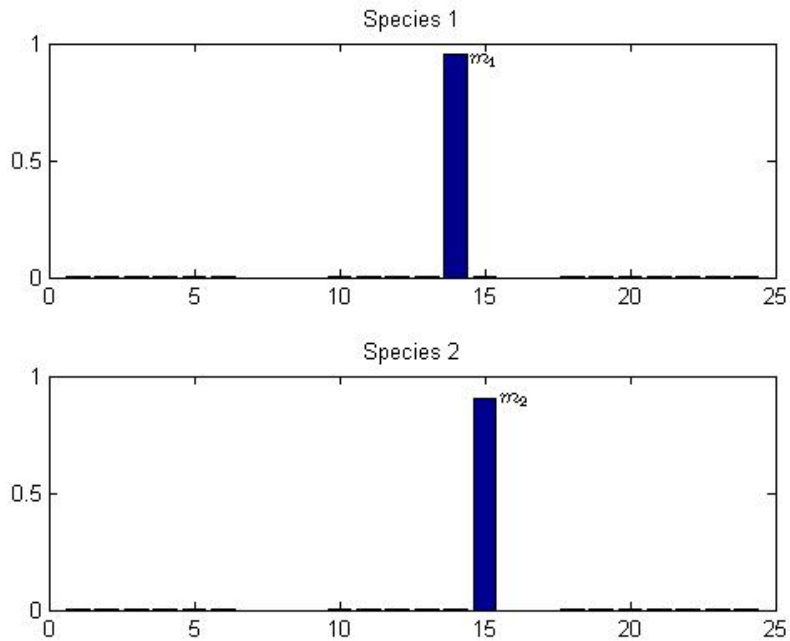

Figure 4.9: Sobol decomposition results for the phytoplankton biomass by species. Parameters in the q vector are on the horizontal axis in order as listed in the vector. The total sensitivity indices S_T are displayed on the vertical axis.

recycling coefficients ε_1 and ε_2 as seen in Figure 4.10. The parameters resulting from the boundary term at the sediment layer, R_{in} and h, have a total sensitivity index on the order of magnitude of 10^{-9} under this procedure. The mortality coefficient m_2 has a total sensitivity index order of magnitude of 10^{-5} and the background attenuation coefficient a_{bg} has a total sensitivity index of order 10^{-8} magnitude. These are significantly smaller than the rankings for the yield and recycling coefficients.

As with the single species variant, the diffusion parameters D_{b_1}, D_{b_2}, and D_R along with the nutrient half-saturation constants $K_{R,1}$ and $K_{R,2}$ have total sensitivity index of order 0 for all three components considered. As stated previously, this result has the same interpretation as it did in the Morris screening.

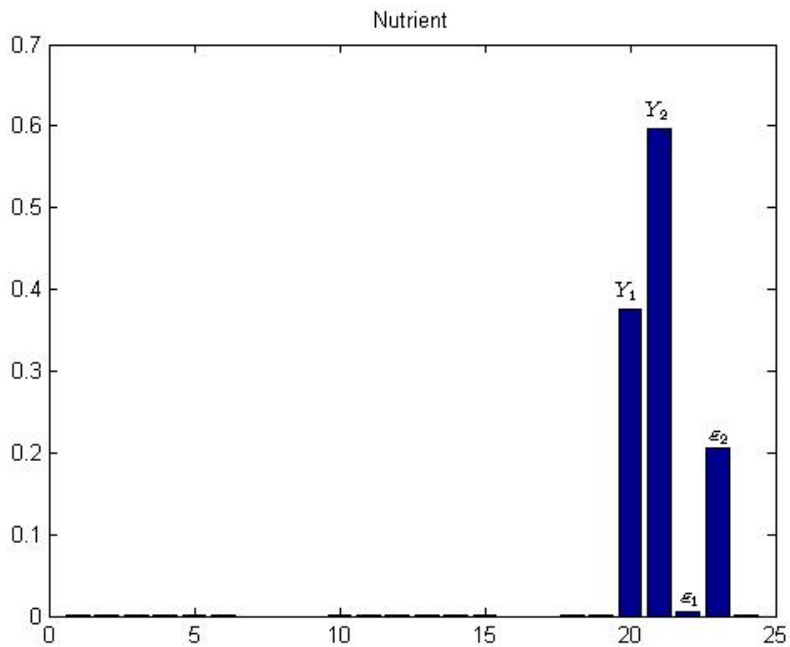

Figure 4.10: Sobol decomposition results for the phytoplankton biomass by species. Parameters in the q vector are on the horizontal axis in order as listed in the vector. The total sensitivity indices S_T are displayed on the vertical axis.

Preferential Nutrient Uptake Model

Unlike the Morris screening results presented in Figure 4.5, the Sobol decomposition results given in Figure 4.11 show that the loss rates m_1 and m_2 have the largest impact on $b_1(z,t)$ and $b_2(z,t)$ respectively. However, this result is consistent with the multi-species Klausmeier and Litchman model. This further highlights the importance these parameters have on the dynamics of the system which is similar to the role the parameter m has in the Klausmeier and Litchman model. The other parameters in the vector q had a sensitivity index S_T of orders of magnitude of 10^{-6} to 0 indicating there was little to no impact on the response variance. From a computational standpoint, this results is consistent to the numerical sensitivity the model has to the mortality coefficients.

The Sobol decomposition results for $R_1(z,t)$ and $R_2(z,t)$ are given in Figure 4.12. As with the Morris screening, the Sobol decomposition method identified the parameters Y_2,

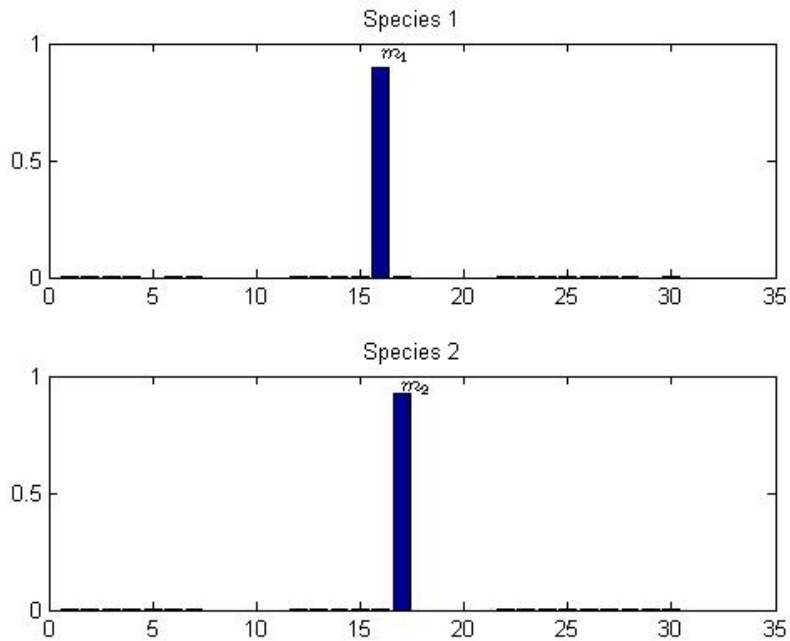

Figure 4.11: Sobol decomposition results for the phytoplankton biomass by species. Parameters in the q vector are on the horizontal axis in order as listed in the vector. The total sensitivity indices S_T are displayed on the vertical axis.

$\varepsilon_{1,2}$, Y_1 and r_2 as having the largest impact on $R_1(z,t)$ and the parameters Y_2, $\varepsilon_{2,2}$, Y_1 and r_2 on $R_2(z,t)$. While this method does identify the parameters r_2 and Y_1 having an impact on the response variance, it is less than what the Morris screening procedure indicates. These parameters are also consistent with the biological assumptions of the model since the growth rates r_1 and r_2 along with the yield coefficients Y_1 and Y_2 impact how much nutrient cells are drawing from the environment and can utilize while the recycling coefficients $\varepsilon_{1,1}, \varepsilon_{1,2}, \varepsilon_{2,1},$ and $\varepsilon_{2,2}$ represent proportions of each nutrient that is released back into the water column upon cell death. This is also consistent with both the single species and multi-species Klausmeier and Litchman models.

Overall, the analysis of the parameter spaces of all three models demonstrates that these class of models is well-suited for experimental data. In addition to having low total error, the inverse problems were able to be successfully solved as the size of the parameter space increased from the base case given by the Klausmeier and Litchman model to the most com-

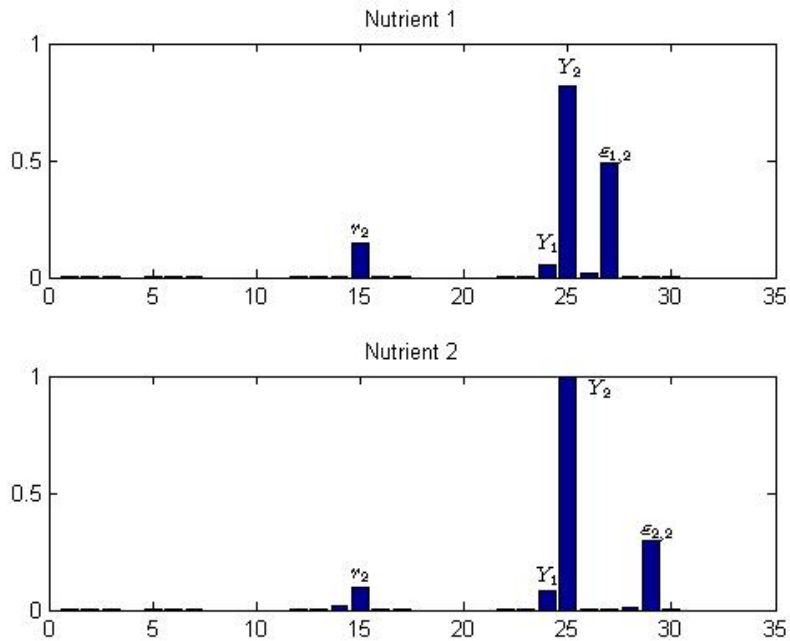

Figure 4.12: Sobol decomposition results for the nutrients. Parameters in the q vector are on the horizontal axis in order as listed in the vector. The total sensitivity indices S_T are displayed on the vertical axis.

plex case given by the proposed preferential uptake model. Further, for all three models, the only parameters which were excluded from the inverse problem were parameter affected the numerical stability of the solution. These results can be improved by removing parameters which can be easily measured from the parameter vector. The incident light parameter, I_{in}, used in all three models fits this requirement.

Additional restrictions to parameters used in the inverse problem can be made by using the insights from the global sensitivity analysis. Certain parameters that were estimated with higher relative error can be eliminated from the parameter vector if it does not show up in sensitivity screening. For example, the parameters K_I, K_R, and K_{swim} in the Klausmeier and Litchman model, the parameters r_2, $K_{R,1}$, and $K_{R,2}$ in the multi-species Klausmeier and Litchman model, and the parameters a_1, $K_{R_1,1}$, $K_{R_2,1}$, $K_{R_2,2}$, $K_{I,1}$, and λ are all parameters that fit this requirement.

Along with gaining insights reducing the complexity of the parameter estimation prob-

lem, the results of the global sensitivity analysis for all three models identify important parameters that govern the dynamics of the system. Given the large number of parameters present in the three models considered and the nonlinear interactions between parameters, it is advantageous to find theoretical approximations to these models which can determine both the location of phytoplankton layers as well as an approximation of the total biomass present. We go about this by considering a game theoretic approach where the depth of phytoplankton layers are treated as the strategy that is adopted. We then solve for the equilibrium distribution of the system.

5 The Evolutionary Stable Strategy

In [35] it is observed that as the swimming velocity ν_{max} increases, the phytoplankton biomass distributions go from a more uniform distribution ($\nu_{max} = 0$) to increasingly concentrated in thin layers. Dimensional analysis done on the Klausmeier and Litchman model shows that the width of a layer of phytoplankton swimming toward a preferred depth and mixed by diffusion processes is proportional to $\dfrac{D}{\nu_{max}}$. From the literature, order of magnitude estimates of these parameters are available. Swimming velocity ν_{max} ranges from 10^1 m d^{-1} to 10^2 m d^{-1} [49]. Typical diffusion coefficients range from $D = 10^1$ m^2 d^{-1} in poorly mixed hypolimnia in stratified water columns to $D = 10^3$ m^2 d^{-1} in well-mixed water columns [31]. Simulations of the Klausmeier and Litchman model (Equations (2.7) - (2.11)) as ν_{max} increases from 0 to 100 m d^{-1} are given in Figure 5.1.

The known parameter ranges imply that the thickness of a layer under poorly mixed conditions ranges from 0.1–1 m while a layer under well mixed conditions ranges from 10–100 m. Given the field observations of thin phytoplankton layers in poorly mixed water columns and the calculations above, Klausmeier and Litchman propose that the location of a layer of phytoplankton can be approximated by an infinitely thin layer in a game theoretical approach [35]. For the game theoretic approach, it is assumed that the phytoplankton form an infinitely thin layer at a depth z_l by setting $b(z) = B\delta_{z_l}(z)$, where $\delta_{z_l}(z)$ is a Dirac delta function and B is the total depth-integrated biomass. That is,

$$B = \int_0^{z_b} b(z)\ dz. \tag{5.1}$$

It is further assumed that active movement is sufficient to overcome biomass mixing $\left(\dfrac{D_b}{\nu_{max}} \ll z_b\right)$ so that $D_b = 0$ is set. From these assumptions, the game theoretic approach outlined in [35] is as follows. Given a layer at z_l, calculate the equilibrium biomass of phytoplankton and distribution of nutrients and light in the absence of movement and then

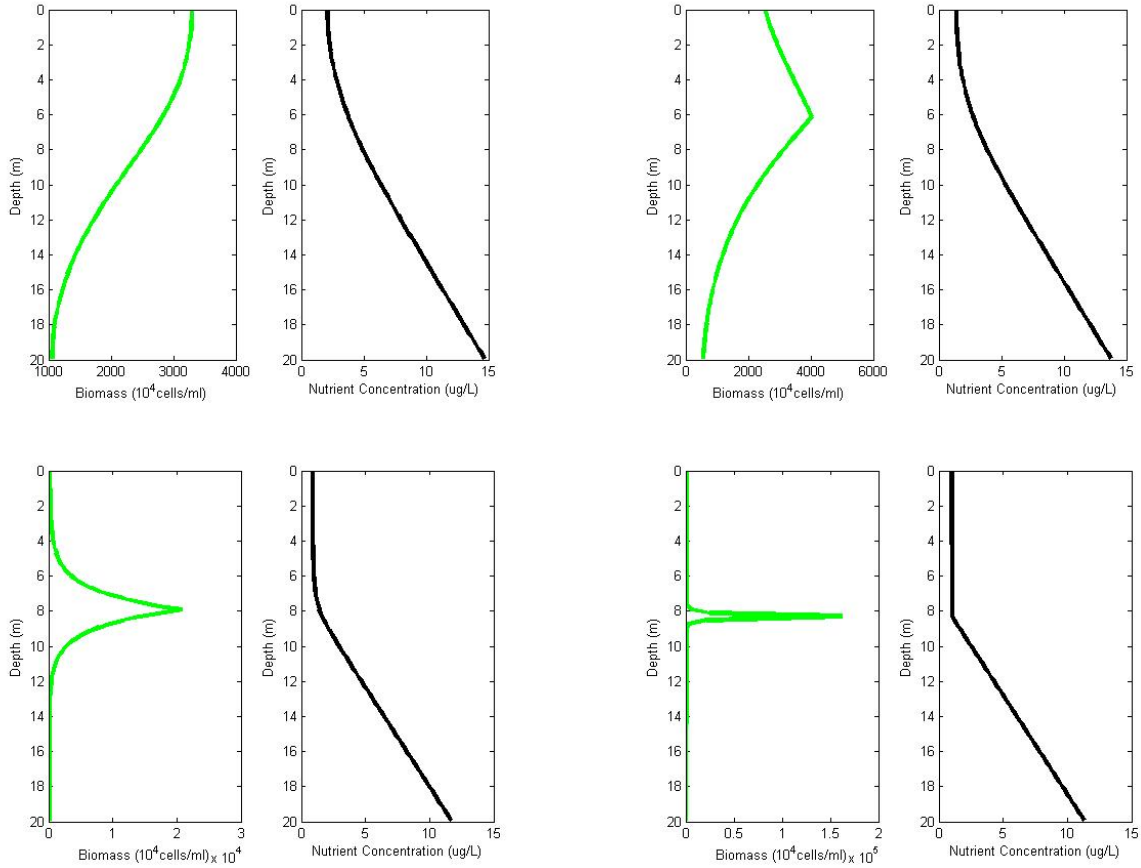

Figure 5.1: Model simulations of Equations (2.7) - (2.11) as ν_{max} increases from 0 m d^{-1} to 100 m d^{-1}. The upper left panel uses $\nu_{max} = 0$ m d^{-1}. The upper right panel uses $\nu_{max} = 1$ m d^{-1}. The lower left panel uses $\nu_{max} = 10$ m d^{-1}. The lower right panel uses $\nu_{max} = 100$ m d^{-1}.

determine whether net growth is possible above or below the layer at z_l. A strategy is said to be **evolutionarily stable** if, when the whole population is using this strategy, any small group of invaders using a different strategy will eventually die off over time [15]. Thus, the **Evolutionary Stable Strategy (ESS) depth**, $\mathbf{z}^\star$, is the depth of a layer that prevents phytoplankton from growing throughout the rest of the water column [18], [42]. Net growth, $g(z)$, fails when $g(z) \leq 0$ and occurs when there are insufficient nutrients, $R(z) \leq R^\star$, or because there is insufficient light, $I(z) \leq I^\star$, where $R^\star$ and $I^\star$ are the minimum nutrient and light levels necessary for growth to occur.

For the Klausmeier and Litchman model, when phytoplankton are absent ($b(z) = 0$), nutrients are uniformly distributed ($R(z) = R_{in}$) and light declines exponentially with depth

due to background attenuation ($I(z) = I_{in}e^{-a_{bg}z}$). Phytoplankton can grow if $R_{in} > R^\star$ and $I_{in} > I^\star$. These assumptions are assumed to be satisfied. Finally, the maximum depth at which phytoplankton can grow is determined by background attenuation of light and is given by

$$z_{max} = \frac{\ln\left(I_{in}/I^\star\right)}{a_{bg}}. \tag{5.2}$$

The equilibrium distributions of the Klausmeier and Litchman model for nutrient, light, and biomass are determined by the following system of equations:

$$0 = \hat{b}(z)\Big(\min\Big(f_I(\hat{I}(z)), f_R(\hat{R}(z))\Big) - m\Big), \tag{5.3}$$

$$0 = -\frac{\hat{b}(z)}{Y}\min\Big(f_I(\hat{I}(z)), f_R(\hat{R}(z))\Big) + D_R\frac{\partial^2\hat{R}}{\partial z^2} + \varepsilon m\frac{\hat{b}(z)}{Y}, \tag{5.4}$$

$$\left.\frac{\partial\hat{R}}{\partial z}\right|_{z=0} = 0, \tag{5.5}$$

$$\left.\frac{\partial\hat{R}}{\partial z}\right|_{z=z_b} = h\left(R_{in} - \hat{R}(z_b)\right), \tag{5.6}$$

$$\hat{I}(z) = I_{in}\exp\left(-\int_0^z (a\hat{b}(w) + a_{bg})\,dw\right). \tag{5.7}$$

Proposition 5.0.1. (The Equilibrium Distributions of $\hat{R}(z)$, $\hat{I}(z)$, and $\hat{B}$) *Assume that f_I and f_R are continuous functions in their respective variables. Then the solution to the system given by Equations (5.3) –(5.7) under the ESS assumptions is given by*

$$\hat{R}(z) = \begin{cases} \hat{R}(z_l), & 0 \le z \le z_l, \\ \hat{R}(z_l) + (z - z_l)\dfrac{R_{in} - \hat{R}(z_l)}{z_b + 1/h - z_l}, & z_l < z \le z_b, \end{cases} \tag{5.8}$$

$$\hat{I}(z) = \begin{cases} I_{in}e^{-a_{bg}z}, & 0 \le z < z_l, \\ I_{in}e^{-a\hat{B} - a_{bg}z}, & z \ge z_l, \end{cases} \tag{5.9}$$

and

$$\hat{B} = \begin{cases} \dfrac{YD_R(R_{in} - R^\star)}{m(1-\varepsilon)(z_b + 1/h - z_l)}, & \text{for a nutrient-limited layer,} \\ \\ \dfrac{\ln(I_{in}/I^\star)}{a} - \dfrac{a_{bg}}{a} z_l, & \text{for a light-limited layer,} \end{cases} \tag{5.10}$$

where

$$\hat{B} = \int_0^{z_b} \hat{b}(z)\, dz. \tag{5.11}$$

Theorem 5.0.2. (Existence of $z^\star$) *The ESS depth $z^\star$ is determined by*

$$\frac{\ln(I_{in}/I^\star)}{a} - \frac{a_{bg}}{a} z^\star = \frac{YD_R(R_{in} - R^\star)}{m(1-\varepsilon)(z_b + 1/h - z^\star)}, \tag{5.12}$$

which corresponds to the case of co-limitation in Equation (5.10). Further, $z^\star$ is convergence stable [16], [18]. That is, the ESS attracts solutions that do not start at the ESS. If $0 < z^\star < z_b$, the layer occurs within the water column and corresponds to a DCM. If $z^\star < 0$ then the layer is a light-limited surface layer and if $z^\star > z_b$ then the layer is a nutrient-limited benthic layer. This solution provides a stable equilibrium of the full model (Equations (2.7) –(2.11)) with $D_b = 0$ and $\nu(\partial g/\partial z)|_{z^\star} = 0$.

Corollary 5.0.3. (The Equilibrium Biomass $\hat{B}$ as a function of $z^\star$) *The equilibrium biomass can be expressed as a function of $z^\star$ as*

$$\hat{B} = \begin{cases} \dfrac{\ln(I_{in}/I^\star)}{a}, & z^\star \leq 0 \text{ (surface layer)} \\ \\ \dfrac{\ln(I_{in}/I^\star)}{a} - \dfrac{a_{bg}}{a} z^\star = \dfrac{YD_R(R_{in} - R^\star)}{m(1-\varepsilon)(z_b + 1/h - z^\star)}, & 0 < z^\star < z_b \text{ (DCM)} \\ \\ \dfrac{YD_R h}{m(1-\varepsilon)}(R_{in} - R^\star), & z^\star \geq z_b \text{ (benthic layer).} \end{cases} \tag{5.13}$$

In this chapter we will solve for the equilibrium distributions of the multi-species version of the Klausmeier and Litchman model in the case when $N = 2$ and the proposed preferential uptake model under the ESS assumptions. Conditions for the existence of the critical depths and convergence will be presented along with numerical demonstrations of increasingly thin layers as the swimming velocities are increased.

5.1 Multi-species Klausmeier and Litchman Model ESS

When $N = 2$ the multi-species Klausmeier and Litchman Model reduces to the following system of integro-partial differential equations:

$$\frac{\partial b_1}{\partial t} = \min\Big(f_{I,1}(I(z,t)), f_{R,1}(R(z,t))\Big)b_1 - m_1 b_1 + D_{b_1}\frac{\partial^2 b_1}{\partial t^2} + \frac{\partial}{\partial z}\left(\nu_1\left(\frac{\partial g_1}{\partial z}\right)b_1\right), \tag{5.14}$$

$$\frac{\partial b_2}{\partial t} = \min\Big(f_{I,2}(I(z,t)), f_{R,2}(R(z,t))\Big)b_2 - m_2 b_2 + D_{b_2}\frac{\partial^2 b_2}{\partial t^2} + \frac{\partial}{\partial z}\left(\nu_2\left(\frac{\partial g_2}{\partial z}\right)b_2\right), \tag{5.15}$$

$$\begin{aligned}\frac{\partial R}{\partial t} &= -\frac{b_1}{Y_1}\min\Big(f_{I,1}(I(z,t)), f_{R,1}(R(z,t))\Big) + \varepsilon_1 m_1\frac{b_1}{Y_1} - \frac{b_2}{Y_2}\min\Big(f_{I,2}(I(z,t)), f_{R,2}(R(z,t))\Big)\\ &+ \varepsilon_2 m_2\frac{b_2}{Y_2} + D_R\frac{\partial^2 R}{\partial z^2},\end{aligned} \tag{5.16}$$

$$I(z,t) = I_{in}\exp\left(\int_0^z (a_1 b_1(w,t) + a_2 b_2(w,t) + a_{bg})\, dw\right). \tag{5.17}$$

The boundary conditions for the partial differential equations are given by:

$$\left[D_{b_1}\frac{\partial b_1}{\partial z} + \nu_1\left(\frac{\partial g_1}{\partial z}\right)b_1\right]\Bigg|_{z=0} = \left[D_{b_1}\frac{\partial b_1}{\partial z} + \nu_1\left(\frac{\partial g_1}{\partial z}\right)b_1\right]\Bigg|_{z=z_b} = 0, \tag{5.18}$$

$$\left[D_{b_2}\frac{\partial b_2}{\partial z} + \nu_2\left(\frac{\partial g_2}{\partial z}\right)b_2\right]\Bigg|_{z=0} = \left[D_{b_2}\frac{\partial b_2}{\partial z} + \nu_2\left(\frac{\partial g_2}{\partial z}\right)b_2\right]\Bigg|_{z=z_b} = 0, \tag{5.19}$$

$$\frac{\partial R}{\partial z}\Bigg|_{z=0} = 0, \tag{5.20}$$

$$\frac{\partial R}{\partial z}\Bigg|_{z=z_b} = h(R_{in} - R(z_b)). \tag{5.21}$$

As shown in Figure 5.2 , when the swimming velocities $\nu_{1_{max}}$ and $\nu_{2_{max}}$ are increased from 0 m d^{-1} to 100 m d^{-1} (all other parameters are consistent with the values listed in Table 2.2), the phytoplankton distributions go from more uniform to increasingly more concentrated in thin layers. Thus, we can approximate the phytoplankton distributions by an infinitely thin layer using the game theoretic approach. To account for multiple species, we now assume that the phytoplankton form infinitely thin layers at depths z_{l_1} and z_{l_2} corresponding to the preferred depths that the species occupy based on their utilization of light and nutrients. Thus we set $b_1(z) = B_1\delta_{z_{l_1}}(z)$ and $b_2(z) = B_2\delta_{z_{l_2}}(z)$ where $\delta_{z_{l_1}}(z)$ and $\delta_{z_{l_2}}(z)$ are Dirac delta functions and B_1 and B_2 are the total depth-integrated biomasses. That is,

$$B_1 = \int_0^{z_b} b_1(z)\ dz, \tag{5.22}$$

and

$$B_2 = \int_0^{z_b} b_2(z)\ dz. \tag{5.23}$$

To find the ESS equilibrium distributions, we set the time derivatives of Equations (5.14) – (5.16) to 0, $D_{b_1} = D_{b_2} = 0$ (active movement is sufficient to overcome biomass mixing). Given layers at z_{l_1} and z_{l_2}, calculate the equilibrium biomasses and distributions of light and free nutrient in the absence of movement, and then determine whether net growth is possible outside of the layers at z_{l_1} and z_{l_2}. This results in the following system of equations:

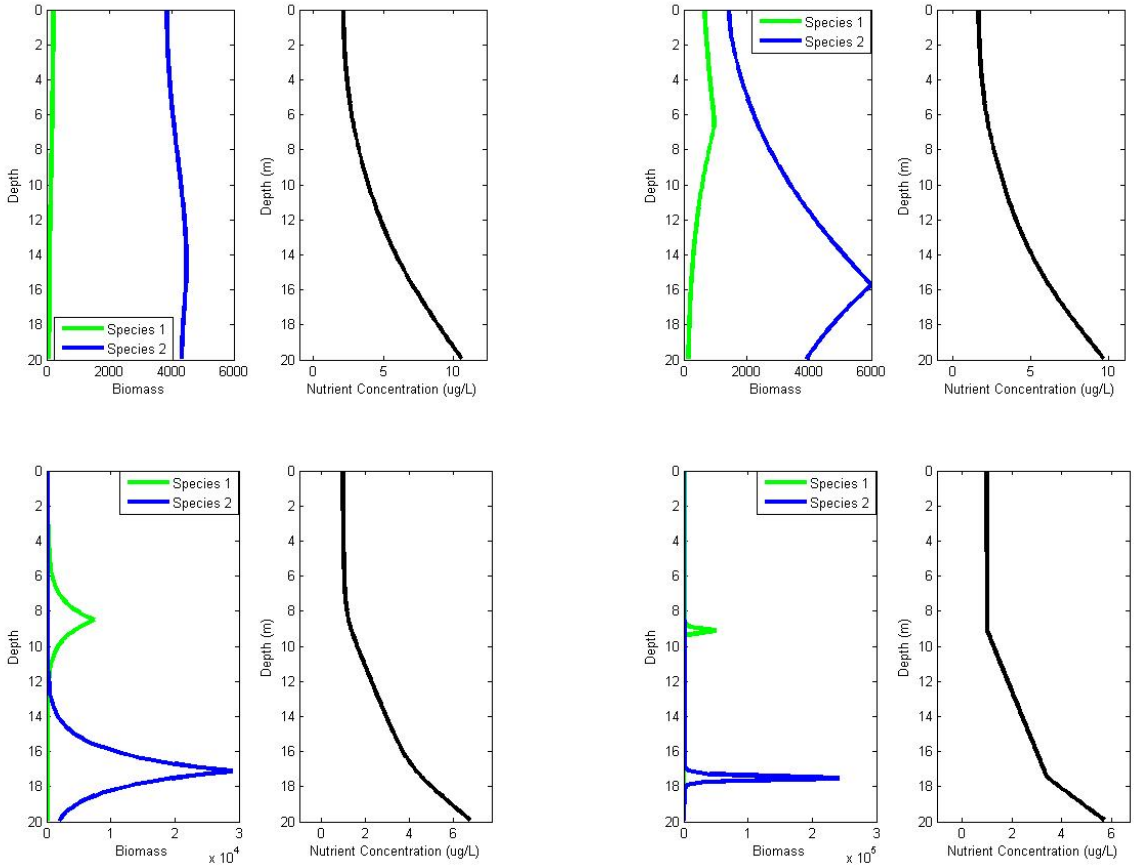

Figure 5.2: Model simulations of Equations (5.14) - (5.21) as $\nu_{1_{max}}$ and $\nu_{2_{max}}$ increases from 0 m d^{-1} to 100 m d^{-1}. The upper left panel uses $\nu_{1_{max}} = \nu_{2_{max}} = 0$ m d^{-1}. The upper right panel uses $\nu_{1_{max}} = \nu_{2_{max}} = 1$ m d^{-1}. The lower left panel uses $\nu_{1_{max}} = \nu_{2_{max}} = 10$ m d^{-1}. The lower right panel uses $\nu_{1_{max}} = \nu_{2_{max}} = 100$ m d^{-1}.

$$0 = \hat{b_1}(z)\Big(\min(f_{I,1}(\hat{I}(z)), f_{R,1}(\hat{R}(z))) - m_1\Big), \tag{5.24}$$

$$0 = \hat{b_2}(z)\Big(\min(f_{I,2}(\hat{I}(z)), f_{R,2}(\hat{R}(z))) - m_2\Big), \tag{5.25}$$

$$0 = -\frac{\hat{b_1}(z)}{Y_1}\min(f_{I,1}(\hat{I}(z)), f_{R,1}(\hat{R}(z))) + \varepsilon_1 m_1 \frac{\hat{b_1}(z)}{Y_1} - \frac{\hat{b_2}(z)}{Y_2}\min(f_{I,2}(\hat{I}(z)), f_{R,2}(\hat{R}(z)))$$
$$+ \varepsilon_2 m_2 \frac{\hat{b_2}(z)}{Y_2} + D_R \frac{\partial^2 R}{\partial z^2}, \tag{5.26}$$

$$\left.\frac{\partial \hat{R}}{\partial z}\right|_{z=0} = 0, \tag{5.27}$$

$$\left.\frac{\partial \hat{R}}{\partial z}\right|_{z=z_b} = h\left(R_{in} - \hat{R}(z_b)\right), \tag{5.28}$$

$$\hat{I}(z) = I_{in}\exp\left(-\int_0^z (a_1\hat{b_1}(w) + a_2\hat{b_2}(w) + a_{bg})\, dw\right). \tag{5.29}$$

The solution to the system of is given below.

Proposition 5.1.1. (The Equilibrium Distributions of $\hat{R}(z)$, $\hat{I}(z)$, $\hat{B}_1$, and $\hat{B}_2$) *Assume that $f_{I,1}$, $f_{I,2}$, $f_{R,1}$, and $f_{R,2}$ are continuous functions in their respective variables. Then the solution to the system of equations given by Equations (5.24) –(5.29) under the ESS assumptions is given by*

$$\hat{R}(z) = \begin{cases} \hat{R}(z_{l_1}), & 0 \le z \le z_{l_1}, \\ \hat{R}(z_{l_1}) + (z - z_{l_1})\dfrac{R_{in} - \hat{R}(z_{l_1})}{z_b + 1/h - z_{l_1}}, & z_{l_1} < z \le z_{l_2}, \\ \hat{R}(z_{l_2}) + (z - z_{l_2})\dfrac{R_{in} - \hat{R}(z_{l_2})}{z_b + 1/h - z_{l_2}}, & z_{l_2} < z \le z_b, \end{cases} \tag{5.30}$$

$$\hat{I}(z) = \begin{cases} I_{in}e^{-a_{bg}z}, & 0 \le z < z_{l_1}, \\ I_{in}e^{-a_1\hat{B}_1 - a_{bg}z}, & z_{l_1} \le z < z_{l_2}, \\ I_{in}e^{-a_1\hat{B}_1 - a_2\hat{B}_2 - a_{bg}z}, & z_{l_2} \le z \le z_b \end{cases} \tag{5.31}$$

$$\hat{B}_1 = \begin{cases} \dfrac{Y_1}{m_1(1-\varepsilon_1)}\left(\dfrac{D_R(R_{in}-R^\star)}{z_b + 1/h - z_{l_2}} - \dfrac{m_2(1-\varepsilon_2)}{Y_2}\hat{B}_2\right), & \text{for a nutrient-limited layer,} \\ \\ \dfrac{\ln(I_{in}/I_1^\star)}{a_1} - \dfrac{a_{bg}}{a_1}z_{l_1}, & \text{for a light-limited layer.} \end{cases} \tag{5.32}$$

and

$$\hat{B}_2 = \begin{cases} \dfrac{Y_2}{m_2(1-\varepsilon_2)}\left(\dfrac{D_R(R_{in}-R^\star)}{z_b + 1/h - z_{l_2}} - \dfrac{m_1(1-\varepsilon_1)}{Y_1}\hat{B}_1\right), & \text{for a nutrient-limited layer,} \\ \\ \dfrac{\ln(I_1^\star/I_2^\star)}{a_2} - \dfrac{a_{bg}}{a_2}(z_{l_2} - z_{l_1}), & \text{for a light-limited layer,} \end{cases} \tag{5.33}$$

where

$$\hat{B}_1 = \int_0^{z_b} \hat{b_1}(z)\ dz, \tag{5.34}$$

and

$$\hat{B}_2 = \int_0^{z_b} \hat{b_2}(z)\ dz. \tag{5.35}$$

Proof. Under the assumption of $b_1(z) = B_1\delta_{z_{l_1}}(z)$ and $b_2 = B_2\delta_{z_{l_2}}(z)$ with B_1 and B_2 as

given in Equations (5.22) and (5.23), Equation (5.26) becomes

$$\frac{\partial^2 \hat{R}}{\partial z^2} = 0,\ 0 \leq z < z_{l_1}, \tag{5.36a}$$

$$\frac{\partial^2 \hat{R}}{\partial z^2} = 0,\ z_{l_1} < z < z_{l_2}, \tag{5.36b}$$

$$\frac{\partial^2 \hat{R}}{\partial z^2} = 0,\ z_{l_2} < z \leq z_b. \tag{5.36c}$$

Now consider Equation (5.36a) with boundary condition (5.27):

$$\begin{cases} \dfrac{\partial^2 \hat{R}}{\partial z^2} = 0, & 0 \leq z < z_{l_1} \\ \\ \left.\dfrac{\partial \hat{R}}{\partial z}\right|_{z=0} = 0. \end{cases} \tag{5.37}$$

Equation (5.37) shows that the diffusion of nutrients equalizes the nutrient concentration above the layer at z_{l_1}. That is, $\hat{R}(z) = \hat{R}(z_{l_1})$ if $0 \leq z \leq z_{l_1}$. Equation (5.37) also implies that nutrients vary linearly below the layer at z_{l_1}, denoted by $z_{l_1}^+$, to z_{l_2}. Thus

$$\left.\frac{\partial \hat{R}}{\partial z}\right|_{z=z_{l_1}^+} = \left.\frac{\partial \hat{R}}{\partial z}\right|_{z=z_{l_2}} = \frac{\hat{R}(z_{l_2}) - \hat{R}(z_{l_1})}{z_{l_2} - z_{l_1}}. \tag{5.38}$$

Now consider Equation (5.36c) with boundary condition (5.28):

$$\begin{cases} \dfrac{\partial^2 \hat{R}}{\partial z^2} = 0, & z_{l_2} < z \leq z_b \\ \\ \left.\dfrac{\partial \hat{R}}{\partial z}\right|_{z=z_b} = h(R_{in} - \hat{R}(z_{l_2})). \end{cases} \tag{5.39}$$

Using the same argument as before, nutrients vary linearly below the layer at z_{l_2}, denoted by $z_{l_2}^+$, to z_b. Thus

$$\left.\frac{\partial \hat{R}}{\partial z}\right|_{z=z_{l_2}^+} = \left.\frac{\partial \hat{R}}{\partial z}\right|_{z=z_b} = \frac{\hat{R}(z_b) - \hat{R}(z_{l_2})}{z_b - z_{l_2}}. \tag{5.40}$$

From Equation (5.40) and Equation (5.28) we obtain

$$h(R_{in} - \hat{R}(z_b)) = \frac{\hat{R}(z_b) - \hat{R}(z_{l_2})}{z_b - z_{l_2}}. \tag{5.41}$$

Solving Equation (5.41) for $\hat{R}(z_b)$ yields

$$\hat{R}(z_b) = \frac{h(z_b - z_{l_2})R_{in} + \hat{R}(z_{l_2})}{1 + h(z_b - z_{l_2})}. \tag{5.42}$$

From Equations (5.40) and (5.42) it follows that

$$\left.\frac{\partial \hat{R}}{\partial z}\right|_{z=z_{l_2}^+} = \frac{\hat{R}(z_b) - \hat{R}(z_{l_2})}{z_b - z_{l_2}} = \frac{\dfrac{h(z_b - z_{l_2})R_{in} + \hat{R}(z_{l_2})}{1 + h(z_b - z_{l_2})} - \hat{R}(z_{l_2})}{z_b - z_{l_2}}$$

$$= \frac{h(R_{in} - \hat{R}(z_{l_2}))}{1 + h(z_b - z_{l_2})} = \frac{R_{in} - \hat{R}(z_{l_2})}{z_b + 1/h - z_{l_2}}. \tag{5.43}$$

Finally, consider (5.36b)

$$\frac{\partial^2 \hat{R}}{\partial z^2} = 0, \;\; z_{l_1} < z < z_{l_2}.$$

The boundary condition for this differential equation can be inferred to be

$$\left.\frac{\partial \hat{R}}{\partial z}\right|_{z=z_{l_2}} = \frac{\hat{R}(z_{l_2}) - \hat{R}(z_{l_1})}{z_{l_2} - z_{l_1}}. \tag{5.44}$$

Using Equations (5.43) and (5.44) we obtain

$$\frac{R_{in} - \hat{R}(z_{l_2})}{z_b + 1/h - z_{l_2}} = \frac{\hat{R}(z_{l_2}) - \hat{R}(z_{l_1})}{z_{l_2} - z_{l_1}}. \tag{5.45}$$

Solving Equation (5.45) for $\hat{R}(z_{l_2})$ gives

$$\hat{R}(z_{l_2}) = \frac{R_{in}(z_{l_2} - z_{l_1}) + \hat{R}(z_{l_1})(z_b + 1/h - z_{l_2})}{z_b + 1/h - z_{l_1}}. \tag{5.46}$$

Substituting the result of Equation (5.46) into Equation 5.44 and simplifying yields

$$\left.\frac{\partial \hat{R}}{\partial z}\right|_{z=z_{l_2}} = \frac{\hat{R}(z_{l_2}) - \hat{R}(z_{l_1})}{z_{l_2} - z_{l_1}} = \frac{\dfrac{R_{in}(z_{l_2} - z_{l_1}) + \hat{R}(z_{l_1})(z_b + 1/h - z_{l_2})}{z_b + 1/h - z_{l_1}} - \hat{R}(z_{l_1})}{z_{l_2} - z_{l_1}}$$

$$= \frac{\dfrac{(z_{l_2} - z_{l_1})(R_{in} - \hat{R}(z_{l_1}))}{z_b + 1/h - z_{l_1}}}{z_{l_2} - z_{l_1}} = \frac{R_{in} - \hat{R}(z_{l_1})}{z_b + 1/h - z_{l_1}}. \tag{5.47}$$

Thus we have shown that the equilibrium distribution for $\hat{R}(z)$ under the ESS assumptions is given by Equation (5.30)

$$\hat{R}(z) = \begin{cases} \hat{R}(z_{l_1}), & 0 \leq z \leq z_{l_1}, \\ \hat{R}(z_{l_1}) + (z - z_{l_1})\dfrac{R_{in} - \hat{R}(z_{l_1})}{z_b + 1/h - z_{l_1}}, & z_{l_1} < z \leq z_{l_2}, \\ \hat{R}(z_{l_2}) + (z - z_{l_2})\dfrac{R_{in} - \hat{R}(z_{l_2})}{z_b + 1/h - z_{l_2}}, & z_{l_2} < z \leq z_b, \end{cases}$$

as desired.

Now consider Equation (5.29)

$$\hat{I}(z) = I_{in} \exp\left(- \int_0^z (a_1 \hat{b_1}(w) + a_2 \hat{b_2}(w) + a_{bg})\, dw \right).$$

Under the assumption of $b_1(z) = B_1 \delta(z_{l_1})$ and $b_2 = B_2 \delta(z_{l_2})$ with B_1 and B_2 as given in Equations (5.22) and (5.23) it is straightforward to see that

$$\hat{I}(z) = \begin{cases} I_{in} e^{-a_{bg} z}, & 0 \leq z < z_{l_1}, \\ I_{in} e^{-a_1 \hat{B}_1 - a_{bg} z}, & z_{l_1} \leq z < z_{l_2}, \\ I_{in} e^{-a_1 \hat{B}_1 - a_2 \hat{B}_2 - a_{bg} z}, & z_{l_2} \leq z \leq z_b \end{cases}$$

due to the nature of the Dirac delta function used when evaluating the integral. Light declines with depth exponentially due to background attenuation and drops a finite amount at the layers due to attenuation by phytoplankton. Thus we have shown that the equilibrium distribution for $\hat{I}(z)$ under the ESS assumptions is given by Equation (5.31) as desired.

Now we will determine the equilibrium biomass. From Equations (5.24) and (5.25), we either have $\hat{b_1}(z) = 0$ and $\hat{b_2}(z) = 0$ or

$$\min\left(f_{I,1}(\hat{I}(z)), f_{R,1}(\hat{R}(z)) \right) = m_1 \tag{5.48}$$

and

$$\min\left(f_{I,2}(\hat{I}(z)), f_{R,2}(\hat{R}(z)) \right) = m_2. \tag{5.49}$$

However, $\hat{b_1}(z) = 0$ and $\hat{b_2}(z) = 0$ are trivial solutions with no phytoplankton in the water column so we assume Equations (5.48) and (5.49) hold. There are two cases to consider:

1. The layers are nutrient-limited so that $\hat{R}(z_{l_1}) = R^\star$, $\hat{R}(z_{l_2}) = R^\star$, $\hat{I}(z_{l_1}) > I_1^\star$ and $\hat{I}(z_{l_2}) > I_2^\star$.

2. The layers are light-limited so that $\hat{I}(z_{l_1}) = I_1^\star$, $\hat{I}(z_{l_2}) = I_2^\star$, $\hat{R}(z_{l_1}) > R^\star$, and $\hat{R}(z_{l_2}) > R^\star$.

First consider the case of nutrient limitation. We use Equations (5.48) and (5.49) in conjuction with Equation (5.26) to solve for $\hat{B}_1$ and $\hat{B}_2$:

$$0 = -\frac{\hat{b_1}(z)}{Y_1}\min(f_{I,1}(\hat{I}(z)), f_{R,1}(\hat{R}(z))) + \varepsilon_1 m_1 \frac{\hat{b_1}(z)}{Y_1} - \frac{\hat{b_2}(z)}{Y_2}\min(f_{I,2}(\hat{I}(z)), f_{R,2}(\hat{R}(z)))$$
$$+ \varepsilon_2 m_2 \frac{\hat{b_2}(z)}{Y_2} + D_R \frac{\partial^2 R}{\partial z^2},$$

$$0 = -\frac{\hat{b_1}(z)}{Y_1} m_1 + \varepsilon_1 m_1 \frac{\hat{b_1}(z)}{Y_1} - \frac{\hat{b_2}(z)}{Y_2} m_2 + \varepsilon_2 m_2 \frac{\hat{b_2}(z)}{Y_2} + D_R \frac{\partial^2 R}{\partial z^2},$$

$$\frac{m_1(1-\varepsilon_1)}{Y_1}\hat{b_1}(z) + \frac{m_2(1-\varepsilon_2)}{Y_2}\hat{b_2}(z) = D_R \frac{\partial^2 \hat{R}}{\partial z^2}. \tag{5.50}$$

Integrating both sides of (5.50) from 0 to z_b results in

$$\int_0^{z_b} \left(\frac{m_1(1-\varepsilon_1)}{Y_1}\hat{b_1}(z) + \frac{m_2(1-\varepsilon_2)}{Y_2}\hat{b_2}(z) \right) dz = \int_0^{z_b} \left(D_R \frac{\partial^2 \hat{R}}{\partial z^2} \right) dz,$$

$$\frac{m_1(1-\varepsilon_1)}{Y_1}\hat{B}_1 + \frac{m_2(1-\varepsilon_2)}{Y_2}\hat{B}_2 = D_R \frac{\partial \hat{R}}{\partial z}\bigg|_0^{z_b},$$

$$\frac{m_1(1-\varepsilon_1)}{Y_1}\hat{B}_1 + \frac{m_2(1-\varepsilon_2)}{Y_2}\hat{B}_2 = D_R h(R_{in} - \hat{R}(z_b)). \tag{5.51}$$

Rewriting this using Equation (5.43) we get

$$\frac{m_1(1-\varepsilon_1)}{Y_1}\hat{B}_1 + \frac{m_2(1-\varepsilon_2)}{Y_2}\hat{B}_2 = D_R \frac{R_{in} - \hat{R}(z_{l_2})}{z_b + 1/h - z_{l_2}}. \tag{5.52}$$

Thus we obtain the implicit solutions

$$\hat{B}_1 = \frac{Y_1}{m_1(1-\varepsilon_1)} \left(\frac{D_R(R_{in} - \hat{R}(z_{l_2}))}{z_b + 1/h - z_{l_2}} - \frac{m_2(1-\varepsilon_2)}{Y_2}\hat{B}_2 \right), \tag{5.53}$$

$$\hat{B}_2 = \frac{Y_2}{m_2(1-\varepsilon_2)}\left(\frac{D_R(R_{in}-\hat{R}(z_{l_2}))}{z_b+1/h-z_{l_2}} - \frac{m_1(1-\varepsilon_1)}{Y_1}\hat{B}_1\right). \tag{5.54}$$

Finally, setting $\hat{R}(z_{l_2}) = R^\star$ gives us

$$\hat{B}_1 = \frac{Y_1}{m_1(1-\varepsilon_1)}\left(\frac{D_R(R_{in}-R^\star)}{z_b+1/h-z_{l_2}} - \frac{m_2(1-\varepsilon_2)}{Y_2}\hat{B}_2\right), \tag{5.55}$$

and

$$\hat{B}_2 = \frac{Y_2}{m_2(1-\varepsilon_2)}\left(\frac{D_R(R_{in}-R^\star)}{z_b+1/h-z_{l_2}} - \frac{m_1(1-\varepsilon_1)}{Y_1}\hat{B}_1\right), \tag{5.56}$$

as desired for the nutrient-limited case. The light level at and immediately under the layer at z_{l_1} and z_{l_2} are given by

$$\hat{I}(z_{l_1}) = I_{in}e^{-\frac{a_1Y_1}{m_1(1-\varepsilon_1)}\left(\frac{D_R(R_{in}-R^\star)}{z_b+1/h-z_{l_2}}-\frac{m_2(1-\varepsilon_2)}{Y_2}\hat{B}_2\right)-a_{bg}z_{l_1}} > I_1^\star \tag{5.57}$$

and

$$\hat{I}(z_{l_2}) = I_{in}e^{-\frac{a_1Y_1}{m_1(1-\varepsilon_1)}\left(\frac{D_R(R_{in}-R^\star)}{z_b+1/h-z_{l_2}}-\frac{m_2(1-\varepsilon_2)}{Y_2}\hat{B}_2\right)-\frac{a_2Y_2}{m_2(1-\varepsilon_2)}\left(\frac{D_R(R_{in}-R^\star)}{z_b+1/h-z_{l_2}}-\frac{m_1(1-\varepsilon_1)}{Y_1}\hat{B}_1\right)-a_{bg}z_{l_2}} > I_2^\star. \tag{5.58}$$

Note that both $\hat{I}(z_{l_1})$ and $\hat{I}(z_{l_2})$ decrease as z_{l_2} increases, so that a deeper nutrient-limited layer implies more shade.

Now consider the case of light-limitation of both layers. Recall

$$\hat{I}(z) = \begin{cases} I_{in}e^{-a_{bg}z}, & 0 \le z < z_{l_1}, \\ I_{in}e^{-a_1\hat{B}_1-a_{bg}z}, & z_{l_1} \le z < z_{l_2}, \\ I_{in}e^{-a_1\hat{B}_1-a_2\hat{B}_2-a_{bg}z}, & z_{l_2} \le z \le z_b. \end{cases}$$

Evaluating at z_{l_1} gives

$$\hat{I}(z_{l_1}) = I_{in}e^{-a_1\hat{B}_1-a_{bg}z_{l_1}}.$$

Solving for $\hat{B}_1$, we obtain

$$\hat{B}_1 = \frac{\ln(I_{in}/\hat{I}(z_{l_1}))}{a_1} - \frac{a_{bg}}{a_1} z_{l_1}. \tag{5.59}$$

Similarly, we evaluate at z_{l_2} to get

$$\hat{I}(z_{l_2}) = I_{in} e^{-a_1 \hat{B}_1 - a_2 \hat{B}_2 - a_{bg} z_{l_2}}.$$

Solving for $\hat{B}_2$, we first obtain

$$\hat{B}_2 = \frac{\ln(I_{in}/\hat{I}(z_{l_2}))}{a_2} - \frac{a_1}{a_2}\hat{B}_1 - \frac{a_{bg}}{a_2} z_{l_2}. \tag{5.60}$$

Rewriting Equation (5.60) using (5.59), we get

$$\hat{B}_2 = \frac{\ln(I_{in}/\hat{I}(z_{l_2}))}{a_2} - \frac{a_1}{a_2}\left(\frac{\ln(I_{in}/\hat{I}(z_{l_1}))}{a_1} - \frac{a_{bg}}{a_1} z_{l_1}\right) - \frac{a_{bg}}{a_2} z_{l_2},$$

and after simplifying we obtain

$$\hat{B}_2 = \frac{\ln(\hat{I}(z_{l_1})/\hat{I}(z_{l_2}))}{a_2} - \frac{a_{bg}}{a_2}(z_{l_2} - z_{l_1}). \tag{5.61}$$

Finally, letting $\hat{I}(z_{l_1}) = I_1^\star$ and $\hat{I}(z_{l_2}) = I_2^\star$, we get

$$\hat{B}_1 = \frac{\ln(I_{in}/I_1^\star)}{a_1} - \frac{a_{bg}}{a_1} z_{l_1}, \tag{5.62}$$

and

$$\hat{B}_2 = \frac{\ln(I_1^\star/I_2^\star)}{a_2} - \frac{a_{bg}}{a_2}(z_{l_2} - z_{l_1}) \tag{5.63}$$

as desired for the light-limited case. The nutrient level at and above the layer at z_{l_2} is given by

$$\hat{R}(z_{l_2}) = R_{in} - \frac{z_b + 1/h - z_{l_2}}{D_R}\left(\frac{m_1(1-\varepsilon_1)}{Y_1}\hat{B}_1 + \frac{m_2(1-\varepsilon_2)}{Y_2}\hat{B}_2\right) \tag{5.64}$$

and from Equations (5.62) and (5.63) it follows that

$$\begin{aligned}\hat{R}(z_{l_2}) &= R_{in} - \frac{z_b + 1/h - z_{l_2}}{D_R}\left(\frac{m_1(1-\varepsilon_1)(\ln(I_{in}/I_1^\star) - a_{bg}z_{l_1})}{a_1 Y_1}\right) \\ &\quad - \frac{z_b + 1/h - z_{l_2}}{D_R}\left(\frac{m_2(1-\varepsilon_2)(\ln(I_1^\star/I_2^\star) - a_{bg}(z_{l_2} - z_{l_1}))}{a_2 Y_2}\right) \\ &> R^\star. \end{aligned} \tag{5.65}$$

Note that $\hat{R}(z_2)$ increases as z_{l_2} increases, so that a shallower light-limited layer depresses nutrient levels more.

Thus we have shown that the equilibrium distribtions for $\hat{B}_1$ and $\hat{B}_2$ under the ESS assumptions are given by Equations (5.32) and (5.33)

$$\hat{B}_1 = \begin{cases} \dfrac{Y_1}{m_1(1-\varepsilon_1)}\left(\dfrac{D_R(R_{in} - R^\star)}{z_b + 1/h - z_{l_2}} - \dfrac{m_2(1-\varepsilon_2)}{Y_2}\hat{B}_2\right), & \text{for a nutrient-limited layer,} \\ \\ \dfrac{\ln(I_{in}/I_1^\star)}{a_1} - \dfrac{a_{bg}}{a_1}z_{l_1}, & \text{for a light-limited layer.} \end{cases}$$

and

$$\hat{B}_2 = \begin{cases} \dfrac{Y_2}{m_2(1-\varepsilon_2)}\left(\dfrac{D_R(R_{in} - R^\star)}{z_b + 1/h - z_{l_2}} - \dfrac{m_1(1-\varepsilon_1)}{Y_1}\hat{B}_1\right), & \text{for a nutrient-limited layer,} \\ \\ \dfrac{\ln(I_1^\star/I_2^\star)}{a_2} - \dfrac{a_{bg}}{a_2}(z_{l_2} - z_{l_1}), & \text{for a light-limited layer.} \end{cases}$$

as desired. □

Theorem 5.1.2. (Existence of $(z_1^\star, z_2^\star)$) *The ESS depths $z_1^\star$ and $z_2^\star$ are determined by the*

system of equations:

$$\begin{cases} \dfrac{Y_1}{m_1(1-\varepsilon_1)}\left(\dfrac{D_R(R_{in}-R^\star)}{z_b+1/h-z_2^\star}-\dfrac{m_2(1-\varepsilon_2)}{Y_2}\hat{B}_2\right)=\dfrac{\ln(I_{in}/I_1^\star)}{a_1}-\dfrac{a_{bg}}{a_1}z_1^\star, \\ \\ \dfrac{Y_2}{m_2(1-\varepsilon_2)}\left(\dfrac{D_R(R_{in}-R^\star)}{z_b+1/h-z_2^\star}-\dfrac{m_1(1-\varepsilon_1)}{Y_1}\hat{B}_1\right)=\dfrac{\ln(I_1^\star/I_2^\star)}{a_2}-\dfrac{a_{bg}}{a_2}(z_2^\star-z_1^\star). \end{cases} \tag{5.66}$$

This solution provides a stable equilibrium of the full model (Equations (5.14) –(5.21)) with $D_{b_1}=D_{b_2}=0$ *and* $\nu_1(\partial g_1/\partial z)|_{z_1^\star}=\nu_2(\partial g_2/\partial z)|_{z_2^\star}=0$.

Proof. Observe that net growth is positive below a nutrient-limited layer since $I>I_1^\star>I_2^\star$ and net growth is positive above a light-limited layer since $R>R^\star$. Thus the ESS depth is obtained by considering the case of a layer under the conditions of co-limitation. That is, the layers are limited by both resources so that $\hat{R}(z_{l_2})=R^\star$, $\hat{I}(z_{l_1})=I_1^\star$, and $\hat{I}(z_{l_2})=I_2^\star$. Thus we need to combine the nutrient-limited and light-limited cases for $\hat{B}_1$ and $\hat{B}_2$ to derive the system needed to solve for the ESS depths $z_1^\star$ and $z_2^\star$. We do this by setting the nutrient-limited and light-limited profiles equal and replace z_{l_1} and z_{l_2} with $z_1^\star$ and $z_2^\star$. Doing this results in the system of equations given in (5.66):

$$\begin{cases} \dfrac{Y_1}{m_1(1-\varepsilon_1)}\left(\dfrac{D_R(R_{in}-R^\star)}{z_b+1/h-z_2^\star}-\dfrac{m_2(1-\varepsilon_2)}{Y_2}\hat{B}_2\right)=\dfrac{\ln(I_{in}/I_1^\star)}{a_1}-\dfrac{a_{bg}}{a_1}z_1^\star, \\ \\ \dfrac{Y_2}{m_2(1-\varepsilon_2)}\left(\dfrac{D_R(R_{in}-R^\star)}{z_b+1/h-z_2^\star}-\dfrac{m_1(1-\varepsilon_1)}{Y_1}\hat{B}_1\right)=\dfrac{\ln(I_1^\star/I_2^\star)}{a_2}-\dfrac{a_{bg}}{a_2}(z_2^\star-z_1^\star). \end{cases}$$

Existence of solutions to this system of equations is guaranteed by the Implicit Function Theorem. The system of equations can be solved in $(z_1^\star, z_2^\star)$, however, the resulting algebraic expressions are uninformative.

The ESS provides a stable equilibrium of the full model (Equations (5.14) –(5.21)) with

$D_{b_1} = D_{b_2} = 0$ and $\nu_1(\partial g_1/\partial z)|_{z_1^\star} = \nu_2(\partial g_2/\partial z)|_{z_2^\star} = 0$ since

$$g_1(z) = \min\Big(f_{I,1}(I_1^\star), f_{R,1}(R^\star)\Big) - m_1 = m_1 - m_1 = 0 \tag{5.67}$$

and

$$g_2(z) = \min\Big(f_{I,2}(I_2^\star), f_{R,2}(R^\star)\Big) - m_2 = m_2 - m_2 = 0 \tag{5.68}$$

for all $z \in [0, z_b]$ under the assumptions that $\hat{b_1} = B_1\delta_{z_{l_1}}(z)$ and $\hat{b_2}(z) = B_2\delta_{z_{l_2}}(z)$. Equations (5.67) and (5.68) follow since $I_1^\star = f_{I,1}^{-1}(m_1)$, $I_2^\star = f_{I,2}^{-1}(m_2)$, and $R^\star = f_{R,1}^{-1}(m_1) = f_{R,2}^{-1}(m_2)$ so that no net growth occurs outside the layers at $z_1^\star$ and $z_2^\star$ for $b_1(z)$ and $b_2(z)$ respectively. □

Corollary 5.1.3. (The Biomass Equilibrium $\hat{B}_1$ and $\hat{B}_2$ as functions of $(z_1^\star, z_2^\star)$) *The equilibrium biomass of $\hat{B}_1$ and $\hat{B}_2$ can be expressed as functions of $(z_1^\star, z_2^\star)$ as*

$$\hat{B}_1 = \begin{cases} \dfrac{\ln(I_{in}/I_1^\star)}{a_1}, & z_1^\star \le 0 \text{ (surface layer)} \\[2ex] \frac{Y_1}{m_1(1-\varepsilon_1)}\left[\frac{D_R(R_{in}-R^\star)}{z_b+1/h-z_2^\star} - \frac{m_2(1-\varepsilon_2)}{Y_2}\left(\frac{\ln(I_1^\star/I_2^\star)}{a_2} - \frac{a_{bg}}{a_2}(z_2^\star - z_1^\star)\right)\right], & 0 < z_1^\star < z_2^\star < z_b \text{ (DCM)} \\[2ex] \dfrac{Y_1 D_R h}{m_1(1-\varepsilon_1)}(R_{in} - R^\star), & z_2^\star \ge z_b \text{ (benthic layer)}, \end{cases} \tag{5.69}$$

and

$$\hat{B}_2 = \begin{cases} \dfrac{\ln(I_1^\star/I_2^\star)}{a_2}, & z_1^\star \ge z_2^\star \text{ (surface layer)} \\[2ex] \frac{Y_2}{m_2(1-\varepsilon_2)}\left[\frac{D_R(R_{in}-R^\star)}{z_b+1/h-z_2^\star} - \frac{m_1(1-\varepsilon_1)}{Y_1}\left(\frac{\ln(I_{in}/I_1^\star)}{a_1} - \frac{a_{bg}}{a_1}z_1^\star\right)\right], & 0 < z_1^\star < z_2^\star < z_b \text{ (DCM)} \\[2ex] \dfrac{Y_2 D_R h}{m_2(1-\varepsilon_2)}(R_{in} - R^\star), & z_2^\star \ge z_b \text{ (benthic layer)}. \end{cases} \tag{5.70}$$

Proof. Recall the equilibrium distribtions for $\hat{B}_1$ and $\hat{B}_2$ under the ESS assumptions are given by Equations (5.32) and (5.33)

$$\hat{B}_1 = \begin{cases} \dfrac{Y_1}{m_1(1-\varepsilon_1)}\left(\dfrac{D_R(R_{in}-R^\star)}{z_b+1/h-z_{l_2}} - \dfrac{m_2(1-\varepsilon_2)}{Y_2}\hat{B}_2\right), & \text{for a nutrient-limited layer,} \\ \\ \dfrac{\ln(I_{in}/I_1^\star)}{a_1} - \dfrac{a_{bg}}{a_1}z_{l_1}, & \text{for a light-limited layer.} \end{cases}$$

and

$$\hat{B}_2 = \begin{cases} \dfrac{Y_2}{m_2(1-\varepsilon_2)}\left(\dfrac{D_R(R_{in}-R^\star)}{z_b+1/h-z_{l_2}} - \dfrac{m_1(1-\varepsilon_1)}{Y_1}\hat{B}_1\right), & \text{for a nutrient-limited layer,} \\ \\ \dfrac{\ln(I_1^\star/I_2^\star)}{a_2} - \dfrac{a_{bg}}{a_2}(z_{l_2}-z_{l_1}), & \text{for a light-limited layer.} \end{cases}$$

To derive the distributions given in Equations (5.69) and (5.70), we combine the cases when one species has a nutrient-limited layer while the other species has a light-limited layer to allow for coexistence of both species. That is, when $\hat{B}_1$ is a nutrient-limited layer, $\hat{B}_2$ is a light-limited layer and when $\hat{B}_1$ is a light-limited layer, $\hat{B}_2$. Making the appropriate substitutions and replacing z_{l_1} and z_{l_2} with $z_1^\star$ and $z_2^\star$ results in

$$\hat{B}_1 = \frac{Y_1}{m_1(1-\varepsilon_1)}\left[\frac{D_R(R_{in}-R^\star)}{z_b+1/h-z_2^\star} - \frac{m_2(1-\varepsilon_2)}{Y_2}\left(\frac{\ln(I_1^\star/I_2^\star)}{a_2} - \frac{a_{bg}}{a_2}(z_2^\star - z_1^\star)\right)\right],$$

and

$$\hat{B}_2 = \frac{Y_2}{m_2(1-\varepsilon_2)}\left[\frac{D_R(R_{in}-R^\star)}{z_b+1/h-z_2^\star} - \frac{m_1(1-\varepsilon_1)}{Y_1}\left(\frac{\ln(I_{in}/I_1^\star)}{a_1} - \frac{a_{bg}}{a_1}z_1^\star\right)\right],$$

which are the expressions describing when the resulting layers are DCMs.

The remaining terms in the biomass distributions are determined by restricting the biomass to the water column. For $\hat{B}_1$, if $z_1^\star \leq 0$ we restrict the biomass to the light-limited surface layer at $z = 0$. Additionally, if $z_2^\star \geq z_b$ we restrict the biomass to the nutrient-limited

benthic layer at $z = z_b$. While the argument is identical for $\hat{B}_2$, the surface layer will occur when $z_2^\star - z_1^\star \leq 0$. $\square$

5.2 Preferential Nutrient Uptake Model ESS

In this section we extend the ESS analysis of the multi-species Klausmeier and Litchman model to the proposed preferential nutrient uptake model. The addition of a second nutrient source that competing phytoplankton can utilize will require the previous analysis to be updated by determining the equilibrium distribution of this additional model component. This change will also impact the game theoretic approximations to the location of the phytoplankton layers given in the previous analysis. We now present a detailed analysis of the ESS equilibrium distributions of the proposed preferential uptake model that was introduced in Chapter 3.

Consider the preferential nutrient uptake model:

$$\frac{\partial b_1}{\partial t} = \min(f_{I,1}(I(z,t)), f_{R,1}(R_1(z,t), R_2(z,t)))b_1 - m_1 b_1 + D_{b_1}\frac{\partial^2 b_1}{\partial z^2} + \frac{\partial}{\partial z}\Big[\nu_1\Big(\frac{\partial g_1}{\partial z}\Big)b_1\Big],$$

$$\frac{\partial b_2}{\partial t} = \min(f_{I,2}(I(z,t)), f_{R,2}(R_1(z,t), R_2(z,t)))b_2 - m_2 b_2 + D_{b_2}\frac{\partial^2 b_2}{\partial z^2} + \frac{\partial}{\partial z}\Big[\nu_2\Big(\frac{\partial g_2}{\partial z}\Big)b_2\Big],$$

$$\frac{\partial R_1}{\partial t} = -\frac{b_1}{Y_1}\min(f_{I,1}(I(z,t)), f_{R,1}(R_1(z,t), R_2(z,t)))\,\frac{\gamma_1(R_1(z,t))}{f_{R,1}(R_1(z,t), R_2(z,t))} + \varepsilon_{1,1} m_1 \frac{b_1}{Y_1}$$

$$- \frac{b_2(z,t)}{Y_2}\min(f_{I,2}(I(z,t)), f_{R,2}(R_1(z,t), R_2(z,t)))\,\frac{\gamma_2(R_1(z,t))}{f_{R,2}(R_1(z,t), R_2(z,t))} + \varepsilon_{2,1} m_2 \frac{b_2}{Y_2}$$

$$+ D_{R_1}\frac{\partial^2 R_1}{\partial z^2},$$

$$\frac{\partial R_2}{\partial t} = -\frac{b_1}{Y_1}\min(f_{I,1}(I(z,t)), f_{R,1}(R_1(z,t), R_2(z,t)))\,\frac{\rho_1(R_1(z,t), R_2(z,t))}{f_{R,1}(R_1(z,t), R_2(z,t))} + \varepsilon_{1,2}m_1\,\frac{b_1}{Y_1}$$

$$-\frac{b_2}{Y_2}\min(f_{I,2}(I(z,t)), f_{R,2}(R_1(z,t), R_2(z,t)))\,\frac{\rho_2(R_1(z,t), R_2(z,t))}{f_{R,2}(R_1(z,t), R_2(z,t))} + \varepsilon_{2,2}m_2\,\frac{b_2}{Y_2}$$

$$+ D_{R_2}\frac{\partial^2 R_2}{\partial z^2},$$

$$I(z,t) = I_{in}\exp\left[-\int_0^z (a_1 b_1(w,t) + a_2 b_2(w,t) + a_{bg})dw\right].$$

The boundary conditions for the partial differential equations are given by:

$$\left[D_{b_1}\frac{\partial b_1}{\partial z} + \nu_1\left(\frac{\partial g_1}{\partial z}\right)b_1\right]\Bigg|_{z=0} = \left[D_{b_1}\frac{\partial b_1}{\partial z} + \nu_1\left(\frac{\partial g_1}{\partial z}\right)b_1\right]\Bigg|_{z=z_b} = 0,$$

$$\left[D_{b_2}\frac{\partial g_2}{\partial z} + \nu_2\left(\frac{\partial g_2}{\partial z}\right)b_2\right]\Bigg|_{z=0} = \left[D_{b_2}\frac{\partial g_2}{\partial z} + \nu_2\left(\frac{\partial g_2}{\partial z}\right)b_2\right]\Bigg|_{z=z_b} = 0,$$

$$\frac{\partial R_1}{\partial z}\Bigg|_{z=0} = 0,\ \frac{\partial R_1}{\partial z}\Bigg|_{z=z_b} = h(R_{in_1} - R_1(z_b))$$

$$\frac{\partial R_2}{\partial z}\Bigg|_{z=0} = 0,\ \frac{\partial R_2}{\partial z}\Bigg|_{z=z_b} = h(R_{in_2} - R_2(z_b)).$$

As shown in Figure 5.3, when the swimming velocities $\nu_{1_{max}}$ and $\nu_{2_{max}}$ are increased from 0 m d^{-1} to 100 m d^{-1} (all other parameters are consistent with the values listed in Table 2.2), the phytoplankton distributions go from more uniform to increasingly more concentrated in thin layers. Thus, we can approximate the phytoplankton distributions by an infinitely thin layer using the game theoretic approach.

To account for multiple species, we use the previous assumption that the phytoplankton form infinitely thin layers at depths z_{l_1} and z_{l_2} corresponding to the preferred depths that the species occupy based on their utilization of light and nutrients. As before, we set $b_1(z) = B_1\delta_{z_{l_1}}(z)$ and $b_2(z) = B_2\delta_{z_{l_2}}(z)$ where $\delta_{z_{l_1}}(z)$ and $\delta_{z_{l_2}}(z)$ are Dirac delta functions and B_1 and B_2 are the total depth-integrated biomasses given by equations (5.22) and (5.23) respectively.

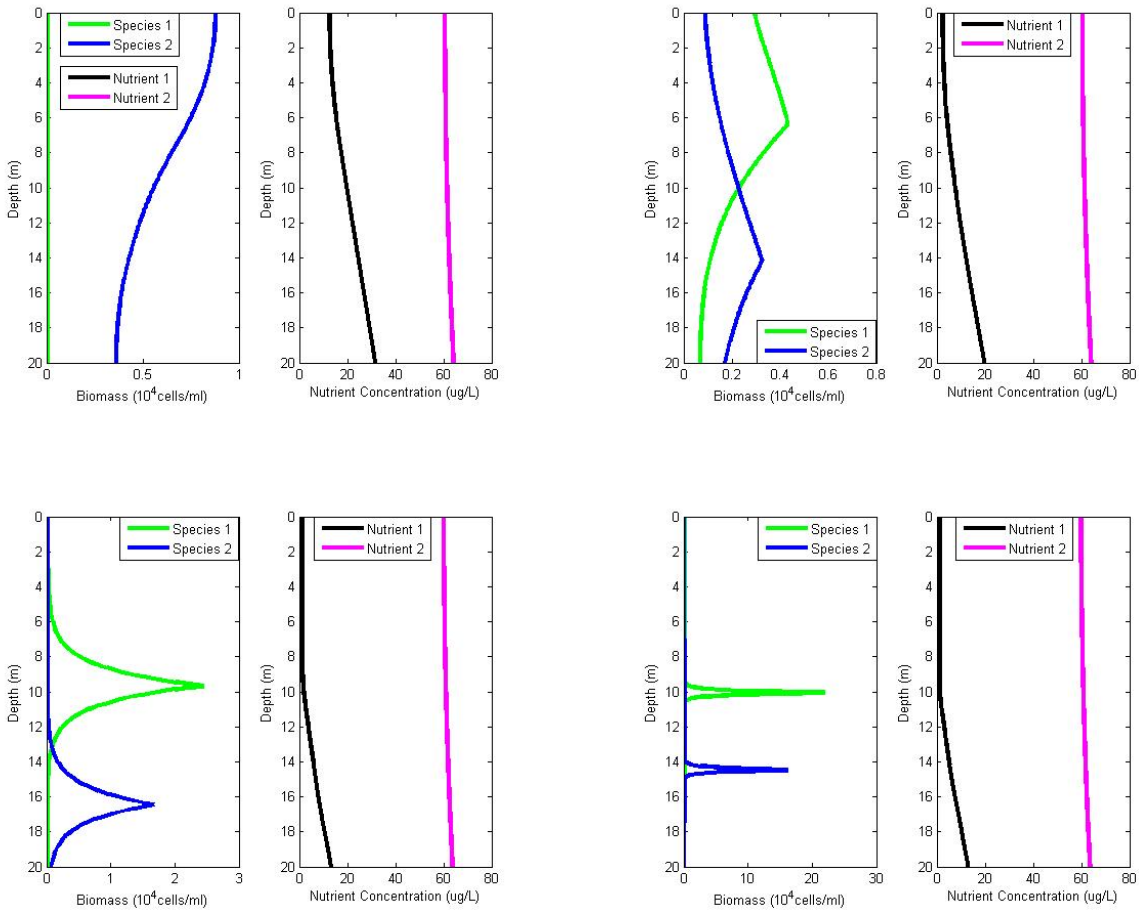

Figure 5.3: Model simulations of Equations (3.1) –(3.17) as $\nu_{1_{max}}$ and $\nu_{2_{max}}$ increases from 0 m d^{-1} to 100 m d^{-1}. The upper left panel uses $\nu_{1_{max}} = \nu_{2_{max}} = 0$ m d^{-1}. The upper right panel uses $\nu_{1_{max}} = \nu_{2_{max}} = 1$ m d^{-1}. The lower left panel uses $\nu_{1_{max}} = \nu_{2_{max}} = 10$ m d^{-1}. The lower right panel uses $\nu_{1_{max}} = \nu_{2_{max}} = 100$ m d^{-1}.

To find the ESS equilibrium distributions, we set the time derivatives of Equations (3.1), (3.2), (3.13), and (3.14) to 0, $D_{b_1} = D_{b_2} = 0$ (active movement is sufficient to overcome biomass mixing), Given layers at z_{l_1} and z_{l_2}, calculate the equilibrium biomasses and distributions of light and free nutrients in the absence of movement, and then determine whether

net growth is possible outside of the layers at z_{l_1} and z_{l_2}. This results in the following system of equations:

$$0 = \hat{b_1}(z)\Big(\min\Big(f_{I,1}(\hat{I}(z)), f_{R,1}(\hat{R}_1(z), \hat{R}_2(z))\Big) - m_1\Big), \tag{5.71}$$

$$0 = \hat{b_2}(z)\Big(\min\Big(f_{I,2}(\hat{I}(z)), f_{R,2}(\hat{R}_1(z), \hat{R}_2(z))\Big) - m_2\Big), \tag{5.72}$$

$$\begin{aligned} 0 = &-\frac{\hat{b_1}(z)}{Y_1} \min\Big(f_{I,1}(\hat{I}(z)), f_{R,1}(\hat{R}_1(z), \hat{R}_2(z))\Big) \frac{\gamma_1(\hat{R}_1(z))}{f_{R,1}(\hat{R}_1(z), \hat{R}_2(z))} + \varepsilon_{1,1} m_1 \frac{\hat{b_1}(z)}{Y_1} \\ &- \frac{\hat{b_2}(z)}{Y_2} \min\Big(f_{I,2}(\hat{I}(z)), f_{R,2}(\hat{R}_1(z), \hat{R}_2(z))\Big) \frac{\gamma_2(\hat{R}_1(z))}{f_{R,2}(\hat{R}_1(z), \hat{R}_2(z))} + \varepsilon_{2,1} m_2 \frac{\hat{b_2}(z)}{Y_1} \\ &+ D_{R_1} \frac{\partial^2 \hat{R}_1}{\partial z^2}, \end{aligned} \tag{5.73}$$

$$\begin{aligned} 0 = &-\frac{\hat{b_1}(z)}{Y_1} \min\Big(f_{I,1}(\hat{I}(z)), f_{R,1}(\hat{R}_1(z), \hat{R}_2(z))\Big) \frac{\rho_1(\hat{R}_1(z), \hat{R}_2(z))}{f_{R,1}(\hat{R}_1(z), \hat{R}_2(z))} + \varepsilon_{1,2} m_1 \frac{\hat{b_1}(z)}{Y_1} \\ &- \frac{\hat{b_2}(z)}{Y_2} \min\Big(f_{I,2}(\hat{I}(z)), f_{R,2}(\hat{R}_1(z), \hat{R}_2(z))\Big) \frac{\rho_2(\hat{R}_1(z), \hat{R}_2(z))}{f_{R,2}(\hat{R}_1(z), \hat{R}_2(z))} + \varepsilon_{2,2} m_2 \frac{\hat{b_2}(z)}{Y_1} \\ &+ D_{R_2} \frac{\partial^2 \hat{R}_2}{\partial z^2}, \end{aligned} \tag{5.74}$$

$$\hat{I}(z) = I_{in} \exp\left(-\int_0^z \left(a_1 \hat{b_1}(w) + a_2 \hat{b_2}(w) + a_{bg}\right)\, dw \right), \tag{5.75}$$

$$\left.\frac{\partial \hat{R}_1}{\partial z}\right|_{z=0} = 0, \tag{5.76}$$

$$\left.\frac{\partial \hat{R}_1}{\partial z}\right|_{z=z_b} = h(R_{in_1} - \hat{R}_1(z_b)), \tag{5.77}$$

$$\tag{5.78}$$

$$\left.\frac{\partial \hat{R}_2}{\partial z}\right|_{z=0} = 0, , \tag{5.79}$$

$$\left.\frac{\partial \hat{R}_2}{\partial z}\right|_{z=z_b} = h(R_{in_2} - \hat{R}_2(z_b)). \tag{5.80}$$

The solution to the system is given below.

Proposition 5.2.1. (The Equilibrium Distributions of $\hat{R}_1(z)$, $\hat{R}_2(z)$, $\hat{I}(z)$, $\hat{B}_1$, and $\hat{B}_2$) *Assume that $f_{I,1}$, $f_{I,2}$, $f_{R,1}$, $f_{R,2}$, γ_1, γ_2, ρ_1, and ρ_2 are continuous functions in their respective variables. Then the solution to the system of equations given by Equations (5.71) –(5.80) under the ESS assumptions is given by*

$$\hat{R}_1(z) = \begin{cases} \hat{R}_1(z_{l_1}), & 0 \le z \le z_{l_1}, \\ \hat{R}_1(z_{l_1}) + (z - z_{l_1})\dfrac{R_{in_1} - \hat{R}_1(z_{l_1})}{z_b + 1/h - z_{l_1}}, & z_{l_1} < z \le z_{l_2}, \\ \hat{R}_1(z_{l_2}) + (z - z_{l_2})\dfrac{R_{in} - \hat{R}_1(z_{l_2})}{z_b + 1/h - z_{l_2}}, & z_{l_2} < z \le z_b, \end{cases} \tag{5.81}$$

$$\hat{R}_2(z) = \begin{cases} \hat{R}_2(z_{l_1}), & 0 \le z \le z_{l_1}, \\ \hat{R}_2(z_{l_1}) + (z - z_{l_1})\dfrac{R_{in_2} - \hat{R}_1(z_{l_1})}{z_b + 1/h - z_{l_1}}, & z_{l_1} < z \le z_b, \end{cases} \tag{5.82}$$

$$\hat{I}(z) = \begin{cases} I_{in}e^{-a_{bg}z}, & 0 \le z < z_{l_1}, \\ I_{in}e^{-a_1\hat{B}_1 - a_{bg}z}, & z_{l_1} \le z < z_{l_2}, \\ I_{in}e^{-a_1\hat{B}_1 - a_2\hat{B}_2 - a_{bg}z}, & z_{l_2} \le z \le z_b, \end{cases} \tag{5.83}$$

$$\hat{B}_1 = \begin{cases} \frac{D_{R_1}P_2(z_{l_2})(z_b+1/h-z_{l_1})(R_{in_1}-R_2^\star)-D_{R_2}\Gamma_2(z_{l_2})(z_b+1/h-z_{l_2})(R_{in_2}-R_1^\star)}{(\Gamma_1(z_{l_1})P_2(z_{l_2})-\Gamma_2(z_{l_2})P_1(z_{l_1}))(z_b+1/h-z_{l_2})(z_b+1/h-z_{l_1})}, & \text{nutrient-limited layer,} \\ \\ \frac{\ln(I_{in}/I_1^\star)}{a_1} - \frac{a_{bg}}{a_1}z_{l_1}, & \text{light-limited layer,} \end{cases} \tag{5.84}$$

and

$$\hat{B}_2 = \begin{cases} \frac{D_{R_2}\Gamma_1(z_{l_1})(z_b+1/h-z_{l_2})(R_{in_2}-R_1^\star)-D_{R_1}P_1(z_{l_1})(z_b+1/h-z_{l_1})(R_{in_1}-R_2^\star)}{(\Gamma_1(z_{l_1})P_2(z_{l_2})-\Gamma_2(z_{l_2})P_1(z_{l_1}))(z_b+1/h-z_{l_2})(z_b+1/h-z_{l_1})}, & \text{nutrient-limited layer,} \\ \\ \frac{\ln(I_1^\star/I_2^\star)}{a_2} - \frac{a_{bg}}{a_2}(z_{l_2} - z_{l_1}), & \text{light-limited layer.} \end{cases} \tag{5.85}$$

The terms $\hat{B}_1$ *and* $\hat{B}_2$ *are as given in (5.34) and (5.35) respectively, and* $\Gamma_1(z)$, $\Gamma_2(z)$, $P_1(z)$, *and* $P_2(z)$ *are defined by*

$$\Gamma_1(z) = \frac{m_1}{Y_1}\left(\frac{\gamma_1(\hat{R}_1(z))}{f_{R,1}(\hat{R}_1(z),\hat{R}_2(z))} - \varepsilon_{1,1}\right), \tag{5.86}$$

$$\Gamma_2(z) = \frac{m_2}{Y_2}\left(\frac{\gamma_2(\hat{R}_1(z))}{f_{R,2}(\hat{R}_1(z),\hat{R}_2(z))} - \varepsilon_{2,1}\right), \tag{5.87}$$

$$P_1(z) = \frac{m_1}{Y_1}\left(\frac{\rho_1(\hat{R}_1(z),\hat{R}_2(z))}{f_{R,1}(\hat{R}_1(z),\hat{R}_2(z))} - \varepsilon_{1,2}\right), \tag{5.88}$$

and

$$P_2(z) = \frac{m_2}{Y_2}\left(\frac{\rho_2(\hat{R}_1(z),\hat{R}_2(z))}{f_{R,2}(\hat{R_1}(z),\hat{R}_2(z))} - \varepsilon_{2,2}\right). \tag{5.89}$$

Proof. As before, under the assumptions of $b_1 = B_1\delta_{z_{l_1}}(z)$ and $b_2 = B_2\delta_{z_{l_2}}(z)$ with B_1 and

B_2 as defined in Equations (5.22) and (5.23) respectively, Equation (5.73) becomes

$$\frac{\partial^2 \hat{R}_1}{\partial z^2} = 0,\ 0 \leq z < z_{l_1} \tag{5.90a}$$

$$\frac{\partial^2 \hat{R}_1}{\partial z^2} = 0,\ z_{l_1} < z < z_{l_2} \tag{5.90b}$$

$$\frac{\partial^2 \hat{R}_1}{\partial z^2} = 0,\ z_{l_2} < z \leq z_b. \tag{5.90c}$$

Now consider Equation (5.90a) with boundary condition 5.76:

$$\begin{cases} \dfrac{\partial^2 \hat{R}_1}{\partial z^2} = 0, & 0 \leq z < z_{l_1} \\ \\ \left.\dfrac{\partial \hat{R}_1}{\partial z}\right|_{z=0} = 0. \end{cases} \tag{5.91}$$

Equation (5.91) shows that the diffusion of the first nutrient equalizes the nutrient concentration above the layer at z_{l_1}. That is, $\hat{R}_1(z) = \hat{R}_1(z_{l_1})$ if $0 \leq z \leq z_{l_1}$. Equation (5.91) also implies that nutrients vary linearly below the layer at z_{l_1}, denoted by $z_{l_1}^+$, to z_{l_2}. Thus

$$\left.\frac{\partial \hat{R}_1}{\partial z}\right|_{z=z_{l_1}^+} = \left.\frac{\partial \hat{R}_1}{\partial z}\right|_{z=z_{l_2}} = \frac{\hat{R}_1(z_{l_2}) - \hat{R}_1(z_{l_1})}{z_{l_2} - z_{l_1}}. \tag{5.92}$$

Now consider Equation (5.90c) with boundary condition given by Equation (5.77):

$$\begin{cases} \dfrac{\partial^2 \hat{R}_1}{\partial z^2} = 0, & z_{l_2} < z \leq z_b \\ \\ \left.\dfrac{\partial \hat{R}_1}{\partial z}\right|_{z=z_b} = h(R_{in_1} - \hat{R}_1(z_b)). \end{cases} \tag{5.93}$$

Using the same argument as before, nutrients vary linearly before the layer at z_{l_2}, denoted by $z_{l_2}^+$, to z_b. Thus

$$\left.\frac{\partial \hat{R}_1}{\partial z}\right|_{z=z_{l_2}^+} = \left.\frac{\partial \hat{R}_1}{\partial z}\right|_{z=z_b} = \frac{\hat{R}_1(z_b) - \hat{R}_1(z_{l_2})}{z_b - z_{l_2}}. \tag{5.94}$$

From Equation (5.94) and (5.77) we obtain

$$h(R_{in_1} - \hat{R}_1(z_b)) = \frac{\hat{R}_1(z_b) - \hat{R}_1(z_{l_2})}{z_b - z_{l_2}}. \tag{5.95}$$

Solving Equation (5.95) for $\hat{R}_1(z_b)$ gives

$$\hat{R}_1(z_b) = \frac{h(z_b - z_{l_2})R_{in_1} + \hat{R}_1(z_{l_2})}{1 + h(z_b - z_{l_2})}. \tag{5.96}$$

From Equations (5.94) and (5.96) it follows that

$$\left.\frac{\partial \hat{R}}{\partial z}\right|_{z=z_{l_2}^+} = \frac{\hat{R}_1(z_b) - \hat{R}_1(z_{l_2})}{z_b - z_{l_2}} = \frac{\dfrac{h(z_b - z_{l_2})R_{in_1} + \hat{R}_1(z_{l_2})}{1 + h(z_b - z_{l_2})} - \hat{R}_1(z_{l_2})}{z_b - z_{l_2}}$$

$$= \frac{h(R_{in_1} - \hat{R}_1(z_{l_2}))}{1 + h(z_b - z_{l_2})} = \frac{R_{in_1} - \hat{R}_1(z_{l_2})}{z_b + 1/h - z_{l_2}}. \tag{5.97}$$

Finally, consider Equation (5.90b)

$$\frac{\partial^2 \hat{R}_1}{\partial z^2} = 0, \;\; z_{l_1} < z < z_{l_2}.$$

The boundary condition for this differential equation can be inferred to be

$$\left.\frac{\partial \hat{R}_1}{\partial z}\right|_{z=z_{l_2}} = \frac{\hat{R}_1(z_{l_2}) - \hat{R}_1(z_{l_1})}{z_{l_2} - z_{l_1}}. \tag{5.98}$$

Using Equations (5.97) and (5.98) we get

$$\frac{R_{in_1} - \hat{R}_1(z_{l_2})}{z_b + 1/h - z_{l_2}} = \frac{\hat{R}_1(z_{l_2}) - \hat{R}_1(z_{l_1})}{z_{l_2} - z_{l_1}}. \tag{5.99}$$

Solving Equation (5.99) for $\hat{R}_1(z_{l_2})$ gives

$$\hat{R}_1(z_{l_2}) = \frac{R_{in_1}(z_{l_2} - z_{l_1}) + \hat{R}_1(z_{l_1})(z_b + 1/h - z_{l_2})}{z_b + 1/h - z_{l_2}}. \tag{5.100}$$

Substituting the result from Equation (5.100) into (5.98) and simplifying yields

$$\left.\frac{\partial \hat{R}}{\partial z}\right|_{z=z_{l_2}} = \frac{\hat{R}_1(z_{l_2}) - \hat{R}_1(z_{l_1})}{z_{l_2} - z_{l_1}} = \frac{\dfrac{R_{in_1}(z_{l_2} - z_{l_1}) + \hat{R}_1(z_{l_1})(z_b + 1/h - z_{l_2})}{z_b + 1/h - z_{l_2}} - \hat{R}_1(z_{l_1})}{z_{l_2} - z_{l_1}}$$

$$= \frac{\dfrac{(z_{l_2} - z_{l_1})(R_{in_1} - \hat{R}_1(z_{l_1}))}{z_b + 1/h - z_{l_1}}}{z_{l_2} - z_{l_1}} = \frac{R_{in_1} - \hat{R}_1(z_{l_1})}{z_b + 1/h - z_{l_1}} \tag{5.101}$$

Thus we have shown that the equilibrium distribution for $\hat{R}_1(z)$ under the ESS assumptions is given by Equation (5.81)

$$\hat{R}_1(z) = \begin{cases} \hat{R}_1(z_{l_1}), & 0 \le z \le z_{l_1}, \\ \hat{R}_1(z_{l_1}) + (z - z_{l_1})\dfrac{R_{in_1} - \hat{R}_1(z_{l_1})}{z_b + 1/h - z_{l_1}}, & z_{l_1} < z \le z_{l_2}, \\ \hat{R}_1(z_{l_2}) + (z - z_{l_2})\dfrac{R_{in} - \hat{R}_1(z_{l_2})}{z_b + 1/h - z_{l_2}}, & z_{l_2} < z \le z_b, \end{cases}$$

as desired.

Now consider Equation (5.74) under the assumptions of $b_1 = B_1\delta(z_{l_1})$ and $b_2 = B_2\delta(z_{l_2})$ with B_1 and B_2 as defined in Equations (5.22) and (5.23) respectively. Since R_1 is as-

sumed (without loss of generality) to be the preferred nutrient source for both phytoplankton species, its uptake is assumed to occur at both infinitely thin concentrations of biomass at z_{l_1} and z_{l_2}. Since R_2 is not the preferred resource, its uptake will occur at the layer of the species which is the better nutrient competitor (and thus a light-limited layer). If we assume without loss of generality that $0 < z_{l_1} < z_{l_2} < z_b$, then this will correspond to the layer at z_{l_1}. Under the ESS assumptions, Equation (5.74) reduces to

$$\frac{\partial^2 \hat{R}_2}{\partial z^2} = 0,\ 0 \leq z < z_{l_1} \tag{5.102a}$$

$$\frac{\partial^2 \hat{R}_2}{\partial z^2} = 0,\ z_{l_1} < z < z_b. \tag{5.102b}$$

Consider (5.102a) with boundary condition given by Equation 5.79

$$\begin{cases} \dfrac{\partial^2 \hat{R}_2}{\partial z^2} = 0, & 0 \leq z < z_{l_1} \\ \\ \left.\dfrac{\partial \hat{R}_2}{\partial z}\right|_{z=0} = 0. \end{cases} \tag{5.103}$$

Solving Equation (5.103) gives $\hat{R}_2(z) = \hat{R}_2(z_{l_1})$ if $0 \leq z \leq z_{l_1}$. Proceeding as we did before, observe that

$$\left.\frac{\partial \hat{R}_2}{\partial z}\right|_{z=z_{l_1}^+} = \left.\frac{\partial \hat{R}_2}{\partial z}\right|_{z=z_b} = \frac{\hat{R}_2(z_b) - \hat{R}_2(z_{l_1})}{z_b - z_{l_1}}. \tag{5.104}$$

Thus, from Equations (5.80) and (5.104) it follows that

$$h(R_{in_2} - \hat{R}_2(z_b)) = \frac{\hat{R}_2(z_b) - \hat{R}_2(z_{l_1})}{z_b - z_{l_1}}. \tag{5.105}$$

Solving (5.105) for $\hat{R}_2(z_b)$ gives

$$\hat{R}_2(z_b) = \frac{h(z_b - z_{l_1})R_{in_2} + \hat{R}_2(z_{l_1})}{1 + h(z_b - z_{l_1})} \tag{5.106}$$

Substituting Equation (5.106) into (5.104) gives

$$\left.\frac{\partial \hat{R}_2}{\partial z}\right|_{z=z_{l_1}^+} = \frac{\hat{R}_2(z_b) - \hat{R}_2(z_{l_1})}{z_b - z_{l_1}} = \frac{\dfrac{h(z_b - z_{l_1})R_{in_2} + \hat{R}_2(z_{l_1})}{1 + h(z_b - z_{l_1})} - \hat{R}_2(z_{l_1})}{z_b - z_{l_1}}$$

$$= \frac{h(R_{in_2} - \hat{R}_2(z_{l_1}))}{1 + h(z_b - z_{l_1})} = \frac{R_{in_2} - \hat{R}_2(z_{l_1})}{z_b + 1/h - z_{l_1}}. \tag{5.107}$$

Thus we have shown that the equilibrium distribution for $\hat{R}_2(z)$ under the ESS assumptions is given by Equation (5.82)

$$\hat{R}_2(z) = \begin{cases} \hat{R}_2(z_{l_1}), & 0 \le z \le z_{l_1}, \\ \hat{R}_2(z_{l_1}) + (z - z_{l_1})\dfrac{R_{in_2} - \hat{R}_1(z_{l_1})}{z_b + 1/h - z_{l_1}}, & z_{l_1} < z \le z_b, \end{cases}$$

as desired.

Now consider Equation (5.75)

$$\hat{I}(z) = I_{in} \exp\left(- \int_0^z (a_1 \hat{b_1}(w) + a_2 \hat{b_2}(w) + a_{bg})\, dw \right).$$

Under the assumption of $b_1(z) = B_1 \delta_{z_{l_1}}(z)$ and $b_2(z) = B_2 \delta_{z_{l_2}}(z)$ with B_1 and B_2 as given in

Equations (5.22) and (5.23) it is straightforward to see that

$$\hat{I}(z) = \begin{cases} I_{in}e^{-a_{bg}z}, & 0 \leq z < z_{l_1}, \\ I_{in}e^{-a_1\hat{B}_1 - a_{bg}z}, & z_{l_1} \leq z < z_{l_2}, \\ I_{in}e^{-a_1\hat{B}_1 - a_2\hat{B}_2 - a_{bg}z}, & z_{l_2} \leq z \leq z_b \end{cases}$$

due to the nature of the Dirac delta function used when evaluating the integral. Light declines with depth exponentially due to background attenuation and drops a finite amount at the layers due to attenuation by phytoplankton. Thus we have shown that the equilibrium distribution for $\hat{I}(z)$ under the ESS assumptions is given by Equation (5.83) as desired.

Finally we will determine the equilibrium biomass distributions for $\hat{B}_1$ and $\hat{B}_2$. Recall equations (5.71) and (5.72)

$$\begin{aligned} 0 &= \hat{b_1}(z)\left(\min\left(f_{I,1}(\hat{I}(z)), f_{R,1}(\hat{R}_1(z), \hat{R}_2(z))\right) - m_1\right), \\ 0 &= \hat{b_2}(z)\left(\min\left(f_{I,2}(\hat{I}(z)), f_{R,2}(\hat{R}_1(z), \hat{R}_2(z))\right) - m_2\right). \end{aligned}$$

It follows that either $\hat{b_1} = 0$ and $\hat{b_2}(z) = 0$ or

$$\min\left(f_{I,1}(\hat{I}(z)), f_{R,1}(\hat{R}_1(z), \hat{R}_2(z))\right) = m_1 \tag{5.108}$$

and

$$\min\left(f_{I,2}(\hat{I}(z)), f_{R,2}(\hat{R}_1(z), \hat{R}_2(z))\right) = m_2, \tag{5.109}$$

that is, the phytoplankton either reduce the nutrient concentration or the light concentration to their break even value at the layers z_{l_1} and z_{l_2}. However, $\hat{b_1} = 0$ and $\hat{b_2}(z) = 0$ are trivial solutions with no phytoplankton in the water column so we assume that Equations (5.108) and (5.109) hold. As before, there are two cases to consider:

1. The layers are nutrient-limited so that $\hat{R}_1(z_{l_2}) = R_2^\star$, $\hat{R}_2(z_{l_1}) = R_1^\star$, $\hat{I}(z_{l_1}) > I_1^\star$, and $\hat{I}(z_{l_2}) > I_2^\star$.

2. The layers are light-limited so that $\hat{I}(z_{l_1}) = I_1^\star$, $\hat{I}(z_{l_2}) = I_2^\star$, $\hat{R}_1(z_{l_2}) > R_2^\star$, and $\hat{R}_2(z_{l_1}) > R_1^\star$.

First consider the case of nutrient limitation. We use Equations (5.108) and (5.109) in conjunction with Equations (5.73) and (5.74) to solve for $\hat{B}_1$ and $\hat{B}_2$:

$$
\begin{aligned}
0 = &-\frac{\hat{b_1}(z)}{Y_1} \min\left(f_{I,1}(\hat{I}(z)), f_{R,1}(\hat{R}_1(z), \hat{R}_2(z))\right) \frac{\gamma_1(\hat{R}_1(z))}{f_{R,1}(\hat{R}_1(z), \hat{R}_2(z))} + \varepsilon_{1,1} m_1 \frac{\hat{b_1}(z)}{Y_1} \\
&- \frac{\hat{b_2}(z)}{Y_2} \min\left(f_{I,2}(\hat{I}(z)), f_{R,2}(\hat{R}_1(z), \hat{R}_2(z))\right) \frac{\gamma_2(\hat{R}_1(z))}{f_{R,2}(\hat{R}_1(z), \hat{R}_2(z))} + \varepsilon_{2,1} m_2 \frac{\hat{b_2}(z)}{Y_1} \\
&+ D_{R_1} \frac{\partial^2 \hat{R}_1}{\partial z^2},
\end{aligned}
$$

$$
\begin{aligned}
0 = &-\frac{\hat{b_1}(z)}{Y_1} \min\left(f_{I,1}(\hat{I}(z)), f_{R,1}(\hat{R}_1(z), \hat{R}_2(z))\right) \frac{\rho_1(\hat{R}_1(z), \hat{R}_2(z))}{f_{R,1}(\hat{R}_1(z), \hat{R}_2(z))} + \varepsilon_{1,2} m_1 \frac{\hat{b_1}(z)}{Y_1}, \\
&- \frac{\hat{b_2}(z)}{Y_2} \min\left(f_{I,2}(\hat{I}(z)), f_{R,2}(\hat{R}_1(z), \hat{R}_2(z))\right) \frac{\rho_2(\hat{R}_1(z), \hat{R}_2(z))}{f_{R,2}(\hat{R}_1(z), \hat{R}_2(z))} + \varepsilon_{2,2} m_2 \frac{\hat{b_2}(z)}{Y_1} \\
&+ D_{R_2} \frac{\partial^2 \hat{R}_2}{\partial z^2}.
\end{aligned}
$$

Which imply:

$$
\begin{aligned}
0 = &-\frac{\hat{b_1}(z)}{Y_1} m_1 \frac{\gamma_1(\hat{R}_1(z))}{f_{R,1}(\hat{R}_1(z), \hat{R}_2(z))} + \varepsilon_{1,1} m_1 \frac{\hat{b_1}(z)}{Y_1} - \frac{\hat{b_2}(z)}{Y_2} m_2 \frac{\gamma_2(\hat{R}_1(z))}{f_{R,2}(\hat{R}_1(z), \hat{R}_2(z))} \\
&+ \varepsilon_{2,1} m_2 \frac{\hat{b_2}(z)}{Y_1} + D_{R_1} \frac{\partial^2 \hat{R}_1}{\partial z^2},
\end{aligned}
$$

$$
\begin{aligned}
0 = &-\frac{\hat{b_1}(z)}{Y_1} m_1 \frac{\rho_1(\hat{R}_1(z), \hat{R}_2(z))}{f_{R,1}(\hat{R}_1(z), \hat{R}_2(z))} + \varepsilon_{1,2} m_1 \frac{\hat{b_1}(z)}{Y_1} - \frac{\hat{b_2}(z)}{Y_2} m_2 \frac{\rho_2(\hat{R}_1(z), \hat{R}_2(z))}{f_{R,2}(\hat{R}_1(z), \hat{R}_2(z))} \\
&+ \varepsilon_{2,2} m_2 \frac{\hat{b_2}(z)}{Y_1} + D_{R_2} \frac{\partial^2 \hat{R}_2}{\partial z^2}.
\end{aligned}
$$

Next,

$$D_{R_1}\frac{\partial^2 \hat{R}_1}{\partial z^2} = \frac{m_1\hat{b_1}(z)}{Y_1}\left(\frac{\gamma_1(\hat{R}_1(z))}{f_{R,1}(\hat{R}_1(z),\hat{R}_2(z))} - \varepsilon_{1,1}\right) + \frac{m_2\hat{b_2}(z)}{Y_2}\left(\frac{\gamma_2(\hat{R}_1(z))}{f_{R,2}(\hat{R}_1(z),\hat{R}_2(z))} - \varepsilon_{2,1}\right)$$

$$D_{R_2}\frac{\partial^2 \hat{R}_2}{\partial z^2} = \frac{m_1\hat{b_1}(z)}{Y_1}\left(\frac{\rho_1(\hat{R}_1(z),\hat{R}_2(z))}{f_{R,1}(\hat{R}_1(z),\hat{R}_2(z))} - \varepsilon_{1,2}\right) + \frac{m_2\hat{b_2}(z)}{Y_2}\left(\frac{\rho_2(\hat{R}_1(z),\hat{R_2}(z))}{f_{R,2}(\hat{R}_1(z),\hat{R}_2(z))} - \varepsilon_{2,2}\right)$$

To simplify notation, we now introduce the terms defined in Equations (5.86) –(5.89) to get

$$D_{R_1}\frac{\partial^2 \hat{R}_1}{\partial z^2} = \Gamma_1(z)\hat{b_1}(z) + \Gamma_2(z)\hat{b_2}(z), \tag{5.110}$$

$$D_{R_2}\frac{\partial^2 \hat{R}_2}{\partial z^2} = P_1(z)\hat{b_1}(z) + P_2(z)\hat{b_2}(z). \tag{5.111}$$

Integrating both sides of Equations (5.110) and (5.111) from 0 to z_b results in

$$\int_0^{z_b} D_{R_1}\frac{\partial^2 \hat{R}_1}{\partial z^2}\, dz = \int_0^{z_b}\left(\Gamma_1(z)\hat{b_1}(z) + \Gamma_2(z)\hat{b_2}(z)\right) dz,$$

$$D_{R_1}h\left(R_{in_1} - \hat{R}_1(z_b)\right) = \Gamma_1(z_{l_1})\hat{B}_1 + \Gamma_2(z_{l_2})\hat{B}_2, \tag{5.112}$$

and

$$\int_0^{z_b} D_{R_2}\frac{\partial^2 \hat{R}_2}{\partial z^2}\, dz = \int_0^{z_b}\left(P_1(z)\hat{b_1}(z) + P_2(z)\hat{b_2}(z)\right) dz,$$

$$D_{R_2}h\left(R_{in_2} - \hat{R}_2(z_b)\right) = P_1(z_{l_1})\hat{B}_1 + P_2(z_{l_2})\hat{B}_2. \tag{5.113}$$

Before solving for $\hat{B}_1$ and $\hat{B}_2$, we rewrite Equations (5.112) and (5.113) using Equations

(5.95), (5.101), (5.105), and (5.107) to obtain

$$\frac{D_{R_1}(R_{in_1} - \hat{R}_1(z_{l_2}))}{z_b + 1/h - z_{l_2}} = \Gamma_1(z_{l_1})\hat{B}_1 + \Gamma_2(z_{l_2})\hat{B}_2, \tag{5.114}$$

$$\frac{D_{R_2}(R_{in_2} - \hat{R}_2(z_{l_1}))}{z_b + 1/h - z_{l_1}} = P_1(z_{l_1})\hat{B}_1 + P_2(z_{l_2})\hat{B}_2. \tag{5.115}$$

Now we solve the system of equations given by Equations (5.114) and (5.115) for $\hat{B}_1$ and $\hat{B}_2$ to obtain

$$\hat{B}_1 = \frac{P_2(z_{l_2})\dfrac{D_{R_1}(R_{in_1} - \hat{R}_1(z_{l_2}))}{z_b + 1/h - z_{l_2}} - \Gamma_2(z_{l_2})\dfrac{D_{R_2}(R_{in_2} - \hat{R}_2(z_{l_1}))}{z_b + 1/h - z_{l_1}}}{\Gamma_1(z_{l_1})P_2(z_{l_2}) - \Gamma_2(z_{l_2})P_1(z_{l_1})}$$

$$= \frac{D_{R_1}P_2(z_{l_2})(z_b + 1/h - z_{l_1})(R_{in_1} - \hat{R}_1(z_{l_2})) - D_{R_2}\Gamma_2(z_{l_2})(z_b + 1/h - z_{l_2})(R_{in_2} - \hat{R}_2(z_{l_1}))}{(\Gamma_1(z_{l_1})P_2(z_{l_2}) - \Gamma_2(z_{l_2})P_1(z_{l_1}))(z_b + 1/h - z_{l_2})(z_b + 1/h - z_{l_1})}, \tag{5.116}$$

and

$$\hat{B}_2 = \frac{\Gamma_1(z_{l_1})\dfrac{D_{R_2}(R_{in_2} - \hat{R}_2(z_{l_1}))}{z_b + 1/h - z_{l_1}} - P_1(z_{l_1})\dfrac{D_{R_1}(R_{in_1} - \hat{R}_1(z_{l_2}))}{z_b + 1/h - z_{l_2}}}{\Gamma_1(z_{l_1})P_2(z_{l_2}) - \Gamma_2(z_{l_2})P_1(z_{l_1})}$$

$$= \frac{D_{R_2}\Gamma_1(z_{l_1})(z_b + 1/h - z_{l_2})(R_{in_2} - \hat{R}_2(z_{l_1})) - D_{R_1}P_1(z_{l_1})(z_b + 1/h - z_{l_1})(R_{in_1} - \hat{R}_1(z_{l_2}))}{(\Gamma_1(z_{l_1})P_2(z_{l_2}) - \Gamma_2(z_{l_2})P_1(z_{l_1}))(z_b + 1/h - z_{l_2})(z_b + 1/h - z_{l_1})}. \tag{5.117}$$

Finally, letting $\hat{R}_1(z_{l_2}) = R_2^\star$ and $\hat{R}_2(z_{l_1}) = R_1^\star$ in Equations (5.116) and (5.117) gives

$$\hat{B}_1 = \frac{D_{R_1}P_2(z_{l_2})(z_b + 1/h - z_{l_1})(R_{in_1} - R_2^\star) - D_{R_2}\Gamma_2(z_{l_2})(z_b + 1/h - z_{l_2})(R_{in_2} - R_1^\star)}{(\Gamma_1(z_{l_1})P_2(z_{l_2}) - \Gamma_2(z_{l_2})P_1(z_{l_1}))(z_b + 1/h - z_{l_2})(z_b + 1/h - z_{l_1})}, \tag{5.118}$$

and

$$\hat{B}_2 = \frac{D_{R_2}\Gamma_1(z_{l_1})(z_b + 1/h - z_{l_2})(R_{in_2} - R_1^\star) - D_{R_1}P_1(z_{l_1})(z_b + 1/h - z_{l_1})(R_{in_1} - R_2^\star)}{(\Gamma_1(z_{l_1})P_2(z_{l_2}) - \Gamma_2(z_{l_2})P_1(z_{l_1}))(z_b + 1/h - z_{l_2})(z_b + 1/h - z_{l_1})}, \tag{5.119}$$

as desired for the nutrient-limited case. The light level at and immediately below the layers at z_{l_1} and z_{l_2} are given by

$$\hat{I}(z_{l_1}) = I_{in} e^{\frac{-a_1(D_{R_1}P_2(z_{l_2})(z_b+1/h-z_{l_1})(R_{in_1}-R_2^\star)-D_{R_2}\Gamma_2(z_{l_2})(z_b+1/h-z_{l_2})(R_{in_2}-R_1^\star))}{(\Gamma_1(z_{l_1})P_2(z_{l_2})-\Gamma_2(z_{l_2})P_1(z_{l_1}))(z_b+1/h-z_{l_2})(z_b+1/h-z_{l_1})} - a_{bg}z_{l_1}} > I_1^\star \tag{5.120}$$

and

$$\hat{I}(z_{l_2}) = \hat{I}(z_{l_1}) e^{\frac{-a_2(D_{R_2}\Gamma_1(z_{l_1})(z_b+1/h-z_{l_2})(R_{in_2}-R_1^\star)-D_{R_1}P_1(z_{l_1})(z_b+1/h-z_{l_1})(R_{in_1}-R_2^\star))}{(\Gamma_1(z_{l_1})P_2(z_{l_2})-\Gamma_2(z_{l_2})P_1(z_{l_1}))(z_b+1/h-z_{l_2})(z_b+1/h-z_{l_1})} - a_{bg}(z_{l_2}-z_{l_1})} > I_2^\star. \tag{5.121}$$

Note that both $\hat{I}(z_{l_1})$ and $\hat{I}(z_{l_2})$ decrease as z_{l_1} and z_{l_2} increase so that a deeper nutrient-limited layer implies more shade.

Now consider the case of light-limitation of both layers. Recall

$$\hat{I}(z) = \begin{cases} I_{in}e^{-a_{bg}z}, & 0 \le z < z_{l_1}, \\ I_{in}e^{-a_1\hat{B}_1 - a_{bg}z}, & z_{l_1} \le z < z_{l_2}, \\ I_{in}e^{-a_1\hat{B}_1 - a_2\hat{B}_2 - a_{bg}z}, & z_{l_2} \le z \le z_b, \end{cases}$$

Evaluating at z_{l_1} gives

$$\hat{I}(z_{l_1}) = I_{in}e^{-a_1\hat{B}_1 - a_{bg}z_{l_1}}.$$

Solving for $\hat{B}_1$, we obtain

$$\hat{B}_1 = \frac{\ln(I_{in}/\hat{I}(z_{l_1}))}{a_1} - \frac{a_{bg}}{a_1}z_{l_1}. \tag{5.122}$$

Similarly, evaluating at z_{l_2} gives

$$\hat{I}(z_{l_2}) = I_{in} e^{-a_1 \hat{B}_1 - a_2 \hat{B}_2 - a_{bg} z_{l_2}}.$$

Solving for $\hat{B}_2$, we first obtain

$$\hat{B}_2 = \frac{\ln(I_{in}/\hat{I}(z_{l_2}))}{a_2} - \frac{a_1}{a_2}\hat{B}_1 - \frac{a_{bg}}{a_2} z_{l_2}. \tag{5.123}$$

Substituting Equation (5.122) into Equation (5.123) and simplifying gives

$$\hat{B}_2 = \frac{\ln(\hat{I}(z_{l_1})/\hat{I}(z_{l_2}))}{a_2} - \frac{a_{bg}}{a_2}(z_{l_2} - z_{l_1}). \tag{5.124}$$

Finally, letting $\hat{I}(z_{l_1}) = I_1^\star$ and $\hat{I}(z_{l_2}) = I_2^\star$, we get

$$\hat{B}_1 = \frac{\ln(I_{in}/I_1^\star)}{a_1} - \frac{a_{bg}}{a_1} z_{l_1}, \tag{5.125}$$

and

$$\hat{B}_2 = \frac{\ln(I_1^\star/I_2^\star)}{a_2} - \frac{a_{bg}}{a_2}(z_{l_2} - z_{l_1}), \tag{5.126}$$

as desired for the light-limited case. Using Equations (5.118), (5.119), (5.125), and (5.126), the nutrient level at and above the layer at z_{l_1} is given by

$$\begin{aligned}
\hat{R}_2(z_{l_1}) = R_{in_2} &- \frac{(z_b + 1/h - z_{l_1})}{2a_1\Gamma_2(z_{l_2})D_{R_2}(z_b + 1/h - z_{l_2})}(\Delta(z_{l_1}, z_{l_2})(z_b + 1/h - z_{l_2})(\ln(I_{in}/I_1^\star) \\
&- a_{bg} z_{l_1})) + \frac{(z_b + 1/h - z_{l_1})}{2a_1 D_{R_2}\Gamma_2(z_{l_2})(z_b + 1/h - z_{l_2})}\left(2a_1 D_{R_2} P_2(z_{l_2})(R_{in_1} - R_2^\star)\right) \\
&- \frac{(z_b + 1/h - z_{l_1})}{2a_2 D_{R_1}\Gamma_1(z_{l_1})(z_b + 1/h - z_{l_2})}(\Delta(z_{l_1}, z_{l_2})(z_b + 1/h - z_{l_2})(\ln(I_1^*/I_2^\star) \\
&- a_{bg}(z_{l_2} - z_{l_1}))) + \frac{(z_b + 1/h - z_{l_1})}{2a_2 D_{R_1}\Gamma_1(z_{l_1})(z_b + 1/h - z_{l_2})}\left(a_2 D_{R_1} P_1(z_{l_1})(R_{in_1} - R_2^\star)\right) \\
&> R_1^\star,
\end{aligned} \tag{5.127}$$

where $\Delta(z_{l_1}, z_{l_2}) = \Gamma_1(z_{l_1})P_2(z_{l_2}) - \Gamma_2(z_{l_2})P_1(z_{l_1})$. Similarly, the nutrient level at and above the layer at z_{l_2} is given by

$$\begin{aligned}
\hat{R}_1(z_{l_2}) = R_{in_1} &- \frac{(z_b + 1/h - z_{l_2})}{2a_1 D_{R_1} P_2(z_{l_2})(z_b + 1/h - z_{l_1})}(\Delta(z_{l_1}, z_{l_2})(z_b + 1/h - z_{l_1})(\ln(I_{in}/I_1^\star) \\
&- a_{bg} z_{l_1})) - \frac{(z_b + 1/h - z_{l_2})}{2a_1 P_2(z_{l_2}) D_{R_1}(z_b + 1/h - z_{l_1})}\,(a_1 D_{R_2}\Gamma_2(z_{l_2})(R_{in_2} - R_1^\star)) \\
&- \frac{(z_b + 1/h - z_{l_2})}{2a_2 P_1(z_{l_1}) D_{R_1}(z_b + 1/h - z_{l_1})}\,(a_2 D_{R_2}\Gamma_1(z_{l_1})(R_{in_2} - R_1^\star)) \\
&+ \frac{(z_b + 1/h - z_{l_2})}{2a_2 P_1(z_{l_1}) D_{R_1}(z_b + 1/h - z_{l_1})}(\Delta(z_{l_1}, z_{l_2})(z_b + 1/h - z_{l_1})(\ln(I_1^\star/I_2^\star) \\
&- a_{bg}(z_{l_2} - z_{l_1})) \\
&> R_2^\star. \qquad (5.128)
\end{aligned}$$

Note that $\hat{R}_1(z_2)$ and $\hat{R}_2(z_{l_1})$ increases as z_{l_1} and z_{l_2} increase so that a shallower light-limited layer depresses nutrient levels more.

Thus we have shown that the equilibrium distributions for $\hat{B}_1$ and $\hat{B}_2$ under the ESS assumptions are given by Equations (5.84) and (5.85)

$$\hat{B}_1 = \begin{cases} \frac{D_{R_1}P_2(z_{l_2})(z_b+1/h-z_{l_1})(R_{in_1}-R_2^\star)-D_{R_2}\Gamma_2(z_{l_2})(z_b+1/h-z_{l_2})(R_{in_2}-R_1^\star)}{(\Gamma_1(z_{l_1})P_2(z_{l_2})-\Gamma_2(z_{l_2})P_1(z_{l_1}))(z_b+1/h-z_{l_2})(z_b+1/h-z_{l_1})}, & \text{nutrient-limited layer,} \\ \frac{\ln(I_{in}/I_1^\star)}{a_1} - \frac{a_{bg}}{a_1}z_{l_1}, & \text{light-limited layer,} \end{cases}$$

and

$$\hat{B}_2 = \begin{cases} \frac{D_{R_2}\Gamma_1(z_{l_1})(z_b+1/h-z_{l_2})(R_{in_2}-R_1^\star)-D_{R_1}P_1(z_{l_1})(z_b+1/h-z_{l_1})(R_{in_1}-R_2^\star)}{(\Gamma_1(z_{l_1})P_2(z_{l_2})-\Gamma_2(z_{l_2})P_1(z_{l_1}))(z_b+1/h-z_{l_2})(z_b+1/h-z_{l_1})} & \text{nutrient-limited layer,} \\ \frac{\ln(I_1^\star/I_2^\star)}{a_2} - \frac{a_{bg}}{a_2}(z_{l_2} - z_{l_1}), & \text{light-limited layer,} \end{cases}$$

as desired. □

Theorem 5.2.2. Existence of $(z_1^\star, z_2^\star)$ *The ESS depths* $z_1^\star$ *and* $z_2^\star$ *are determined by the*

system of equations:

$$\begin{cases} \frac{D_{R_1}P_2(z_{l_2})(z_b+1/h-z_1^\star)(R_{in_1}-R_2^\star)-D_{R_2}\Gamma_2(z_{l_2})(z_b+1/h-z_2^\star)(R_{in_2}-R_1^\star)}{(\Gamma_1(z_{l_1})P_2(z_{l_2})-\Gamma_2(z_{l_2})P_1(z_{l_1}))(z_b+1/h-z_2^\star)(z_b+1/h-z_1^\star)} = \frac{\ln(I_{in}/I_1^\star)}{a_1} - \frac{a_{bg}}{a_1}z_1^\star, \\ \\ \frac{D_{R_2}\Gamma_1(z_{l_1})(z_b+1/h-z_2^\star)(R_{in_2}-R_1^\star)-D_{R_1}P_1(z_{l_1})(z_b+1/h-z_1^\star)(R_{in_1}-R_2^\star)}{(\Gamma_1(z_{l_1})P_2(z_{l_2})-\Gamma_2(z_{l_2})P_1(z_{l_1}))(z_b+1/h-z_2^\star)(z_b+1/h-z_1^\star)} = \frac{\ln(I_1^\star/I_2^\star)}{a_2} - \frac{a_{bg}}{a_2}(z_2^\star - z_1^\star). \end{cases} \tag{5.129}$$

This solution provides a stable equilibrium of the full preferential nutrient uptake model (Equations (3.1) –(3.17)) with $D_{b_1} = D_{b_2} = 0$ *and* $\nu_1(\partial g_1/\partial z)|_{z_1^\star} = \nu_2(\partial g_2/\partial z)|_{z_2^\star} = 0$.

Proof. Observe that net growth is positive below a nutrient-limited layer since $I > I_1^\star > I_2^\star$ and net growth is positive above a light-limited layer since $R > R_1^\star > R_2^\star$. Thus the ESS depth is obtained by considering the case of a layer under the conditions of co-limitation. That is, the layers are limited by both resources so that $\hat{R}_2(z_{l_1}) = R_1^\star$, $\hat{R}_1(z_{l_2}) = R_2^\star$, $\hat{I}(z_{l_1}) = I_1^\star$, and $\hat{I}(z_{l_2}) = I_2^\star$. Thus we need to combine the nutrient-limited and light-limited cases for $\hat{B}_1$ and $\hat{B}_2$ to derive the system needed to solve for the ESS depths $z_1^\star$ and $z_2^\star$. We do this by setting the nutrient-limited and light-limited profiles equal and replace z_{l_1} and z_{l_2} with $z_1^\star$ and $z_2^\star$. Doing this results in the system of equations given in (5.129):

$$\begin{cases} \frac{D_{R_1}P_2(z_{l_2})(z_b+1/h-z_1^\star)(R_{in_1}-R_2^\star)-D_{R_2}\Gamma_2(z_{l_2})(z_b+1/h-z_2^\star)(R_{in_2}-R_1^\star)}{(\Gamma_1(z_{l_1})P_2(z_{l_2})-\Gamma_2(z_{l_1})P_1(z_{l_1}))(z_b+1/h-z_2^\star)(z_b+1/h-z_1^\star)} = \frac{\ln(I_{in}/I_1^\star)}{a_1} - \frac{a_{bg}}{a_1}z_1^\star, \\ \\ \frac{D_{R_2}\Gamma_1(z_{l_1})(z_b+1/h-z_2^\star)(R_{in_2}-R_1^\star)-D_{R_1}P_1(z_{l_1})(z_b+1/h-z_1^\star)(R_{in_1}-R_2^\star)}{(\Gamma_1(z_{l_1})P_2(z_{l_2})-\Gamma_2(z_{l_2})P_1(z_{l_1}))(z_b+1/h-z_2^\star)(z_b+1/h-z_1^\star)} = \frac{\ln(I_1^\star/I_2^\star)}{a_2} - \frac{a_{bg}}{a_2}(z_2^\star - z_1^\star). \end{cases}$$

Existence of solutions to this system of equations is guaranteed by the Implicit Function Theorem. The system of equations can be solved in $(z_1^\star, z_2^\star)$, however, the resulting algebraic expressions are uninformative.

The ESS provides a stable equilibrium of the full model (Equations (3.1) –(3.17)) with

$D_{b_1} = D_{b_2} = 0$ and $\nu_1(\partial g_1/\partial z)|_{z_1^\star} = \nu_2(\partial g_2/\partial z)|_{z_2^\star} = 0$ since

$$g_1(z) = \min\Big(f_{I,1}(I_1^\star), f_{R,1}(R_1^\star, R_2^\star)\Big) - m_1 = m_1 - m_1 = 0 \tag{5.130}$$

and

$$g_2(z) = \min\Big(f_{I,2}(I_2^\star), f_{R,2}(R_1^\star, R_2^\star)\Big) - m_2 = m_2 - m_2 = 0 \tag{5.131}$$

for all $z \in [0, z_b]$. Equations (5.130) and (5.131) follow since $I_1^\star = f_{I,1}^{-1}(m_1)$, $I_2^\star = f_{I,2}^{-1}(m_2)$, $R_1^\star = f_{R,1}^{-1}(m_1, m_2)$, and $R_2^\star = f_{R,2}^{-1}(m_1, m_2)$ so that no net growth occurs outside the layers at $z_1^\star$ and $z_2^\star$ for $b_1(z)$ and $b_2(z)$ respectively. □

Corollary 5.2.3. (The Biomass Equilibrium $\hat{B}_1$ and $\hat{B}_2$ as functions of $(z_1^\star, z_2^\star)$) *The equilibrium biomass can be expressed as a function of* $(z_1^\star, z_2^\star)$ *as*

$$\hat{B}_1 = \begin{cases} \dfrac{\ln(I_{in}/I_1^\star)}{a_1}, & z_1^\star \leq 0 \\ & \text{(surface layer)}, \\ \frac{D_{R_1}P_2(z_{l_2})(R_{in_1}-R_2^\star)}{\Delta(z_{l_1},z_{l_2})(z_b+1/h-z_2^\star)} - \frac{D_{R_2}\Gamma_2(z_{l_2})(R_{in_2}-R_1^\star)}{\Delta(z_{l_1},z_{l_2})(z_b+1/h-z_1^\star)} = \frac{\ln(I_{in}/I_1^\star)}{a_1} - \frac{a_{bg}}{a_1}z_1^\star, & 0 < z_1^\star < z_2^\star < z_b \\ & \text{(DCM)}, \\ \dfrac{D_{R_1}P_2(z_{l_2})(R_{in_1} - R_2^\star) - D_{R_2}\Gamma_2(z_{l_2})(R_{in_2} - R_1^\star)}{\Delta(z_{l_1}, z_{l_2})}, & z_2^\star \geq z_b \\ & \text{(benthic layer)}, \end{cases} \tag{5.132}$$

and

$$\hat{B}_2 = \begin{cases} \dfrac{\ln(I_1^\star/I_2^\star)}{a_2}, & z_1^\star \geq z_2^\star \\ & \text{(surface layer)}, \\ \frac{D_{R_2}\Gamma_1(z_{l_1})(R_{in_2}-R_1^\star)}{\Delta(z_{l_1},z_{l_2})(z_b+1/h-z_1^\star)} - \frac{D_{R_1}P_1(z_{l_1})(R_{in_1}-R_2^\star)}{\Delta(z_{l_1},z_{l_2})(z_b+1/h-z_2^\star)} = \frac{\ln(I_1^\star/I_2^\star)}{a_2} - \frac{a_{bg}}{a_2}(z_2^\star - z_1^\star), & 0 < z_1^\star < z_2^\star < z_b \\ & \text{(DCM)}, \\ \dfrac{D_{R_2}\Gamma_1(z_{l_1})(R_{in_2}-R_1^\star) - D_{R_1}P_1(z_{l_1})(R_{in_1}-R_2^\star)}{\Delta(z_{l_1},z_{l_2})}, & z_2^\star \geq z_b \\ & \text{(benthic layer)}. \end{cases} \tag{5.133}$$

Proof. The DCM layers present in Equations (5.132) and (5.133) are a direct consequence of Theorem 5.2.2. The remaining terms in the biomass distributions are determined by restricting the biomass to the water column. For $\hat{B}_1$, if $z_1^\star \leq 0$ we restrict the biomass to the light-limited surface layer at $z = 0$. Additionally, if $z_2^\star \geq z_b$ we restrict the biomass to the nutrient-limited benthic layer at $z = z_b$. While the argument is identical for $\hat{B}_2$, the surface layer will occur when $z_2^\star - z_1^\star \leq 0$. □

6 Conclusion and Suggestions for Future Work

The proposed preferential nutrient uptake model presented is able to qualitatively replicate common depth profiles and offer insights into what physical and physiological parameters are important to consider in model calibration. The parameter estimation problem was able to be successfully solved on 26 of the model's parameters. While simulated data was used in this presentation, this approach offered insights into parameters that are numerically difficult to estimate. Of these, the incident light I_{in} is the easiest to resolve with measurement and can be fixed for simulations done on data generated from field observations. When the model was analyzed under the Morris screening and Sobol decomposition procedures, the model's full parameter space was considered to determine a ranking of the parameters and their impact on the model's output for $b_1(z,t)$, $b_2(z,t)$, $R_1(z,t)$, and $R_2(z,t)$. The results of the screening algorithm for the biomass were consistent with biological intuition and highlighted the importance of parameters associated with how phytoplankton species use light. The Sobol decomposition method highlighted the possible numerical instability of the solutions when the loss coefficients are made too large. For the nutrient, the yield coefficients were ranked as most important in both methods. Since the yield coefficients Y_1 and Y_2 have a large range of values reported in the literature and are susceptible to being estimated with error, care should be taken with these parameters in simulations. These finds are remarkably consistent with the analysis done on the Klausmeier and Litchman model and the multi-species variant of their model as well.

In Chapter 5 we derived special equilibrium solutions to the multi-species Klausmeier and Litchman model (an extension of the work done in [35]) and the preferential nutrient uptake model. The analysis of both multi-species models show that presence of light and nutrient gradients are essential in controlling biomass abundance. In particular, the co-existence of phytoplankton populations can be attributed to how different species specialize in the utilization of light and nutrients. This work can be extended to analyze the competition

between two consumers for multiple resources in a spatially continuous habitat in which resource distributions are impacted by biological factors. Research in this direction for a multi-species phytoplankton competition model can be found in [51]. Using a similar analysis, the impact of preferential nutrient uptake can be better understood.

Going forward, there are multiple avenues of study which can be considered relating to this current body of research. An often overlooked component of aquatic ecosystems is the impact that viral populations have in the microbial loop. Studies have shown that there can be up to an order of magnitude of 10^{10} viruses per liter in surface water and are an important factor in controlling algal blooms [17]. Currently most models that study the vertical distributions of phytoplankton and forms of coexistence do not incorporate a viral component. Additionally, the invasion of zebra and quagga mussels in North American freshwater ecosystems and the Great Lakes poses further modeling challenges. Mussels are filter feeders which attach to the substrate and adults are capable of filtering one or more liters of water per day where they remove phytoplankton, zooplankton, and algae and discharge particle free water. In order to adapt the existing models to this environment, a biologically active layer at the boundary would need to be added, resulting in a term which would be the solution of an ordinary differential equation used to model mussel growth. Some work has been done in this regard and can be found in [59].

In addition to extending the existing models to incorporate further biological complexities, different modeling approaches can also be considered. In particular, the use of agent based models and cellular automata models, along with models which incorporate machine learning techniques such as evolutionary computation, autoregressive fuzzy models, and artificial neural network models are of great interest. Agent based and cellular automata models are discrete models which simulate a group of individuals. Population level behavior emerges as the sum of the agent behaviors and how the agents interact with the environment. These models provide a natural contrast to the differential equation models and can offer further insights into the phytoplankton layering phenomenon and forms of coexistence. In

particular, combining these methods with other models which incorporate machine learning techniques which have been previously used successfully to forecast the formation of harmful algal blooms is of interest. This framework would allow us to not only see how those forecasts compare to others based on field data, but to further contrast the existing differential equation models and reduce the number of input parameters needed for a robust forecasting system.

REFERENCES

[1] Anderson, Donald M., Gilbert, Patricia M., and Burkholder, JoAnn M. (2002) *Harmful algal blooms and eutrophication: nutrient sources, composition, and consequences.* Estuaries 25-4: 704-726.

[2] Ashino, Ryuichi, Nagase, Michihiro, and Nagase, Vaillancourt, Rémi (2000) *Behind and beyond the MATLAB ODE suite.* Computers & Mathematics with Applications 40: 491-512.

[3] Auguéres, Anne-Sophie, and Loreau, Michel. (2015) *Can organisms regulate global biogeochemical cycles?* Ecosystems 18-5: 813-825.

[4] Banks, H.T., and Bihari, K.L. (2001) *Modeling and estimating uncertainty in parameter estimation.* Inverse Problems 17: 95-111.

[5] Brooks, A.S. and Torke, B.G. (1977) *Vertical and seasonal distribution of Chlorophyll a in Lake Michigan.* Journal of the Fisheries Research Board of Canada 34:2280-2287.

[6] Brooks, A.S. and Edginton, D.N. (1994) *Biogeochemical control of phosphorus cycling and primary production in Lake Michigan* Limnology and Oceanography 39-4: 961-968.

[7] Chattopadhyay, J., Pal, S., and Sarkar, R.R. (2004) *Mathematical modeling of harmful algal blooms supported by experimental findings.* Ecological Complexity 1: 225-235.

[8] DeManche, J.M., Curl, Jr, H.C., Lundy, D.W., Donaghay, P. L. (1979). *The rapid responses of the marine diatom Skeletonema costatum in external and internal nutrient concentration.* Marine Biology 53: 323-333.

[9] Domis, Lisette, Waal, Dedmer, Helmsing, Nico, Donk, Ellen, and Mooij, Wolf (2014). *Community stoichiometry in a changing world: combined effects of warming and eutrophication on phytoplankton dynamics.* Ecology 95-6: 1485 - 1495.

[10] Dortch, Q. (1990) *The interaction between ammonium and nitrate uptake in phytoplankton.* Marine ecology press series. Oldendorf, 61-1: 183-201.

[11] Du, Yihong and Hsu, Sze-Bi (2008) *Concentration phenomena in a nonlocal quasi-linear problem modeling phytoplankton I: existence*. SIAM Journal of Mathematical Analysis 40-4: 1419-1440.

[12] Du, Yihong and Hsu, Sze-Bi (2008) *Concentration phenomena in a non-local quasi-linear problem modeling phytoplankton II: limiting profile*. SIAM Journal of Mathematical Analysis 40-4: 1441-1470.

[13] Du, Yihong and Hsu, Sze-Bi (2010) *On a non-local reaction-diffusion problem arising from the modeling of phytoplankton growth*. SIAM Journal of Mathematical Analysis 42-3 : 1305-1333.

[14] Du, Yihong and Mei, Linfeng (2011) *On a non-local reaction-diffusion-advection equation modeling phytoplankton dynamics*. Nonlinearity 24: 319-349.

[15] Easley, David and Kleinberg, Jon (2010) *Networks, Crowds, and Markets: Reasoning about a Highly Connected World*. Cambridge University Press

[16] Eshel, I. (1983) *Evolutionary and continuous stability*. Journal of Theoretical Biology 103: 99-111.

[17] Fuhrman, K.M., Pinter, G.A. and Berges, J.A. (2011) *Dynamics of a virus-host model with an intrinsic quota*. Mathematical and Computer Modeling 53: 716-730.

[18] Geritz, S.A.H., A.J. Metz, E., Kisdi, and G. Meszeńa. (1998) *Evolutionary singular strategies and the adaptive growth and branching of the evolutionary tree*. Evolutionary Ecology 12: 35-57.

[19] Gilbert, Patricia M., Wilkerson, Frances P., Dugdale, Richard C., Raven, John A., Dupont, Christopher L., Leavitt, Peter R., . . . ,Kana, Todd M. (2015) *Pluses and minuses of ammonium and nitrate uptake and assimilation by phytoplankton and implications for productivity and community composition, with emphasis on nitrogen-enriched conditions*. Limnology and Oceanography 61-1: 165-197.

[20] Haghighi, Erfan, Madani, Kaveh, and Hoekstra, Arjen (2018). *The water footprint of water conservation using shade balls in California*. Nature Sustainability 1: 358-360.

[21] Hays G.C., Richardson, A.J. Robinson, C. (2005) *Climate change and marine plankton.* Trends in Ecology & Evolution 20: 337-334.

[22] Hoagland, P., Andersson, D.M., Karou, Y., and White, A.W. (2002) *The economic effects of harmful algal blooms in the United States: Estimates, assessment issues, and information needs.* Estuaries 25-4: 819-837.

[23] Horner, Rita A., Garrison, David L., and Plumey, F. Gerald (1997) *Harmful algal blooms and red tide problems on the U.S. West Coast.* Limnology and Oceanography 42-5: 1076-1088.

[24] Howard, Alan (2001) *Modeling movement patterns of the cyanobacterium Microcystis.* Ecological Applications 11-1: 304-310.

[25] Hsu, Sze-Bi and Lou, Yan. (2010) *Single phytoplankton species growth with light and advection in a water column.* SIAM Journal of Applied Mathematics 70-8: 2942-2974.

[26] Hsu, S.B. and Waltman, P. (1993) *On a system of reaction diffusion equations arising from competition in an unstirred chemostat.* SIAM Journal of Applied Mathematics 53-4: 1026-1044.

[27] Huisman, Jef and Sommeijer, Ben (2002) *Simulation techniques for the population dynamics of sinking phytoplankton in light-limited environments.* Modeling, Analysis and Simulation: 1-17.

[28] Huisman, Jef and Weissing, Franz J. (1994) *Light-limited growth and competition for light in well-mixed aquatic environments: an elementary model.* Ecology 75-2: 507-520.

[29] Huisman, Jef and Weissing, Franz J. (1995) *Competition for nutrients and light in a mixed water column: a theoretical analysis.* The American Naturalist 146-4: 536-564.

[30] Hutchinson, G.E. (1961) *The paradox of the plankton.* The American Naturalist 95-882: 137-145.

[31] Imboden, D. M. (1990) *Mixing and transport in lakes: Mechanisms and ecological relevance,* p. 47-80. *In* M. Tilzer and S. Serruya [eds.], Large lakes: Ecological structure and function. Springer.

[32] Jassby, Alan D. and Pratt, Trevor. (1976) *Mathematical formulation of the relationship between photosynthesis and light for phytoplankton.* Limnology and Oceanography 21-4: 540-547.

[33] Keller, E.F. and Segel, L.A. (1971) *Traveling bands of chemotactic bacteria: A theoretical analysis.* Journal of Theoretical Biology 30: 235-248.

[34] Kirk, J.T.O. (1975) *Theoretical-analysis of contribution of algal cells to attenuation of light within natural waters 1. General treatment of suspensions of pigmented cells.* New Phytologist 75: 11-20.

[35] Klausmeier, Christopher A. and Litchman, Elena (2001) *Algal games: the vertical distribution of phytoplankton in poorly mixed water columns.* Limnology and Oceanography 46-8: 1998-2007.

[36] Krause-Jensen, Dorte, and Sand-Jensen, Kaj (1998) *Light attenuation and photosynthesis of aquatic plant communities.* Limnology and Oceanography 43-3: 396-407.

[37] Lagarias, J.C., Reeds, J.A., and Wright, P.E. (1998) *Convergence properties of the Nelder-Mead simplex method in low dimensions.* SIAM Journal of Optimization 9-1: 112-147.

[38] Leibold, M.A. (1990) *Resources and predators can affect the vertical distributions of zooplankton.* Limnology and Oceanography 35: 33-45.

[39] Litchman, Elena, and Klausmeier, Christopher A. (2008) *Trait-based community ecology of phytoplankton.* Annual Review of Ecology, Evolution, and Systematics 39: 615-639.

[40] Losada, M. and Guerro, M.G. (1979) *The photosynthetic reduction of nitrate and its regulation.* Photosynthesis in Relation to Model Systems (J. Barber, ed.). Elsevier/North Holland Biomedical Press, Amsterdam: 365408.

[41] MacArthur, Robert and Levins, Richard (1964) *Competition, habitat selection, and character displacement in a patchy environment.* Proceedings of the National Academy of Sciences (USA) 51: 1207-1210.

[42] Maynard Smith, J., and Price, G. (1973) *The logic of animal conflicts.* Nature 246: 15-18.

[43] Mellard, Jared P., Yoshiyama, Kohei, Lichtman, Elena, Klausmeier, Christopher A. (2011) *The vertical of phytoplankton in stratified water columns.* Journal of Theoretical Biology 269-1: 16-30.

[44] Morris, I. (1974). *Nitrogen assimilation and protein synthesis.* Algal physiology and biochemistry (Steward, W.D.P, ed.) University of California Press, Berkley and Los Angeles: 583-609.

[45] Mortonson, J.A. and Brooks, A.S. (1980) *Occurrence of a deep nitrate maximum in Lake Michigan* Canadian Journal of Fisheries and Aquatic Science 37:1025-1027.

[46] Okubo, A. (1980) *Diffusion and ecological problems: mathematical models.* Springer-Verlag

[47] Phillips, O. M. (1973) *The equilibrium and stability of simple marine biological systems I. Primary nutrient consumers.* The American Naturalist 107-953: 73-93.

[48] Recknagel,F., Ostrovsky, I., Cao, H., Zhang, X. (2013) *Ecological relationships, thresholds and time-lags determining phytoplankton community dynamics of Lake Kinnert, Israel elucidated by evolutionary computation and wavelets.* Ecological Modeling 255: 70-86.

[49] Reynolds, C.S. (1984) *The ecology of freshwater phytoplankton.* Cambridge University Press.

[50] Rhee, G-Yull and Gotham, Ivan J. (1981) *The effect of environment factors on phytoplankton growth: light and the interactions of light with nitrate limitation.* Limnology and Oceanography 26-4: 649-659.

[51] Ryabov, Alexei B. and Blasius, Bernd. (2008) *Population growth and persistence in a heterogeneous environment: the role of diffusion and advection.* Math. Model. Nat. Phenom. 3-3: 42-86.

[52] Ryabov, Alexei B. and Blasius, Bernd. (2010) *Vertical distribution and composition of phytoplankton under the influence of an upper mixed layer*. Journal of Theoretical Biology 263: 120-133.

[53] Ryabov, Alexei B. and Blasius, Bernd. (2011) *A graphical theory of competition on spatial resource gradients*. Ecology Letters 14: 200-228.

[54] Smayda, T.J. (1970) *The suspension and sinking of phytoplankton in the sea*. Annual Review of Oceanography and Marine Biology 8: 353-414.

[55] Smith, Ralph C. (2014) *Uncertainty quantification: theory, implementation, and applications*. Society for Industrial and Applied Mathematics.

[56] Smith, H.L. and Waltman, P.E. (1995) *The theory of the chemostat: dynamics of microbial competition*. Cambridge studies in mathematical biology.

[57] Stakgold, Ivar. (2000) *Boundary value problems of mathematical physics Volume I*. Society for Industrial and Applied Mathematics.

[58] Stewart, Frank M. and Levin, Bruce R. (1973) *Partitioning of resources and the outcome of interspecific competition: a model and some general considerations*. The American Naturalist 107-954: 171-198.

[59] Swan, Breanna Patrice. (2016) *The influence of currents and bathymetry on the phytoplankton growth dynamics in a deep lake: an applicaation of the Lattice Boltzmann Method*, Theses and Dissertations.

[60] Syrett, P. J. (1981). *Nitrogen metabolism of microalgae.* Physiological Bases of Phytoplankton Ecology (Platt, T., ed), Bull No. 210, Canadian Government Publishing Center, Hull, Quebec, Candada: 182-210.

[61] Waal, Dedmer, Verschoor, Antoine, Verspagen, Jolanda, Donk, Ellen, and Huisman, Jef. (2010) *Climate-driven changes in the ecological stoichiometry of aquatic ecosystems.* Frontiers in Ecology and the Environment 8-3: 145-152.

[62] Wentworth, Mami T., Smith, Ralph C., and Banks H.T. (2015, February 15) *Parameter selection and verification techniques based on global sensitivity analysis illustrated for an HIV model*. Retrieved from https://www.ncsu.edu/crsc/reports/ftp/pdf/crsc-tr15-01.pdf

[63] Wu, J., Nie, H., and Wolkowicz, G.S.K. (2004) *A mathematical model of competition for two essential resources in the unstirred chemostat*. SIAM Journal of Applied Mathematics 65-1: 209-229.

[64] Xiao, Xi and He, Junyu and Huang, Haomin and Miller, Todd R. and Christakos, George and Reichwaldt, Elke S. and Ghadouani, Anas and Lin, Shengpan and Xu, Xinhua and Shi, Jiyan. (2017) *A novel single-parameter approach for forecasting algal blooms*. Water Research 108: 222-231.

CURRICULUM VITAE

Thomas G. Stojsavljevic Jr.

Education:

Master of Science, Mathematics

University of Wisconsin-Milwaukee, Milwaukee, WI, May 2014

Bachelor of Science, Pure Mathematics

University of Wisconsin-Milwaukee, Milwaukee, WI, May 2012

Honors and Awards:

Ernst Schwandt Teaching Award May 2018, May 2014

Elsevier Student Award for the most notable paper by a student May 2014

Undergraduate Morris and Miriam Marden Award May 2012

Alice Siu-Fun Leung Award May 2012

UWM Undergraduate Research Symposium First Place Research Presentation in the Natural Sciences April 2010

Professional Memberships:

American Mathematical Society September 2012 –Present

Mathematical Association of America September 2012 –Present

Association for Women in Mathematics February 2018 –Present

Graduate Student Research Symposium Organizing Committee September 2016 –May 2017

Phi –Beta –Kappa May 2012 –Present

Research Interests:

Applied Mathematics

- Mathematical biology, computational mathematics, agent based/cellular automata models, optimization

Statistics

- Parameter estimation, global sensitivity analysis, machine learning

Publications:

1. Stojsavljevic, T., G.A. Pinter, I. Lauko, and N. Myers (2019) *Parameter identification and global sensitivity analysis for a phytoplankton competition model.* Quart. Appl. Math. 77: 1-18.

2. Béchette, A., T. Stojsavljevic, M. Tessmer, J.A. Berges, G.A. Pinter and E.B. Young. (2013) *Mathematical modeling of bacteria–virus interactions in Lake Michigan incorporating phosphorus content.* J. Great Lakes Res. 39(4): 646-654.

    - This paper won the JGLR/Elsevier Student Award for the most notable paper by a student in 2014.

Conferences and Presentations:

1. Joint Mathematics Meeting, Baltimore, MD: *Mathematical modeling and analysis of a phytoplankton competition model incorporating preferential nutrient uptake.* January 2019; Talk

2. Joint Mathematics Meeting, San Diego, CA: *Evolutionary stable strategy for a multi-species phytoplankton competition model.* January 2018; Talk

3. Mathematical Association of America Wisconsin Regional Meeting, UWM: *Global sensitivity analysis for a phytoplankton competition model.* April 2017; Talk

4. UWM Graduate Student Seminar:*Parameter identification and global sensitivity analysis for a phytoplankton competition model.* February 2017; Talk

5. UWM Graduate Student Research Symposium: *Global sensitivity analysis for a phytoplankton competition model.* October 2016; Poster Presentation

6. Joint Mathematics Meeting Seattle, WA: *Parameter identification and sensitivity analysis for a phytoplankton competition model.*, January 2016; Talk

7. Joint Mathematics Meeting San Antonio, TX: *Mathematical modeling of competition for light and nutrients between phytoplankton species in a poorly mixed water column.* January 2015; Talk

8. UWM Applied Math Seminar: *Evolutionary Stable Strategy for Phytoplankton Competition in a Poorly Mixed Water Column.* November 2014; Talk

9. Mathematical Association of America Wisconsin Regional Meeting, UW-Stout: *Dynamic Modeling of Aquatic Viruses with a Phosphorus Quota.* (Béchette, A., T. Stojsavljevic M. Tessmer) April 2011; Talk

10. Second Annual Undergraduate Research Conference at the Interface of Biology and Mathematics NIMBios, University of Tennessee Knoxville: *Dynamic Modeling of Aquatic Viruses with an Internal Phosphorus Quota.* (Béchette, A., T. Stojsavljevic, M. Tessmer,) November 2010; Talk

11. UWM Undergraduate Research Symposium: *Is the simplest model the most desirable? Parsimony in a lake ecosystem.* (Béchette, A. Hughes A., C. Murphy, T. Stojsavljevic, M. Tessmer) April 2010; Poster Presentation

- The presentation was awarded the symposiums first prize in the Natural Sciences category.

Recent Service:

Judge for UWM Undergraduate Research Symposium April 2019, 2018, 2014

AWM student chapter outreach at Oostburg Christian School February 2019

Chair for MAA General Contributed Paper Session on Applied Mathematics II at Joint Mathematics Meeting Baltimore, MD January 2019

Chair for AMS Contributed Session on Modeling Disease and Biological Processes at Joint Mathematics Meeting San Diego, CA January 2018

Moderator for the MAA Wisconsin Regional Meeting April 2017

Organized UWM Graduate Student Research Symposium October 2016

Teaching Experience:

Teaching Assistant September 2012 –Present

University of Wisconsin-Milwaukee, Milwaukee, WI

Primary instructor for the following courses:

- Math 092/102: Mathematical Literacy for College Students I/II (co-requisite flipped classroom model for non-STEM majors)
- Math 098: Algebraic Literacy I (developmental math course)
- Math 105: Introduction to College Algebra
- Math 116: College Algebra
- Math 117: Trigonometry
- Math 211: Survey in Calculus and Analytical Geometry

- Math 231: Calculus and Analytical Geometry I
- Math 232: Calculus and Analytical Geometry II

Taught discussion sections for the following courses:

- Math 105: Introduction to College Algebra
- Math 211: Survey in Calculus and Analytical Geometry
- Primary responsibilities: office hours, grading, discussion of homework problems, and exam reviews

Grader for Math 321: Vector Analysis

Graduate Student Mentor for NSF Supported Undergraduate Research in Biology and Mathematics UBM Program January 2015 –May 2016

- Conducted study sessions for the mathematical modeling sequence Math 405/Math 675
- Advised undergraduate students on research projects, poster presentations, and conference presentations.

Mathematics Teacher Summers 2015, 2016, 2017

UWM Upward Bound Trio & Precollege Programs

- Primary instructor for AP Calculus

Classroom Aid September 2008 –May 2012

Preparation for College Mathematics/Beginning Algebra Intermediate Algebra Combined

- I worked with students one on one answering questions ranging from basic algebra and geometry up to Pre-Calculus using the ALEKS software.

Classroom Aid June 2011 –August 2011

Student Support Services Summer Bridge Program

- Made program announcements, graded worksheets, and generated assessments